REPORT NO.
UCD/CGM-01/05

CENTER FOR GEOTECHNICAL MODELING

DYNAMIC PROPERTIES OF SHERMAN ISLAND PEAT: PHASE II STUDY

BY

TIMOTHY M. WEHLING
ROSS W. BOULANGER
LESLIE F. HARDER, JR.
MICHAEL W. DRILLER

Research supported by the California Department of Water Resources (CDWR), State of California. The National Science Foundation (NSF) funded development of the triaxial testing equipment under NSF award number BCS-9310669, and acquisition of the digital oscilloscope, function generator, and other components used to perform the bender element tests under award number CMS-9502530. The views and conclusions contained in this document are those of the authors and should not be interpreted as necessarily representing the official policies, either expressed or implied, of the U.S. Government or the State of California.

DEPARTMENT OF CIVIL & ENVIRONMENTAL ENGINEERING
COLLEGE OF ENGINEERING
UNIVERSITY OF CALIFORNIA AT DAVIS

MARCH 2001

DYNAMIC PROPERTIES OF SHERMAN ISLAND PEAT: PHASE II STUDY

by

Timothy M. Wehling and Ross W. Boulanger
Department of Civil & Environmental Engineering, University of California, Davis, CA

Leslie F. Harder, Jr. and Michael W. Driller
Department of Water Resources, State of California, Sacramento, CA

Report No. UCD/CGM-01/05

Center for Geotechnical Modeling
Department of Civil & Environmental Engineering
University of California
Davis, California

March 2001

Abstract

This report summarizes the results of a laboratory study of the dynamic properties of peaty organic soil (or "peat" for brevity) at the south levee of Sherman Island near the western side of the Sacramento-San Joaquin Delta in California. This Phase II laboratory study complements the laboratory testing that was completed in 1998 and addresses a major source of uncertainty in the evaluations of seismic hazards in the Delta. High quality samples were obtained using standard and modified Shelby tubes at locations ranging from beneath the free-field to beneath the levee crest. The peat was very soft and highly compressible in the free-field where consolidation stresses were very low (e.g., 12 kPa) and was moderately firm beneath the levee crest where consolidation stresses were substantially larger (e.g., 130 kPa). Ash contents ranged from 48% to 79% and water contents ranged from 171% to 588%. Cyclic triaxial tests were used to measure the stress-strain behavior of 13 samples at cyclic shear strains ranging from 5×10^{-4} % to 10%. Bender element tests provided shear wave velocities for most of the specimens during triaxial testing. The test results show how the dynamic properties of Sherman Island peat are affected by consolidation stress, prior overstraining, reconsolidation, creep, and loading frequency. Recommendations are given for modulus reduction and damping relations to be used in evaluating seismic site response.

Acknowledgements

Support for this research was provided by the California Department of Water Resources (CDWR), State of California. The National Science Foundation (NSF) funded development of the triaxial testing equipment under NSF award number BCS-9310669, and acquisition of the digital oscilloscope, function generator, and other components used to perform the bender element tests under award number CMS-9502530. The views and conclusions contained in this document are those of the authors and should not be interpreted as necessarily representing the official policies, either expressed or implied, of the U.S. Government or the State of California.

Associate development engineer Bill Sluis and development technician Daret Kehlet of the University of California at Davis (UCD) provided assistance in the development and assembly of the triaxial testing apparatus and piezoceramic bender elements.

Drilling and sampling services for this research were provided by the CDWR. Brent Lampkin of the CDWR assisted with the drilling and sampling work.

Fellow UCD graduate students Tara Hutchinson, Jon Boland, Erik Malvick, and “Kula” Kulasingam, provided assistance during sample preparation.

All of the above support and assistance is greatly appreciated.

Table of Contents

Introduction

This report summarizes the results of a laboratory study of the properties of peaty organic soil (or "peat" for brevity) at the south levee of Sherman Island near the western side of the Sacramento-San Joaquin Delta. This Phase II laboratory study complements the laboratory test results obtained for this site by Boulanger et al. (1998).

Seismic Stability of the Delta Levee System

The Sacramento-San Joaquin Delta system is made up of over 1000 km of levees that direct various rivers and sloughs to the San Francisco Bay and channel two-thirds of all the water consumed in California. The levees make up a mesh of waterways that surround over 60 low-lying "islands" with ground levels below sea level. Failure of the levees during an earthquake would inundate the inner islands and could have an adverse effect on water quality in the Delta.

The dynamic response of the levees depends on site characteristics, such as the dynamic properties and thicknesses of the underlying soil layers, and on earthquake characteristics, such as level of shaking, duration of shaking, and frequency content. Most of this information can be obtained, or at least reasonably approximated, from recent technical literature. However, only limited information exists regarding the dynamic properties of peaty organic soils or peats, which greatly influence the expected dynamic response of the levees.

Delta levees are commonly comprised of uncompacted sands, silts, clays and peat built atop a thick layer of peaty organic soils. The dynamic properties, such as shear modulus and damping ratio, of these peaty organic soils must be determined to adequately evaluate their expected response to earthquake shaking. Estimating the seismic response of the levees is an important prerequisite to evaluating the potential for liquefaction of the uncompacted sands and silts within the levees. The immediate concern is the amount of damage that the levees will suffer from a near-by earthquake of sizable magnitude (CDWR 1992).

Previous Research

The available literature on dynamic properties of organic soil were reviewed by Boulanger et al. (1998), and so the following discussion is limited to a few key points. Seed and Idriss (1970) analyzed site response records at Union Bay and concluded that the peat (which had very low consolidation stresses) exhibited stronger nonlinearity and higher damping ratios than clays. Stokoe (1994) conducted resonant column and torsional shear tests on two peat specimens from near Queensboro Bridge in New York with in situ vertical effective stresses of about 114 kPa that showed relatively linear behavior up to strains of about 1%. Kramer (1996) performed several resonant column tests on Mercer Slough peat with in situ vertical effective stresses of 2 to 30 kPa, and observed strong nonlinearity, but with the degree of nonlinearity decreasing with increasing confining pressure. Boulanger et al. (1998) performed cyclic triaxial tests on peaty organic soils from beneath the levee crest at Sherman Island, where the in situ vertical effective stress

was approximately 130 kPa. The results showed relatively linear behavior with the shear modulus reduction and damping relations being comparable to those expected for high plasticity clays. Kramer (2000) combined results from Boulanger et al. (1998), Stokoe et al. (1994), and Kramer (1996, 1993) to show a general trend of increasing linearity with increasing effective confining pressure for different peats (Figure 2). Similarly, a general trend of decreasing damping with increasing effective confining pressure was observed.

The effect of loading frequency on modulus and damping ratios was also studied by Stokoe et al. (1994), Kramer (1996,1993) and Boulanger et al. (1998). These studies are consistent in showing that shear modulus generally increases by about 10% over a log-cycle increase in loading frequency. Damping ratios, however, are more complicated since they tend to decrease with increasing frequency up to about 0.1 Hz and then increase with increasing frequency above 0.1 Hz (Kramer 2000).

Overconsolidation was shown to have little effect on modulus reduction and damping relations for the peat samples tested by Boulanger et al. (1998). The test samples had in situ vertical effective stresses of about 130 kPa and were tested at effective consolidation stresses ranging from about 66 kPa to 200 kPa.

Current Study

This study further evaluates the dynamic properties of the peaty organic soil at Sherman Island in the Sacramento-San Joaquin Delta. The previous laboratory study by Boulanger et al. (1998) only tested samples from beneath the levee crest (Figure 1) where the effective vertical stress was about 130 kPa. In the present study, samples were obtained from beneath the levee bench, the levee mid-toe, and the free-field (Figure 1). The purpose of this additional testing was to cover the full range of in situ stress conditions for the peaty organic soils that influence the dynamic response of the levees.

This report summarizes the results of cyclic triaxial tests on 13 high-quality samples of the peaty organic soil: 2 samples from the levee bench, 5 samples from the mid-toe, and 6 samples from the free-field. The sample characteristics and test details are summarized in Table 1. The site conditions, in situ test data, sampling procedures, laboratory testing equipment, and testing procedures are described in this report. Experimental results are presented in detail because of the limited data currently available for peat. The effects of consolidation stress, prior overstraining, prior overstraining with reconsolidation, creep, and loading frequency are evaluated. The resulting experimental dynamic properties of peat at Sherman Island are compared with published results for other peaty soils. Recommendations are provided for modulus reduction and damping relations to be used in seismic site response analyses.

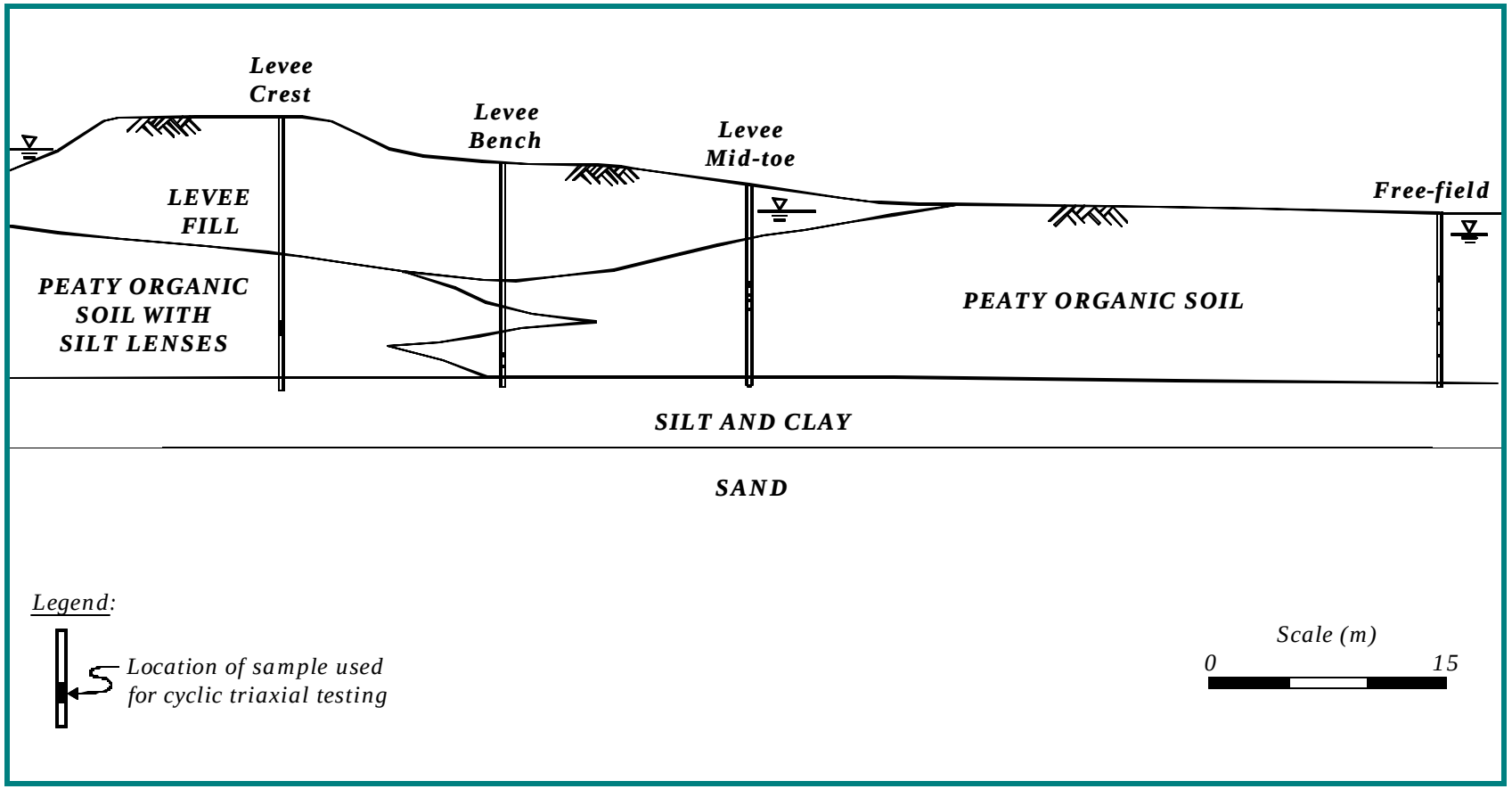

Figure 1: Soil profile at Sherman Island levee

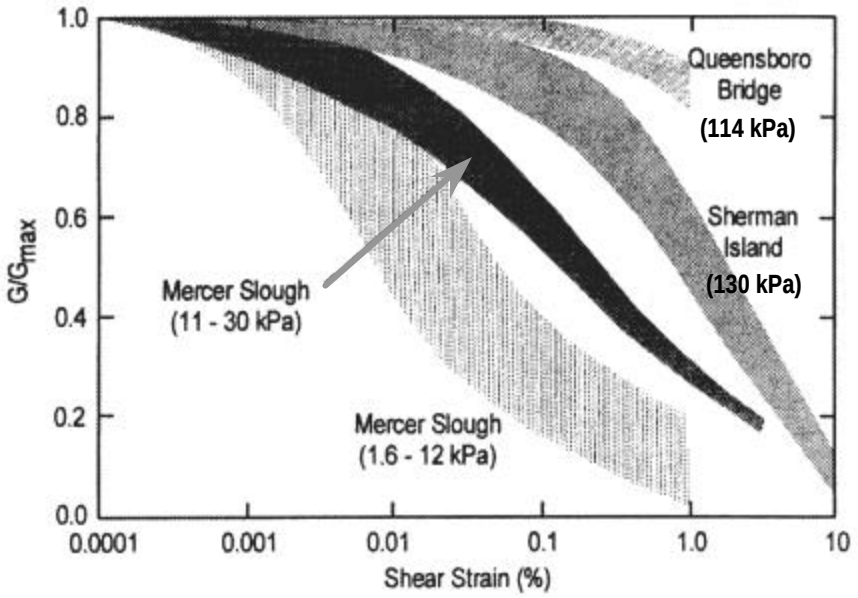

Figure 2: Modulus reduction behavior of peat soils at different vertical effective confining pressures (Kramer 2000)

Table 1: Summary of cyclic triaxial tests and bender element tests from this study

Boring Location[1]	Shelby Tube No.	Test Sample No.	Depth (m)	Initial Water Content[2] (%)	Ash Content[3] (%)	Initial Density (Mg/m^3)	In Situ σ_{vo}' (kPa)	Triaxial σ_{3c}' (kPa)	Bender Element V_s (m/s)
Bench (DHP-5H3)	S-2	3	12.0	185	62	1.198	78	78	95
	S-3	12	12.7	171	68	1.236	78	78	72
Mid-toe (DHP-5I1)	S-3	1	7.3	265	64	1.100	45	45	41
	S-3	6	6.9	334	49	1.102	45	45	*
	S-2	8	6.4	409	52	1.079	43	86	58
	S-2	9	6.2	406	53	1.168	43	86	*
	S-4	13	7.8	279	69	1.119	46	46	*
Free-field (DHP-5J1)	S-6	2	6.1	430	66	1.145	12	12	21
	S-7	4	7.0	442	63	1.116	13	13	23
	S-9	7	9.0	236	79	1.197	14	14	*
	S-4	10**	4.2	433	57	1.095	11	22	*
	S-4	11	4.0	588	48	1.066	11	22	*
	S-3	14	2.7	512	63	1.062	11	11	*

1. Designation in parenthesis refers to wooden stakes set by California Department of Water Resources.
2. Water content determined by oven-drying at 90 ^{o}C as recommended by Landva et al. (1983).
3. Ash contents determined from igniting at 440 ^{o}C corresponding to method C of ASTM (1996) D 2974 standard.

* Not measurable.

** Contained a decomposed wood knot with a maximum dimension of about 70 mm.

Site Characteristics

Geographic Location

The peat samples for this study were obtained by the Department of Water Resources, State of California (CDWR), from three boreholes at the south levee on Sherman Island, just east of the Highway 160 bridge that connects the island to Antioch across the San Joaquin River (Figure 3). The three sampling locations (free-field, levee mid-toe, and levee bench) and the sampling location (levee crest) used in the previous Sherman Island study were arranged in a line perpendicular to the levee. A schematic cross-section of the levee with the sampling locations is shown in Figure 1. Notice that the free-field ground surface elevation is below the elevation of the adjacent river water surface.

Geologic History

Peat began forming naturally in the Delta about 11,000 years ago from decomposed plant material. Occasional flooding of the rivers developed small natural levees made from fine-grained mineral deposits. Once the gold rush erupted in California, beginning in 1848, hydraulic mining upstream from the Delta built up hundreds of thousands of tons of silt in the Delta waterways. This caused more frequent flooding and raised the natural levees (CDWR 1992).

During the late 1800's, Delta inhabitants began raising the existing natural levees and drained the flooded inner Delta islands for agricultural use. Migrant laborers began construction of the man-made levees, and later horse-drawn carts were used to place uncompacted sand and other dredged materials, including peat, clay, and silty sand on the levees. By the early 1900's laborers were replaced with machines like the sidedraft clamshell dredge, which floated on a barge and had a clamshell bucket (CDWR 1992). Today, rehabilitation and maintenance are continually being done on the levees to prevent instability and piping.

General Characteristics of Peat Layer

The schematic cross-section in Figure 1 shows the main strata at Sherman Island, including the 7.5- to 10.5-m-thick peaty organic soil stratum. This organic soil stratum has been compressed under the overlying levee such that it is thinnest beneath the levee crest and thickest in the free-field. The levee fill is highly heterogeneous, consisting of sand, silt, clay, and peat. In the free-field the upper 0.5 m of soil overlying the peaty organic soil layer is also an organic soil but with a higher content of silt and sand. The peat stratum is underlain by a 4.2- to 4.6-m-thick layer of medium plasticity, medium stiff clay, which is underlain by dense sands and stiff to very stiff clays.

The peat samples had average initial water contents that ranged from 171% to 185% (178% average) beneath the levee bench to 236% to 588% (440% average) at the free-field, 58 m north of the levee bench (Figure 1). These differences in water content reflect the differences in consolidation stresses at these locations. Ash contents of the peat

samples ranged from 48% to 79% (61% average) with no apparent trend in ash contents between the different locations.

All peat specimens were highly fibrous with individual fibers ranging from fine, hairlike threads to 7-mm-wide blades. Samples could be separated along horizontal planes more easily than vertical planes, indicating a preferential orientation for the fibers. Of specific interest is sample 3 from the levee bench, which showed particularly weak bedding planes dipping at about 20^{o}. After testing, it was observed that these weak planes contained smooth, wide fibrous blades.

CPT and shear wave velocity (V_s) data beneath the levee crest are shown in Figure 4, and shear wave velocity data from the free-field boring are shown in Figure 5. V_s values in the peat stratum ranged from 80 m/s to 165 m/s beneath the levee crest, and from 21 m/s to 30 m/s in the free-field. These V_s profiles were obtained by Agbabian Associates (levee crest) and Geovision (free-field) using an OYO suspension logging system.

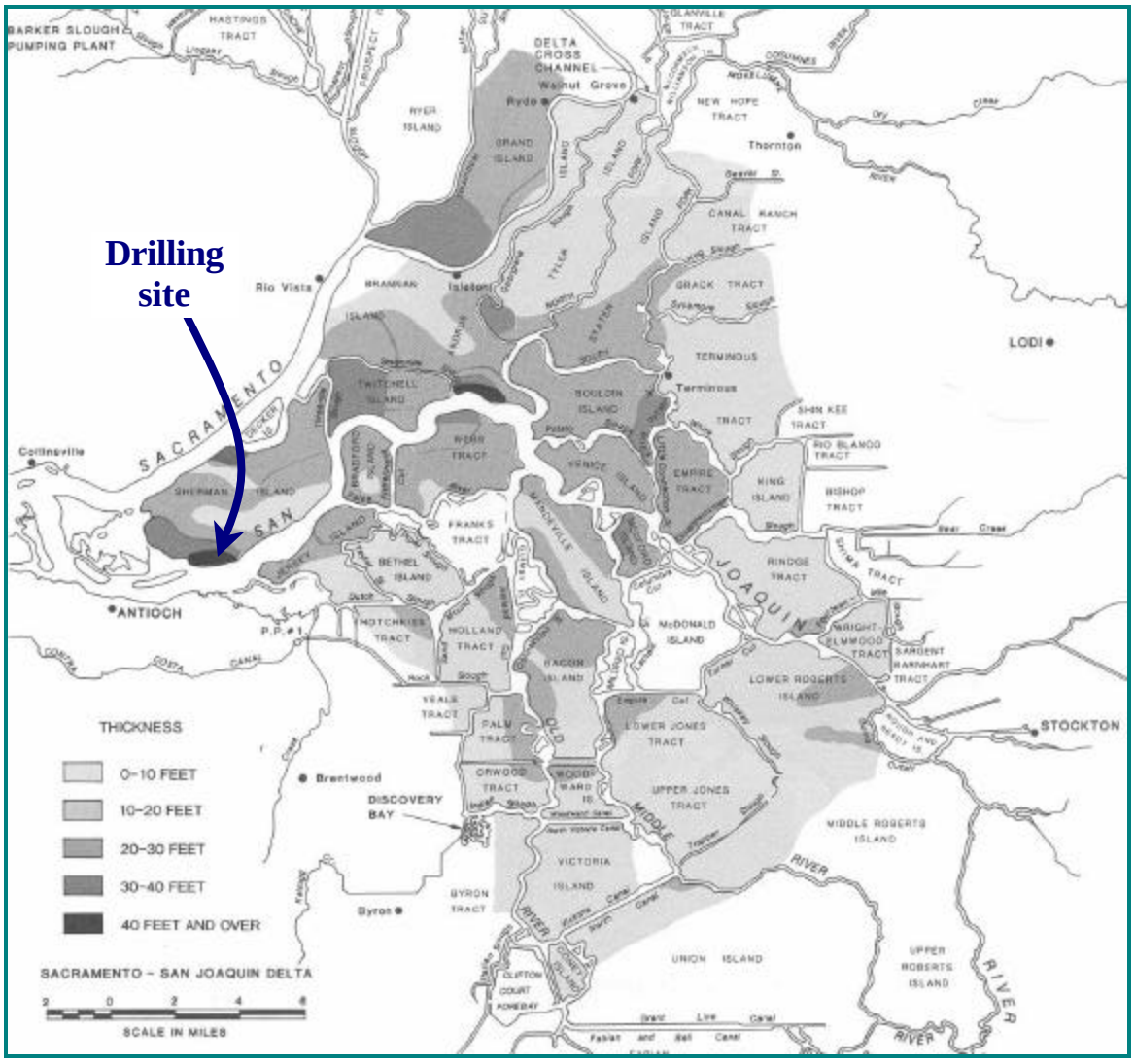

Figure 3: Location of Sherman Island (after CDWR 1993)

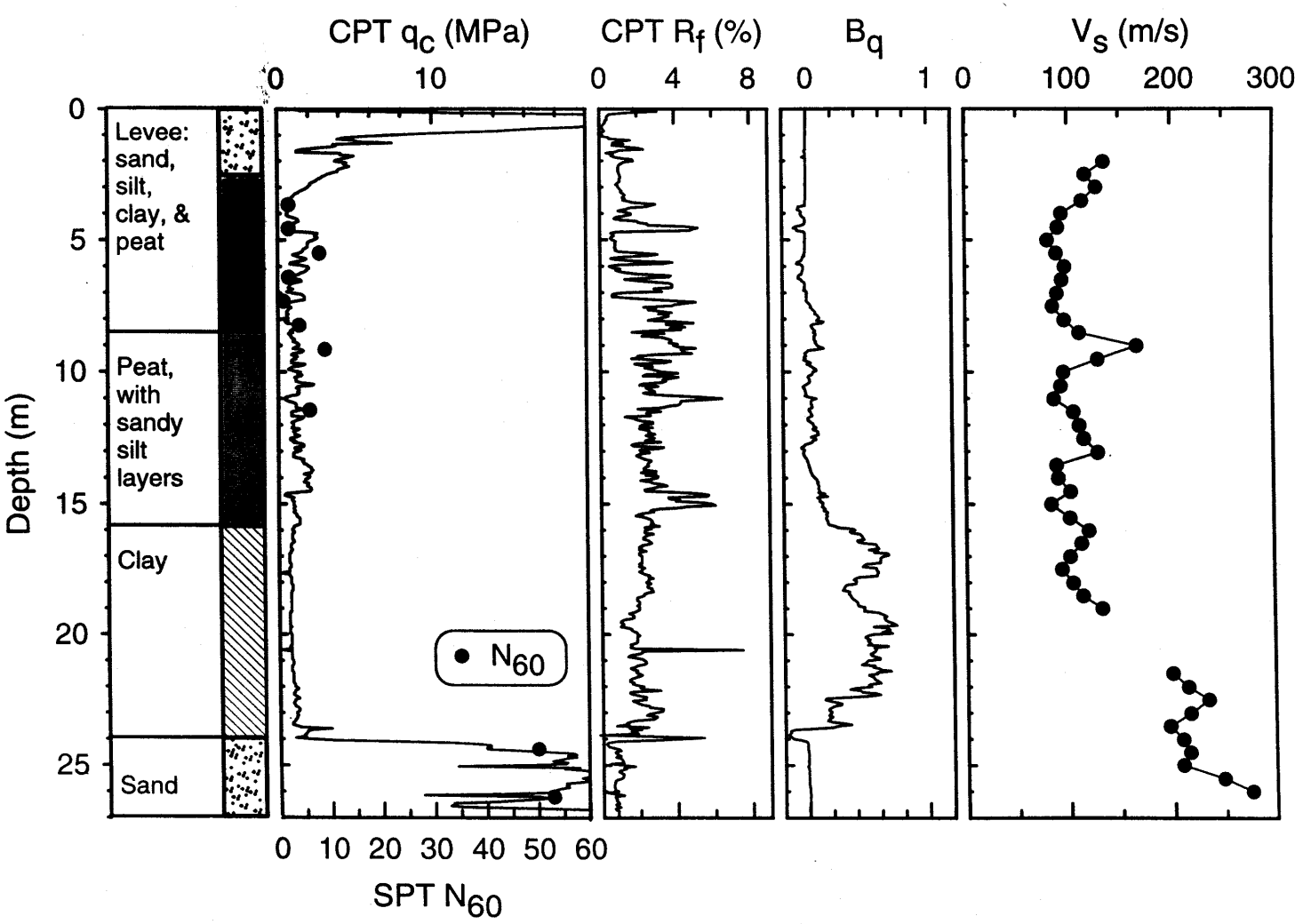

Figure 4: CPT and shear wave velocity data from beneath the levee crest at Sherman Island (Boulanger et al. 1998)

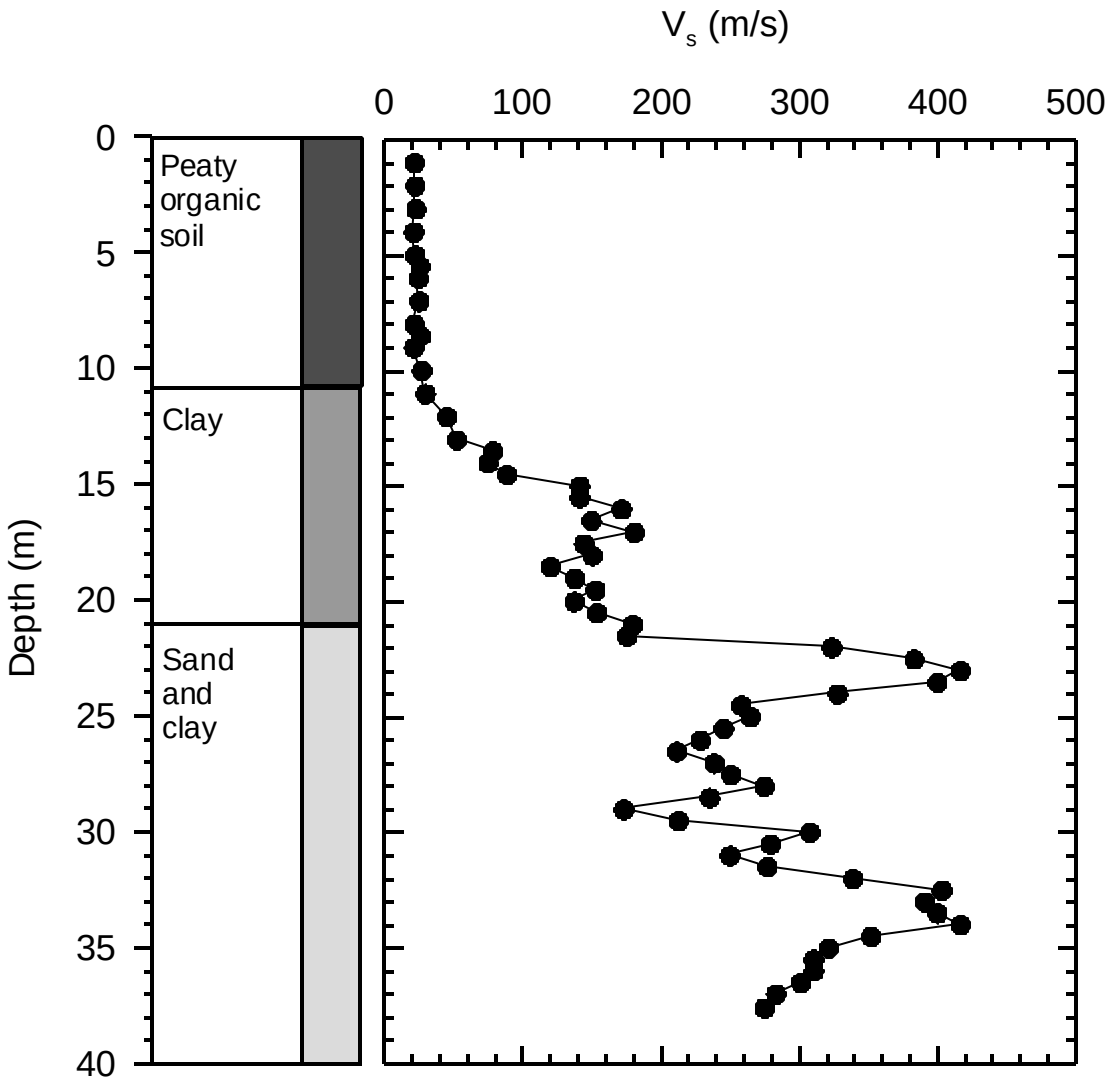

Figure 5: Shear wave velocity data from the free-field at Sherman Island

Sampling Procedures

Continuous Sampling

Continuous sampling was first conducted at all three boring locations (bench, mid-toe, and free-field) to obtain complete downhole cross-sections. Borings were performed using a track mounted drill rig with hollow stem augurs. The water level inside the hollow stem augurs was kept as high as possible during drilling and sampling to prevent boiling of sands and silty sands at the borehole bottom.

Disturbed samples were obtained using a 1.5-m-long, 7.1-cm inner diameter split-spoon sampler driven by the same method used for the Standard Penetration Test (SPT). The split-spoon sampler disturbed the samples but provided a good understanding of the soil stratigraphy, including the limits of the peat layer and the location of concentrations of silt lenses in the peat layer.

Thin-walled tube sampling techniques were also evaluated during these exploratory borings because of the known difficulties with sampling these types of soils. Shelby tubes shortened to lengths of 46 cm with sharpened ends often provided better sample recoveries than standard Shelby tubes. The standard 76-cm-long Shelby tubes often allowed the entire sample to fall out of the tube as it was pulled out of the borehole. All samples from continuous sampling were extruded on site and placed into plastic boxes for storage.

Tube Sampling for Laboratory Tests

High quality tube samples were obtained from three new boreholes at the bench, mid-toe, and free-field. Again, the water level inside the hollow stem augurs was kept as high as possible during drilling and sampling to prevent boiling of sands and silty sands at the borehole bottom. Some of the samples were obtained using the Shelby tubes that were shortened to 46 cm with sharpened cutting edges. Sample tubes were sealed with packers, plastic caps, and duct tape immediately following sample recovery. After labeling, each tube was placed in a heavily padded wood box to be transported to the laboratory. All samples taken for laboratory tests were stored vertically in an environmental chamber with a relative humidity of 98% and temperature of 13 ^{o}C.

Triaxial Testing Equipment

Instrumentation Set-up

The triaxial testing apparatus used for this study was designed for measuring stress-strain behavior for shear strains ranging from 5×10^{-4} % to 10%. The apparatus is very similar to the equipment described by Gookin et al. (1996) with the main difference being a new small-strain load applicator, which is described in the following section. This triaxial testing apparatus uses internal (inside the triaxial chamber) and external (outside the triaxial chamber) measurements of stress and strain over three different strain ranges. Figure 6 shows the general set-up including the frame, volume change device, and various instruments used during testing.

Inside the Plexiglas chamber (Figure 7) two noncontacting proximity transducers and one LVDT were positioned above the top cap of the sample to measure axial displacement. The proximity transducers were capable of measuring displacements that correspond to shear strains from 5×10^{-4} % to 0.01% over a typical triaxial specimen. Using two of these transducers on opposite sides of the top end cap eliminated measuring error due to rocking of the top end cap. The LVDT internal to the chamber was able to measure shear strains from 0.001% to 1%, well above the range of strain that was affected by any minute rocking of the top end cap.

A protected load cell, also inside the chamber, was bolted to the top of the top end cap where it meets the load rod (Figure 7). This internal load cell was able to measure axial deviator stresses from 5×10^{-3} kPa to 18 kPa.

These internal force and displacement transducers are unaffected by frictional resistance and mechanical compliance that occur between the top end cap and any instruments external to the chamber. Internal transducers are widely recognized as essential for accurate measurements at small shear strains.

An external LVDT and load cell were used to measure axial displacements and stresses outside the measuring range of the internal LVDT and load cell. At these levels of strain, mechanical compliance at threaded connections and frictional resistance of the load rod are relatively insignificant.

The entire triaxial frame was supported on rubber bearings seated on the concrete floor. These bearings reduced the level of ambient vibration in the triaxial apparatus which can be important when measuring shear strains of 5×10^{-4} % (i.e., requiring displacement measurement at the micron level). Special attention was also given to reducing other sources of low-level noise in the measurements through careful shielding and separation of cables and band-pass filtering of high frequency electronic noise.

Small-strain Load Applicator

Cyclic shear strains of less than 1×10^{-3} % were difficult to control with the hydraulic actuator despite the low-flow servo valve. At these strain levels, the actuator would cause a jittery loading on the sample, which may be partly related to mechanical compliance between the actuator and the sample.

For this reason, a pressure vessel (Figure 8) was used in place of a hydraulic actuator to apply strain-controlled loading at shear strains of 1×10^{-4} % to 0.02%. The pressure vessel was made from PVC and was designed to elastically elongate as the pressure inside the vessel was varied. The pressure inside the vessel was controlled by a closed-loop servo-valve control system, and could be cycled by amounts ranging from ± 1 kPa to ± 300 kPa.

Conceptually, changing the pressure inside the pressure vessel will cause displacements (strains) in the vessel, triaxial frame, and triaxial specimen that depend on their relative stiffnesses. However, the cyclic elongation of the pressure vessel is imposed on the triaxial specimen as essentially a displacement-controlled loading because the axial stiffness of the pressure vessel and triaxial frame are orders of magnitude greater than the stiffness of a triaxial soil specimen. Generally, the pressure vessel was capable of generating ± 0.02% shear strain on a 15-cm-tall triaxial specimen when subjected to the maximum available air pressure of ± 300 kPa from a starting pressure of 300 kPa.

Piezoceramic Bender Elements

The two aluminum end caps for the triaxial specimen were each equipped with a piezoceramic bender element (Figure 9) capable of generating or measuring shear waves transmitted through the sample. Charged with pulses of ± 10 volts from a function generator, the lower bender element would bend, causing a shear wave to travel up through the sample. When the shear wave reached the upper bender element, the shear wave would induce bending in the upper bender element and cause a voltage to be generated. A digital oscilloscope (Fluke PM3384A) measured the voltage-time histories of the transmitting and receiving bender elements.

Travel time (Dt) for the shear wave was determined as the time difference between the first characteristic peaks in the transmitted and received signals. The strongest signals were obtained for frequencies (f) that produced wavelengths ($l = V_s / f$) that were 8 to 15 times the bender element length (L_b). Within this frequency range, travel times were found to be insensitive to the transmitting pulse frequency. The travel distance of the shear wave was taken as the distance between the bender element tips (L_{tt}), and thus the shear wave velocity (V_s) calculated as:

$$V_s = \frac{L_{tt}}{?t} \tag{1}$$

Successful V_s measurements are shown in Appendix A. Additional details on the equipment, procedures, and potential errors in these measurements are given by Arulnathan et al. (1998). Note that the G_{max} obtained as $G_{max} = \rho V_s^2$ is not directly comparable to the G_{max} obtained from the stress-strain measurements because of sample anisotropy and other influencing factors (Boulanger et al. 1998).

Calibration of Small Strain Instruments

The calibration of the triaxial device for small-strain measurements (i.e., particularly the internal displacement transducers and load cell) was verified using an aluminum sample (Figure 10) instrumented with 8 strain gages. This dummy sample was a thin-walled (0.889 mm), 50.8-mm-diameter tube made of alloy 3003 aluminum tubing. The strains measured by the full-bridge strain gages matched well with the strains measured by the proximity transducers. At axial strains of about 1×10^{-4} % to 3×10^{-4} %, the measured Young's modulus for the aluminum was within 3% of the listed Young's modulus (68.9 GPa) for all cycles in a loading sequence.

The damping ratio of a soil sample (χ_s) was calculated from the deviator stress and axial strain measurements taken during cyclic triaxial testing by the expression:

$$\chi_s = \frac{\Delta W_s}{4\pi W_{s,s}} \tag{2}$$

where DW_s = work dissipated in the soil specimen, and $W_{s,s}$ = the maximum elastic energy stored in the soil specimen during the loading cycle. However, the measured hysteretic work (DW_m) includes not only the work dissipated in the soil specimen (DW_s), but also an additional amount of work dissipated in components of the triaxial device (DW_d). Therefore,

$$\Delta W_s = \Delta W_m - \Delta W_d \tag{3}$$

The work dissipated by the triaxial device (DW_d) was evaluated using the cyclic loading results for the aluminum sample. One significant source of DW_d was found to be the internal (gaging) LVDT. Other sources of DW_d are believed to come from friction against cable movements and from hysteresis in the load cell. The DW_d measured from the dummy sample was conceptualized as:

$$\Delta W_d = \beta_1 \Delta_{PP} \left(\frac{1}{A_0 L_0} \right) + \beta_2 F_{PP} \left(\frac{1}{A_0 L_0} \right) \tag{4}$$

where β_1 represents apparent work losses that are proportional to displacement of the top cap (e.g. friction on cables) and β_2 represents apparent work losses that are proportional to axial deviator load on the sample (e.g. hysteresis in the load cell). Also, D_{PP} and F_{PP} are peak-to-peak axial displacement and peak-to-peak deviator force, respectively. The

above expression is divided by the sample's cross-sectional area A_0 and length L_0 to obtain the work per sample volume. b_1 and b_2 were calibrated against measurements of DW_d, D_{PP}, and F_{PP} on the aluminum dummy sample. The resulting values were $b_1 = 10.1 \times 10^{-3}$ N and $b_2 = 8 \times 10^{-11}$ m. Then the results of tests on soil samples were adjusted by subtracting the work dissipated in the testing device (calculated using Equation 4) from the work measured during the test (Equation 3).

The effect that the above correction has on equivalent damping ratios depends on the sample dimensions, stiffness, and strain level. For a typical peat specimen (diameter = 73 mm, length = 160 mm) with a shear modulus of 5 MPa, the correction corresponds to 1.02% damping at 10^{-3} % shear strain, 0.10% damping at 10^{-2} % shear strain, and 0.01% damping at 10^{-1} % shear strain. Thus the correction is most important in the small strain range, and is progressively less important as the level of strain increases.

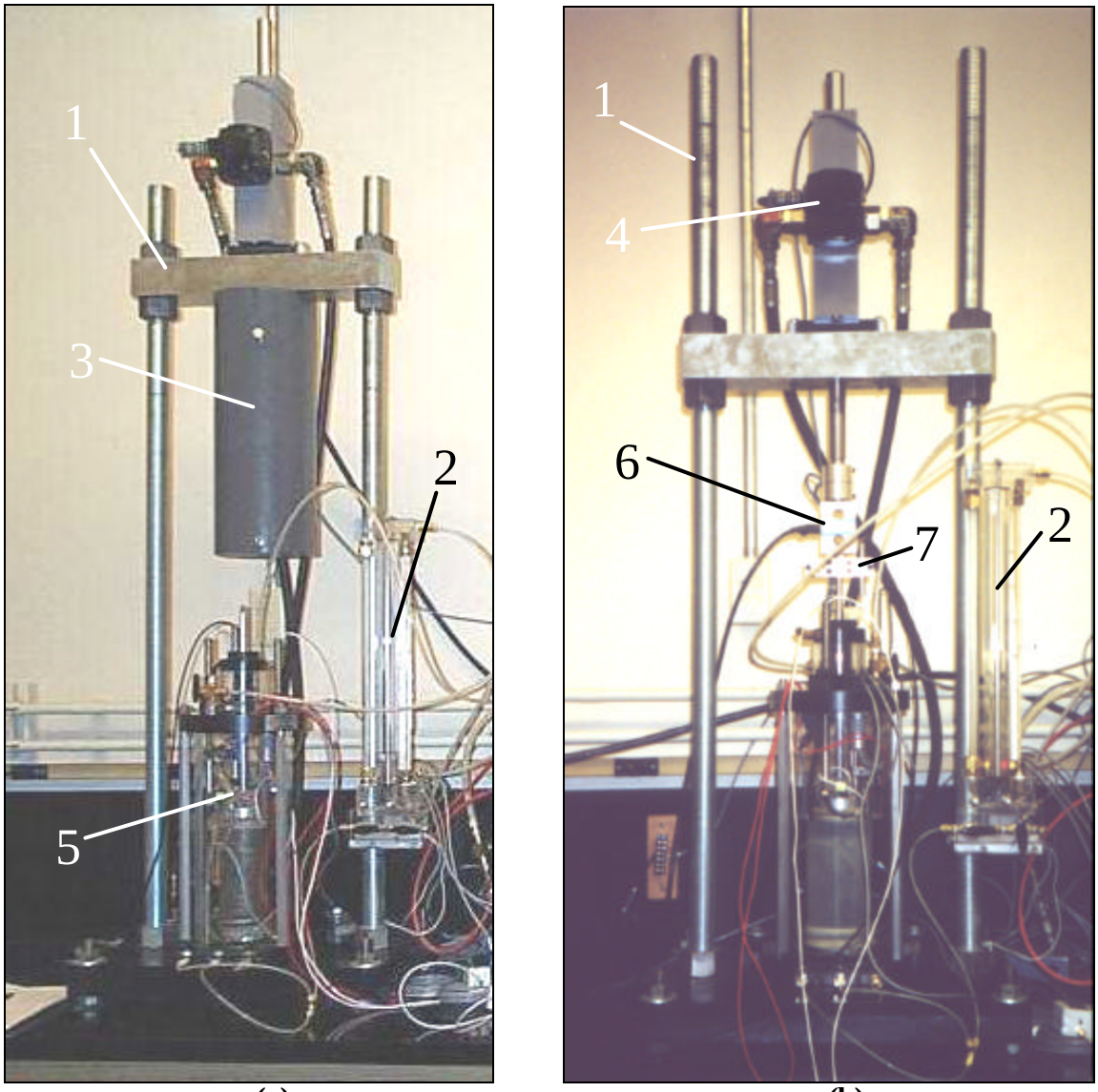

(a) **(b)**

1. Steel frame
2. Volume change device
3. Pressure vessel
4. Hydraulic actuator
5. Instruments inside the triaxial chamber (internal transducers)
6. External load cell
7. External LVDT

Figure 6: General set-up of load cells, displacement transducers, and other instruments used during cyclic triaxial testing for both (a) small strain loading and (b) large strain loading

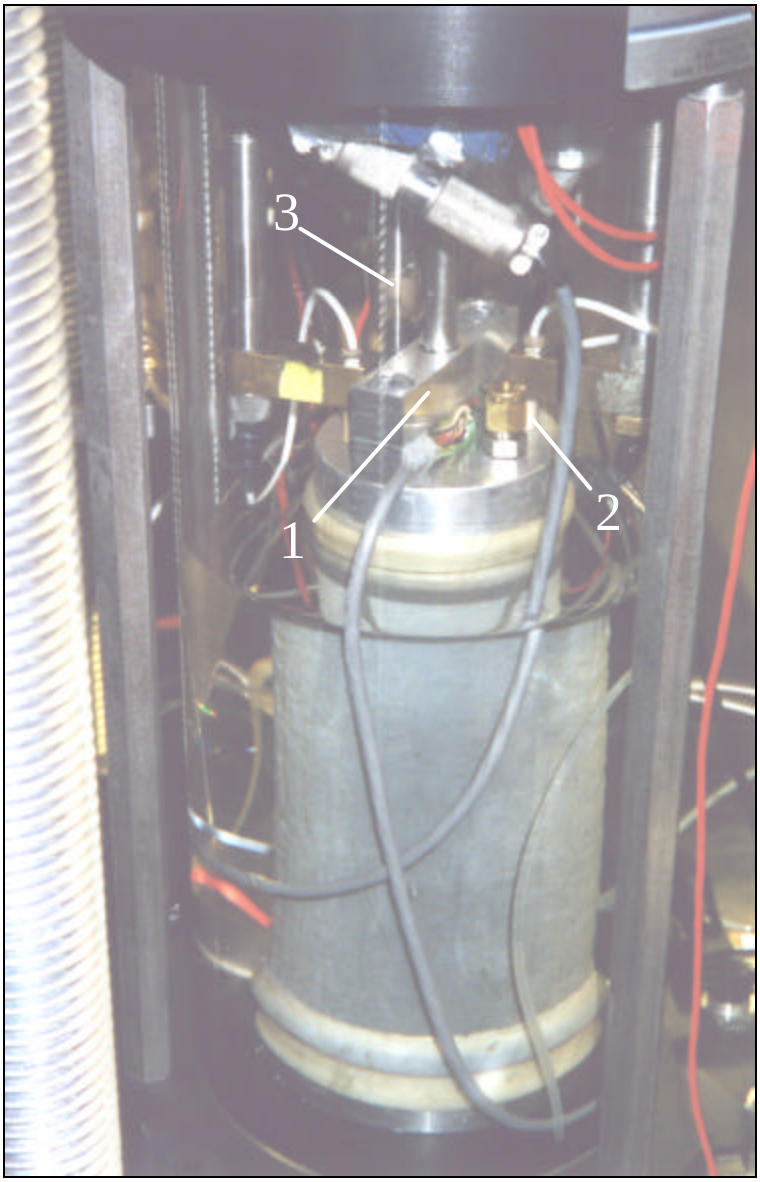

1. Protected load cell
2. Proximity transducer (one on either side of top cap)
3. Internal LVDT

Figure 7: Instruments internal to the triaxial chamber used to measure deviator load and displacement at small strains

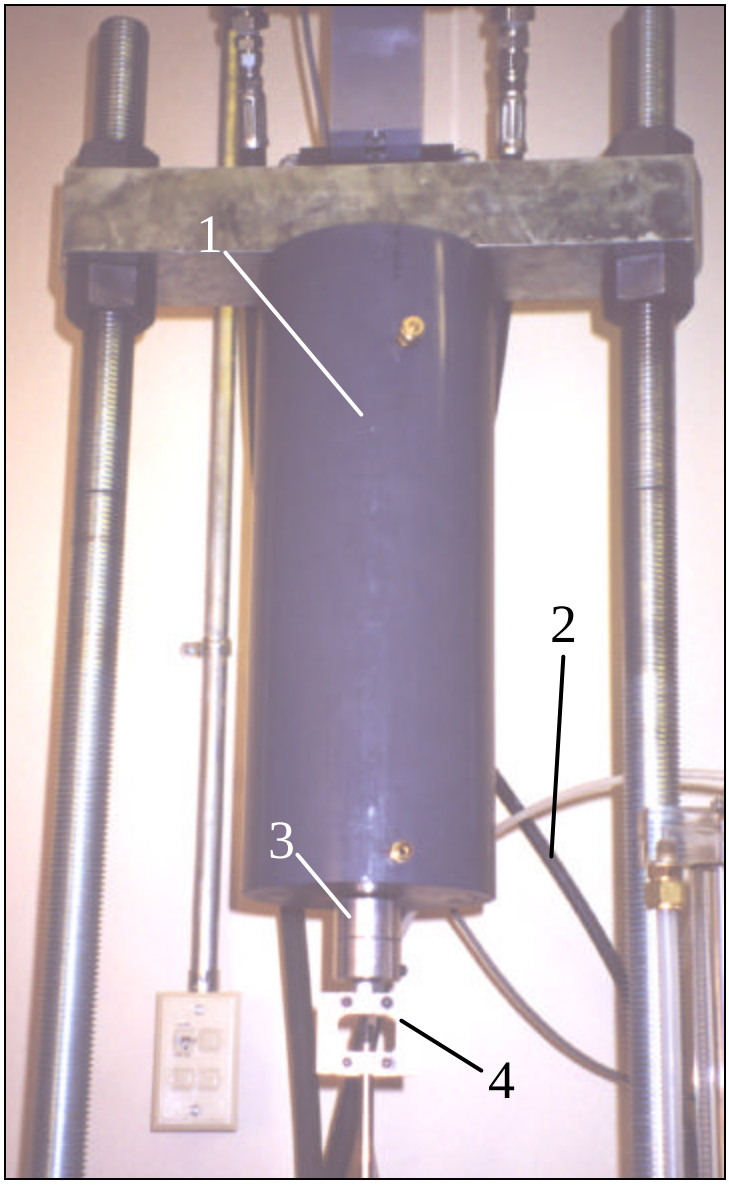

1. Pressure vessel
2. Tubing that applies cyclic pressure to pressure vessel
3. Universal joint
4. Connection between pressure vessel and load rod

Figure 8: Pressure vessel used to apply strain-controlled loading during cyclic triaxial tests

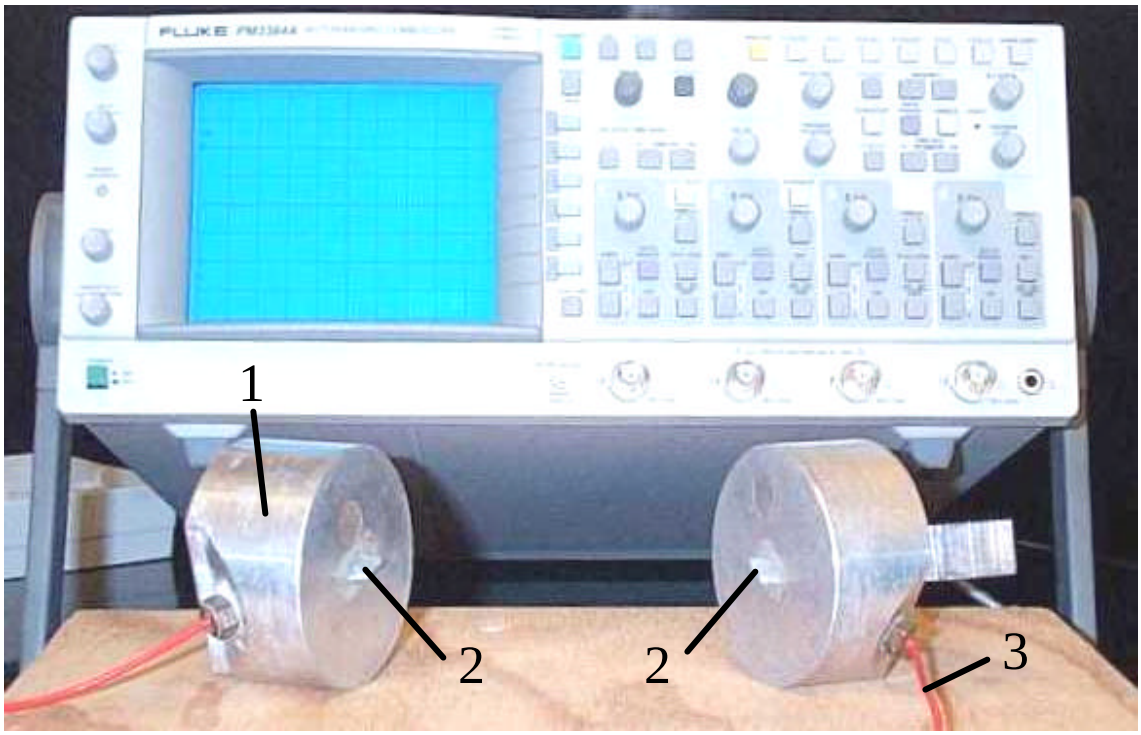

1. Bottom end cap (diameter of 71.12 mm)
2. Bender elements (one on each end cap)
3. Bender element cable

Figure 9: Top and bottom end caps showing location of piezoceramic bender elements

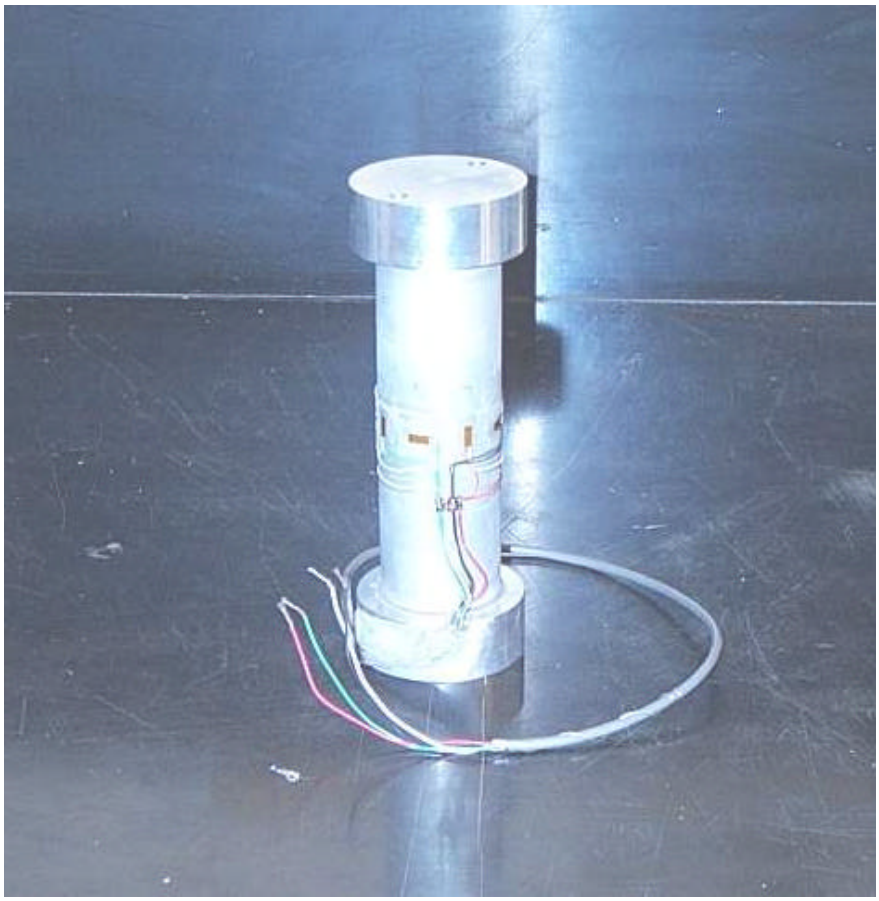

Figure 10: Aluminum dummy sample used to measure the shear modulus of alloy 3003 aluminum at small strains

Triaxial Testing Procedures

Sample Preparation

Samples were stored in an environmental chamber (Figure 11) that kept the relative humidity at 98% and temperature at 13 ^{o}C. The first sample was tested about 4 weeks after drilling and the twelfth sample was tested about 11 weeks after drilling. The thirteenth sample was tested about 27 weeks after drilling.

Disturbance during the extrusion of the peat samples from the Shelby tubes was minimized by carefully cutting the Shelby tube down to a 200-mm-long section prior to extruding the sample. The Shelby tube was slid into a very stiff steel ring that was then clamped in a vice (Figure 12). This stiffener ring prevented the strong clamping force of the vice from deforming the Shelby tube. A pipe cutter was then used to score a hairline groove around the perimeter of the tube. Using this scored groove as a guide, the Shelby tube was then cut with a Dremel® high-speed rotary cutting tool (Figure 13). This cutting tool produced very little vibration and heat, which helped limit sample disturbance.

The 200-mm portion of the Shelby tube sample was extruded using a hydraulic piston (Figure 14). First, the top 20 mm of the sample was extruded, trimmed off with a razor blade, and weighed for a water content determination. At this time the razor blade was used to cut an 8-mm-long slot on the top of the sample that the bender element would later fit into. The rest of the sample was then extruded and, similarly, the bottom 20 mm was trimmed off and its water content determined.

The sample was then mounted between the aluminum end caps, and enclosed in a rubber membrane sealed by o-rings against the caps. A small vacuum was applied to the sample while it was being positioned in the triaxial chamber. Once the instruments were positioned, the chamber was filled with de-aired water up to the top of the sample. Having instruments inside the chamber precluded filling it completely with de-aired water.

Isotropic Consolidation

All peat samples were initially consolidated isotropically to their estimated in situ stresses, including their in situ total stress, pore pressure, and effective stress. These consolidation stresses had to be incrementally applied slow enough for pore pressures to equilibrate throughout the sample and hence avoid temporarily (and unknowingly) exceeding the in situ effective stress.

Volumetric strain measurements were recorded to track the sample's consolidation during and after application of the in situ stresses. Generally, samples were consolidated for ten to twelve hours after the last increment of chamber pressure was applied, ensuring the end of primary consolidation. The chamber water had to be drained every twelve hours and replenished with de-aired water to avoid diffusion of dissolved air from the chamber water through the membrane into the sample.

Bender Element Tests

The shear wave velocity of the sample was measured by means of a bender element test prior to cyclic loading, and sometimes later during testing. The shear wave velocity (V_s) and the density (r) of each sample was used to calculate the small-strain shear modulus (G_{max}) of the sample.

$$G_{max} = r\ V_s^2 \tag{5}$$

This value of G_{max} was then compared to the secant shear modulus measured during small-strain cyclic loading of the sample. However, not all samples provided measurable shear wave velocities, either due to the extreme softness of the samples or due to poor contact between the bender elements and the peat.

Staged Cyclic Loading

Each peat sample was subjected to a sequence of cyclic loading stages designed to evaluate certain aspects of cyclic behavior. Each stage typically consisted of 5 uniform cycles of undrained, strain-controlled loading at a frequency of 1 Hz (unless otherwise noted). The first stage was usually performed at about 5×10^{-4} % shear strain. The next stage of 5 cycles would occur at a shear strain level about one-half of a log cycle greater than the previous stage (i.e., about 3 times greater). It is believed that such a large jump in level of shear strain will diminish any effects of the prior 5 cycles of loading. The final stage of cyclic loading would be at about 10% shear strain. Then the specimen would be weighed and dissected for the purpose of determining the sample's density, water content, ash content, and visual/manual classification. At this time any unusual observations would be noted, such as heterogeneity and concentrated shear zones.

A complete set of experimental results is shown for one representative sample in Appendix B. For every stage of cyclic loading, plots are presented for: (1) stress, strain, and pore pressure ratio (r_u) versus time, and (2) stress versus strain for each loading cycle. Note that $r_u = Du/s'_{3c}$ where Du is the change in pore pressure during undrained cyclic loading. Measurements of Du during 1 Hz loading on low permeability samples are generally unreliable, but the data illustrate that very little Du was observed even for large shear strains.

The following section describes the test results, including descriptions of any variations in the cyclic loading protocol. Detailed data from every test is summarized in Appendix A, including sample characteristics, test conditions, modulus and damping values for every load cycle, and plots of modulus reduction and damping versus strain.

Figure 11: Environmental chamber with humidity and temperature controls

Figure 12: Shelby tube with stiffener ring to prevent tube distortion

Figure 13: Cutting Shelby tube with low-vibration, high-speed rotary cutting tool

Figure 14: Extruding sample to be tested

Test Results

Results for Samples from Different Boring Locations

Nine samples were tested after being consolidated to their in situ stresses, including two samples from beneath the bench, three samples from beneath the mid-toe, and four samples from beneath the free-field (Table 1, Figure 1). Typical results for one sample from each of these three locations are used to illustrate the general differences in behavior.

First, a typical set of stress-strain curves are shown in Figure 15 for sample 9 from beneath the levee mid-toe. These stress-strain curves show almost linear behavior for shear strains up to about 0.1% (0.06% axial strain) and very little degradation of shear modulus with increasing number of loading cycles. Figure 16 shows the stress-strain curves for three shear strain levels (0.88%, 2.9%, and 8.2%) on the same plot to illustrate the change in stiffness and hysteretic behavior with increasing strain. For purely hysteretic damping, one would expect to see corners at either end in the stress-strain curve upon load reversal. The rounded peaks in Figure 16, particularly in the first cycle of load, are suggestive of a significant viscous component of damping. It is possible that some of the rounding could be attributed to the digital filtering of the data. It was confirmed, however, that the filtering had negligible effect on G and x.

Plots of secant shear modulus (G) and equivalent damping ratio (x) versus shear strain (single amplitude) are shown in Figure 17 for samples 12, 8, and 4 from the bench, mid-toe, and free-field, respectively. The sample from beneath the levee bench has higher shear moduli than the sample from beneath the mid-toe, which in turn has higher shear moduli than the sample from the free-field. The samples from beneath the levee bench and mid-toe have shear moduli that are relatively linear up to shear strains of about 0.1%, whereas the free-field sample's shear modulus reduces continuously with increasing shear strain beginning at shear strains as small as 0.001%. Despite the differences in stiffness, damping ratios from the bench and mid-toe locations are very similar, while samples from the free-field generally had slightly higher damping ratios at all strain levels.

Figure 18 summarizes the modulus reduction (G/G_{max}) and damping relations for all peat samples that were consolidated to their estimated in situ vertical effective stresses from the three sampling locations. Most notably, the samples from the free-field, within their very low in situ confining stresses, show the highest degree of non-linearity in shear modulus. As a result, the damping values for the free-field samples were consistently higher than damping values from the other locations that have more confinement.

Surprisingly, samples from the levee bench show greater reductions in secant shear modulus than the mid-toe samples beyond a shear strain of 0.1%. Close inspection of sample 3 from beneath the bench showed it contained inclined bedding planes (~20^o from horizontal) that were substantially weaker (i.e., more easily separated) than almost all other samples. Consequently, this aspect of modulus reduction behavior may represent

the effects of sample bedding plane characteristics rather than an effect of differences in consolidation stress.

Loading Frequency

The effects of loading frequency and cyclic degradation are illustrated in Figure 19 through Figure 24 for two samples from beneath the mid-toe and one sample from the free-field. For these samples, select stages of cyclic loading consisted of 30 uniform strain-controlled cycles arranged as alternating sets of five cycles at 1.0 Hz and 0.01 Hz.

Figure 19 through Figure 21 show the effects that loading frequency and cyclic degradation have on the secant shear modulus. Generally, the secant shear modulus increases by about 15% to 22% with an increase in loading frequency from 0.01 Hz to 1.0 Hz for samples from either location.

The data in these three figures also show that cyclic degradation of the secant shear modulus was very minor even at higher shear strains. The effect of cyclic degradation can be expressed by the degradation index (d), which is the ratio of the secant modulus in cycle N (G_N) to the secant modulus in the first cycle (G_1). The value of d decreases with increasing cycles, and can be approximately represented as (Idriss et al. 1978)

$$d = N^{-t} \tag{6}$$

where t is the degradation parameter. Figure 19 through Figure 21 show that the value of t was only 0.024 or less for shear strains at almost 1%. Similarly, Boulanger et al. (1998) tested peat samples from beneath the levee crest and determined that the value of t was only about 0.017 at cyclic shear strains of 1%.

Figure 22 through Figure 24 show the effect of loading frequency and loading cycles on the equivalent damping ratio. The results show no consistent trend, with the higher frequency sometimes resulting in slightly greater or slightly smaller damping ratios. For strains of about 0.01% to 1%, the greatest difference was about 1.5% (e.g., x of 9.5% vs. 8%).

Effect of Consolidation Stress

Additional information on the effect of consolidation stress on cyclic behavior was obtained through tests on four samples (two from the mid-toe and two from the free-field) that were consolidated in the laboratory to effective stresses (s'_{3c}) that were twice their in situ vertical effective stresses (s'_{vc}). The effect of doubling the consolidation stress on the free-field samples is shown in Figure 25, with results shown for two samples consolidated to their in situ stresses of about 13 kPa to 14 kPa and for two samples consolidated to 22 kPa (twice their in situ values). The higher consolidation stress caused the free-field peat samples to behave more linearly, as expressed through higher G/G_{max} curves and lower damping ratios. With a higher confining stress, these originally very soft samples behave more like samples taken from beneath the levee mid-toe, which had greater in situ vertical effective stresses.

Similarly, the effect of doubling the consolidation stress for the mid-toe samples, from about 45 kPa to 46 kPa (3 samples) to 86 kPa (2 samples) is shown in Figure 26. For these samples, doubling the consolidation stress had only a very slight effect on modulus reduction (slightly more linear) and damping relations (mixed effect). These results suggest that there is some threshold in situ consolidation stress, above which the modulus reduction (G/G_{max}) and damping (x) properties of the peat are relatively independent of consolidation stress. At the same time, doubling the consolidation stress did result in an increase in the secant stiffness (G) of the samples. This is shown by the stress-strain loops for sample 13 (consolidated to in situ stresses) and sample 9 (consolidated to twice the in situ stresses) in Figure 27.

For peaty soils with in situ confinements less than this threshold effective stress, the effect of the consolidation stress on G/G_{max} may be attributed to the evolution of fiber-to-fiber interactions (e.g., fabric) within the soil. When first deposited (with $s'_{vc} \cong 1$ kPa), the fibers may have very few direct interactions and hence are easily dislodged or shifted under an applied shear stress. The resulting permanent or plastic deformations are manifested as highly nonlinear shear resistance. As s'_{vc} increases, fibers may be pressed closer together, developing interactions with numerous other fibers. Shear resistance at smaller shear strains (say ≤ 1%) may then be dominated by elastic deformations and stretching of the fibers, with relatively less permanent slippage between fibers, resulting in a more linear macro behavior. Nonlinear behavior at higher shear strains would then develop as the fibers slip and break under the greater shear stresses. For $s'_{vc} > 40$ kPa, it appears that the fiber matrix has reached a condition where further increases in s'_{vc} do not significantly change the relative micro mechanisms of nonlinearity and hence the macro G/G_{max} and x relations are relatively unaffected.

A related issue is how isotropic consolidation in the lab versus anisotropic consolidation in situ may affect the micro mechanisms of nonlinearity in these fibrous soils and hence the macro G/G_{max} and x relations. Unfortunately, the current configuration of the triaxial device limits its use to isotropic consolidation because of the small range of deviator stresses that the internal load cell can measure. The issues of stress anisotropy and material anisotropy for these types of soils warrant further study.

Prior Overstraining

The effect of prior undrained “overstraining” was investigated for three samples, one from each of the bench, mid-toe, and free-field locations. Overstraining is used to refer to the case where a sample was cyclically loaded to some level of virgin strain and then cyclically loaded at some smaller level of strain.

Levee Bench

Sample 3 from beneath the levee bench was first loaded cyclically in stages from 0.001% to 0.4% shear strain (Figure 28). For 5 cycles of loading at 0.4% shear strain the shear modulus had reduced to $G/G_{max} = 0.57$. The sample was then loaded cyclically at about 0.06% shear strain and the shear modulus recovered to be almost equal to the value for

virgin loading at 0.06% shear strain (G/G_{max} = 0.95). The full recovery of shear modulus was accompanied by almost no change in damping.

For 5 cycles of loading at about 9% shear strain, the shear modulus had reduced to G/G_{max} = 0.09. This sample was then cyclically loaded again at a shear strain of about 0.06%. This time the shear modulus substantially recovered to a G/G_{max} = 0.66, but its stiffness still was significantly less than its virgin shear modulus at this shear strain (i.e., G/G_{max} = 0.95). Also, notice that the reduction in stiffness due to prior overstraining increased the damping ratios slightly.

Mid-toe of Levee

The effect of prior overstraining for a sample from beneath the mid-toe of the levee is shown in Figure 29. This sample was first loaded in stages from 0.001% to 0.02% shear strain. The sample was then loaded cyclically at about 0.001% shear strain. The shear modulus was essentially equal to the value for virgin loading at this strain level. This was expected because the sample was still almost linear elastic at 0.02% shear strain.

The partial recovery of shear modulus after prior overstraining to shear strains of about 1% and 9%, as shown in Figure 29, are quantitatively similar to that shown for sample 3 from beneath the bench (Figure 28). Again, prior overstraining to 9% shear strain caused small increases in damping ratios during subsequent loading at smaller strain levels.

Free-field

The effect of prior overstraining for a sample from beneath the free-field is shown in Figure 30. Overstraining to 1% shear strain had very little effect on shear modulus or damping ratios during subsequent loading at 0.1% shear strain despite the strong nonlinearity of free-field samples in this strain range. Overstraining to 9% shear strain had similar effects as previously described for mid-toe and bench samples.

Effect of Prior Overstraining with Reconsolidation

The effect of reconsolidation following prior undrained overstraining was evaluated for three samples, one from each of the bench, mid-toe, and free-field locations. These specimens were cyclically loaded in stages from 10^{-3} % to 10% shear strain and then allowed to reconsolidate to their original (in situ) effective stresses. The duration of reconsolidation was long enough (6 hr or more) to allow excess pore pressures that developed during testing to dissipate. Then each specimen was again cyclically loaded undrained with the same stages of cyclic strain up to 10% shear strain.

The shear modulus, modulus reduction ratio, and damping relations for sample 12 from beneath the levee bench are shown in Figure 31. After reconsolidation the sample showed a reduction in secant shear modulus of about 20% over the entire range of cyclic shear strains. This nearly uniform reduction in shear modulus after reconsolidation produces very similar normalized secant shear modulus (G/G_{max}) curves, provided the “virgin” and “after reconsolidation” portions of the test are normalized by their own respective low-

strain maximum shear modulus values. Not surprisingly, the two damping curves are also very similar over the entire range of shear strains.

The shear modulus, modulus reduction, and damping relations for sample 13 from beneath the levee mid-toe are shown in Figure 32. The effect of reconsolidation on these relations are very similar to what was described for sample 12, given the same method of normalizing the "virgin" and "after reconsolidation" shear modulus values. While the secant shear modulus was reduced by about 10% over its entire range of strain, G/G_{max} and x for each strain level were essentially unchanged after reconsolidation.

For sample 14 from the free-field, the effects of reconsolidation following prior undrained overstraining are again very similar to those described for samples 12 and 13 from the levee bench and mid-toe, respectively. Figure 33 shows that the secant shear modulus, modulus reduction, and damping relations for this free-field sample.

Summary of Modulus Reduction and Damping Data

A summary of modulus reduction (G/G_{max}) and damping (x) data for all Sherman Island samples tested at in situ vertical effective consolidation stresses was obtained for two sets of conditions: one set with $s'_{vc} \cong 12$ kPa and a second set with $s'_{vc} \geq 40$ kPa. The median and $\pm$ 1 standard deviation G/G_{max} and x relations are shown in Figure 34. The standard deviation in G/G_{max} or x varies with strain level, and was determined by sorting the data into bins that spanned 1 log-cycle of shear strain each. A smooth function for standard deviation versus shear strain was then fit to the values of standard deviation determined in each bin.

Effect of Creep on Shear Modulus and Damping

The effect of creep on the measured shear modulus and damping values was investigated for a sample from each location: the bench (sample 12), mid-toe (sample 13), and free-field (sample 10). These three samples were intermittently cyclically loaded undrained at a shear strain of about 0.002% over a period of 4.5 hr. At this strain level, the samples underwent a total of 20 cycles of loading in which four sets of 5 cycles were performed at 0, 0.5, 1.5, and 4.5 hr. During this time the drain lines remained closed and creep caused pore pressures to increase, reducing the effective stress in the samples by as much as 25% to 40%. The shear moduli measured during these tests are given in the summary sheets for cyclic triaxial tests in Appendix A. The shear modulus values for these samples remained within 3% of the maximum shear modulus, and damping values were essentially unaffected (within scatter), despite the influence of undrained creep over a 4.5-hr period.

Maximum Shear Modulus versus Consolidation Stress

Maximum shear modulus (G_{max}) values from all tested peat samples, including those from beneath the levee crest (Boulanger et al. 1998), are plotted versus consolidation stress (s'_{3c}) in Figure 35. First, results are shown in Figure 35(a) for samples that had

laboratory consolidation effective stresses equal to their in situ vertical effective stresses. The relation between G_{max} and s'_{3c} was assumed to have the following form:

$$\frac{G_{\max}}{P_a} = C_o \left(\frac{s'_{3c}}{P_a} \right)^n \tag{7}$$

where P_a is atmospheric pressure (101.3 kPa). The constant C_o and exponent n were obtained by regression against the data shown in Figure 35(a), excluding sample 7 which had considerably less organic material (ash content 79%) than the other samples. The resulting values were C_o = 72.3 and n = 0.96.

Arulnathan (2000) and Arulnathan et al. (2001) presented measurements of shear wave velocity versus consolidation stress for reconstituted, normally consolidated, peat specimens, as shown in Figure 36. When the variation in density (r) with s'_{vc} (in Arulnathan 2000) is taken into account, then their data produce C_o = 73.7 and n = 0.87 by Equation 7. Thus, there is good agreement between the values of C_o and n determined for high quality tube samples (Figure 35) and reconstituted, normally consolidated peat specimens. Note that the reconstituted peat used by Arulnathan was obtained from beneath the levee crest at Sherman Island.

Figure 35(b) shows the same data from part (a) plus the maximum shear moduli of peat samples tested at consolidation stresses other than their in situ effective stresses. Two samples from beneath the levee crest, two from the levee mid-toe, and two from the free-field were consolidated to 1.5, 2.0, and 2.0 times their in situ consolidation stresses, respectively. Two more samples from beneath the levee crest were consolidated to their in situ stresses and then rebounded to half that stress. Testing these peat samples at consolidation stresses below, or above, their in situ stresses had relatively little effect (on average) on their maximum shear moduli. This observation was surprising because the peat layer should be normally consolidated in situ based on its geologic history and the in situ G_{max} was just shown to be strongly affected by s'_{3c} (Figure 35(a)). Therefore, doubling s'_{3c} in the lab would presumably cause a consistent and significant increase in G_{max}. A reasonable explanation for G_{max} not being sensitive to the laboratory s'_{3c} is that the peat developed a "quasi-preconsolidation pressure" due to substantial secondary compression (creep) over its geologic life, as described later in this section.

The effect of OCR on G_{max} can be incorporated using the form:

$$\frac{G_{\max}}{P_a} = C_1 OCR^m \left(\frac{s'_{3c}}{P_a} \right)^n \tag{8}$$

where $C_1 OCR^m$ replaces the constant C_o. Arulnathan (2000) determined that the exponent m was 0.58 for reconstituted peat specimens with specimen ages of less than one week and mechanically-imposed overconsolidation. The determination of appropriate C_1 and m values for the field samples under in situ conditions is complicated by the difficulty in

determining the equivalent pre-consolidation pressure (and hence *OCR*). However, it can be shown that the slope of the $log(G_{max} / P_a)$ versus $log(\sigma'_{3c} / P_a)$ plot for overconsolidated samples with the same σ'_{vp} would be equal to $n - m$. The linear slopes (s) between the G_{max} versus σ'_{3c} data for each sampling location, as shown in Figure 37, are 0.31, 0.21, and 0.03, with the slope becoming smaller with increasing σ'_{3c}. If the samples from each location remained overconsolidated in the laboratory tests, then the values of m might be estimated as

$$m = n - s \tag{9}$$

With n = 0.96, the above assumption and equation results in m values of 0.65, 0.75, and 0.93 for the free-field, mid-toe, and crest locations, respectively. However, if any of the samples became normally consolidated under the larger consolidation stresses used in the laboratory, then the exponent m would be underestimated by the above approximation. The value of m, as determined by the above approximation, appears to increase with increasing effective consolidation stress. These aspects of behavior will be explored further in subsequent studies.

Figure 38 shows a schematic illustration of how long-term secondary compression may produce a quasi-preconsolidation pressure that may reasonably contribute to the insensitivity of G_{max} to changes in σ'_{3c} in the laboratory. As shown in this figure, the relation between void ratio (e), consolidation stress (σ'_{vc}), and time can conceptually be defined by the end-of-primary $e\text{-}log(\sigma'_{vc})$ curve, the recompression index C_r, and the coefficient of secondary compression C_a [e.g., see Leonards and Altschaeffl (1964) and Mesri and Castro (1987) regarding quasi-preconsolidation in clays]. Now consider the following idealized example. Suppose a peaty soil layer forms and reaches the end of primary consolidation (t_p) in about 1 day, and then the soil undergoes secondary compression under a constant in situ vertical effective stress for hundreds of years. Assume our peaty organic soil has C_c = 2.1 [which is the value Arulnathan (2000) obtained for his reconstituted peat samples], a recompression index C_r = 0.2 C_c, and a coefficient of secondary compression C_a = 0.05 C_c [reasonable for highly organic plastic soils (Mesri and Castro 1987)]. The theoretical progression of secondary compression from t_p = 1 day through 1 year to 400 years is shown in Figure 38. Then, if a sample of this aged peaty soil was loaded in the laboratory, within a timeframe of about 1 day, to a stress greater than σ'_{vo}, the peat would move to the normal consolidation line corresponding to an age of about 1 day. The sample would appear as if it was overconsolidated, with the preconsolidation stress σ'_{vp} corresponding to the break in the $e\text{-}log(\sigma'_{v})$ plot. Notice that σ'_{vp} is on the order of about 1.5 to 2.2 times the value of σ'_{vo} for ages between 1 and 400 years in this problem. Thus, secondary compression can, in certain conditions, feasibly cause an apparent *OCR* of about 2 in the laboratory. Now recall that Equation 8 shows that G_{max} is a function of both *OCR* and σ'_{3c}. If the value of $n - m$ is close to zero, as shown in Figure 37 for samples from the levee crest, and if the laboratory consolidation stresses do not exceed the quasi-preconsolidation stress, then G_{max} becomes a function primarily of σ'_{vp} and independent of σ'_{3c}. The above, idealized example is only meant to qualitatively illustrate the potential importance of secondary compression. Quantitative estimates of the actual effects of secondary compression are

complicated by the unknown influence of decomposition, time varying soil properties (e.g., C_a), cementation, pore fluid composition, geologic loading history, and other factors.

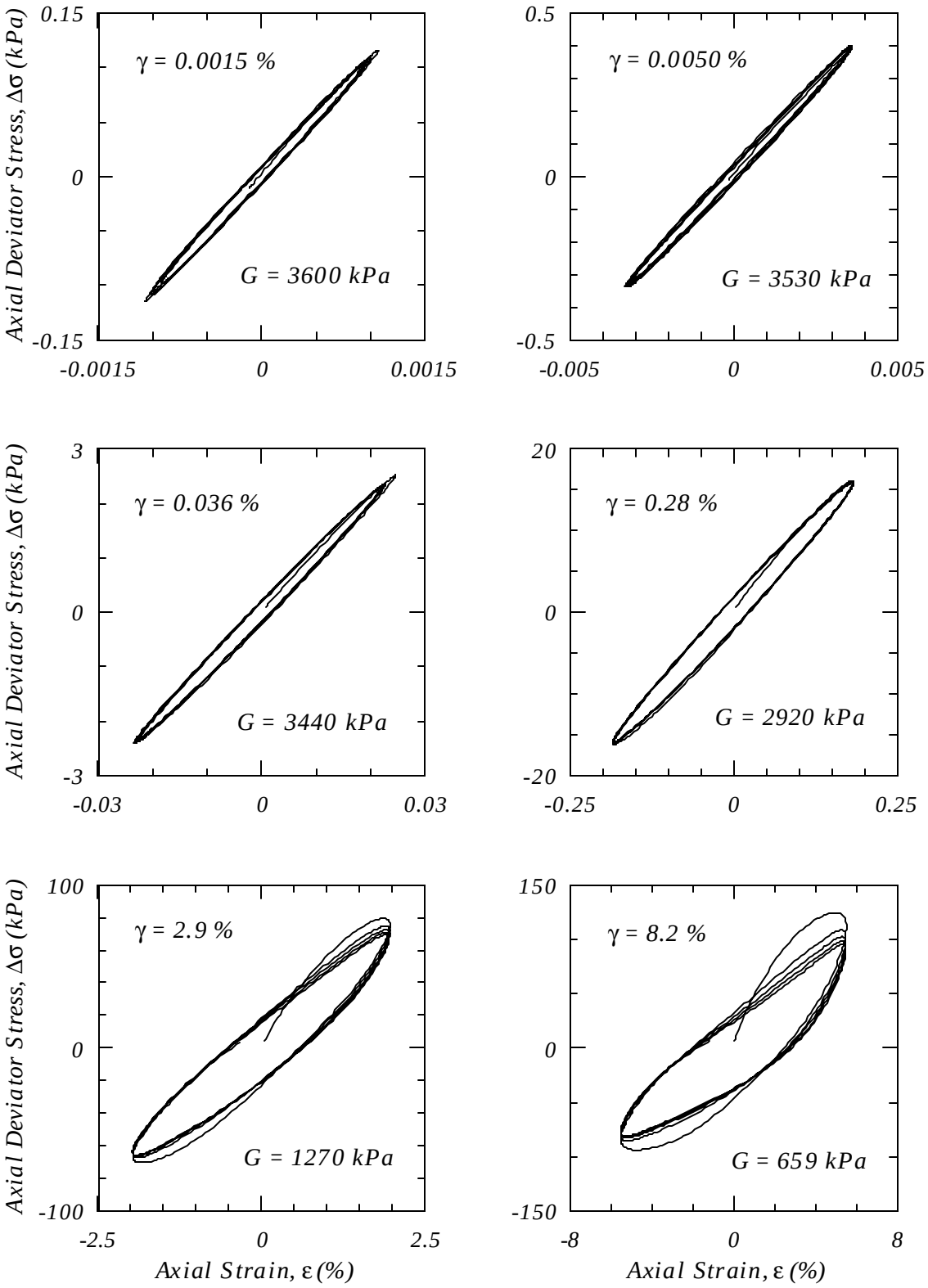

Figure 15: Stress-strain curves for sample 9 from beneath the levee mid-toe showing the secant shear modulus of the first loading cycle for each strain level

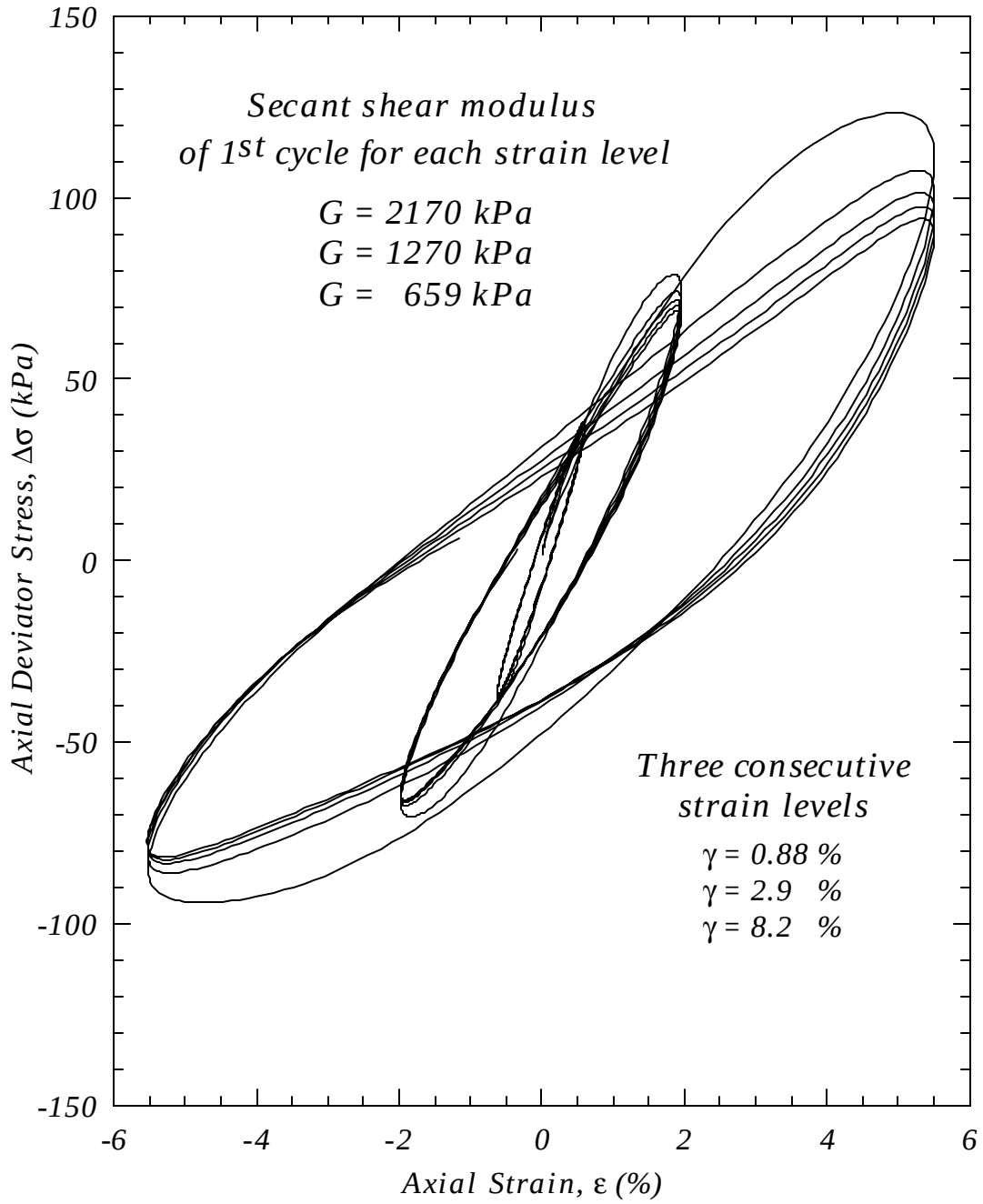

Figure 16: Stress-stain curves for three consecutive strain levels for sample 9 from the levee mid-toe

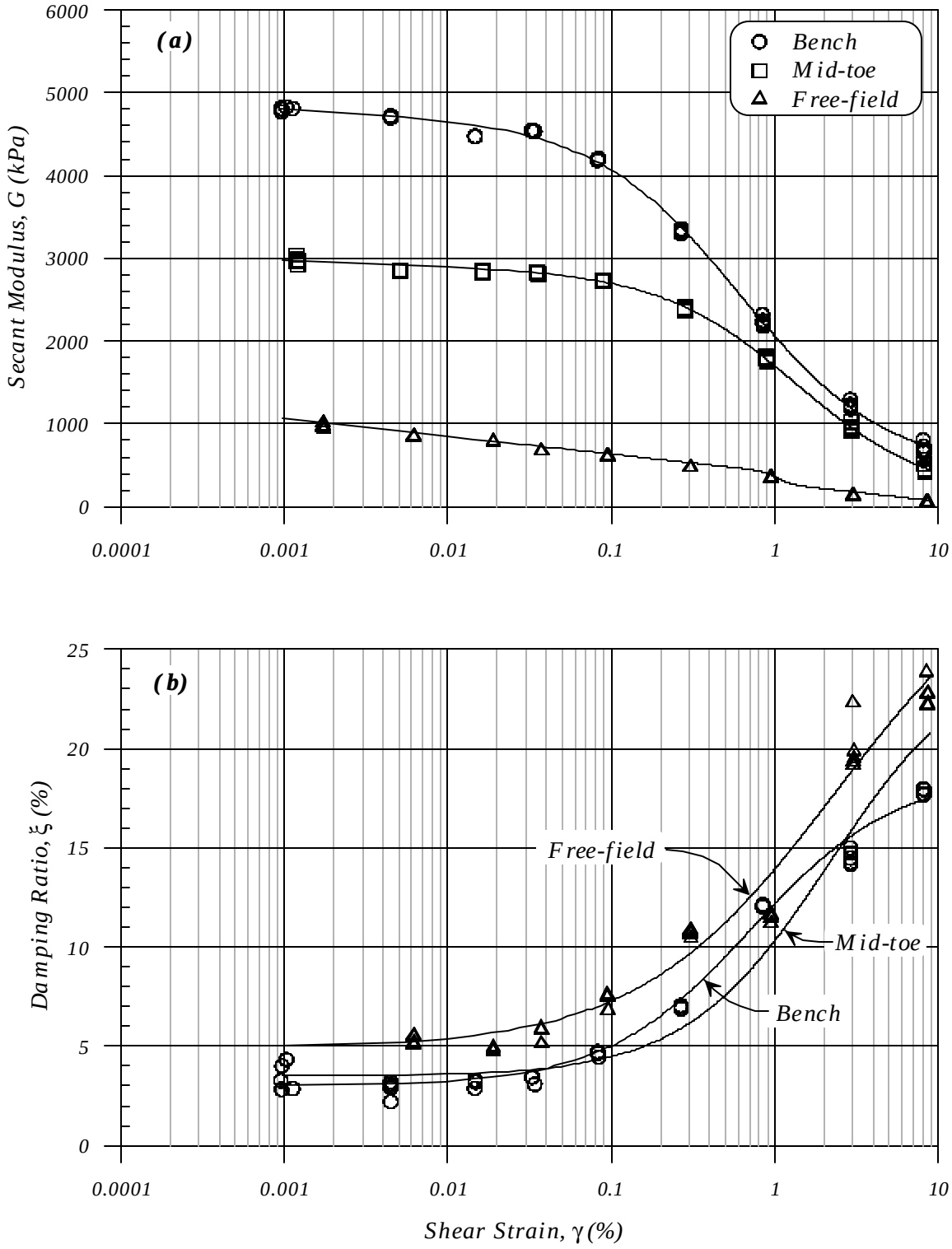

Figure 17: Typical results for samples from the levee bench (Sample 12), levee mid-toe (Sample 8), and free-field (Sample 4): (a) secant shear modulus and (b) equivalent damping ratio

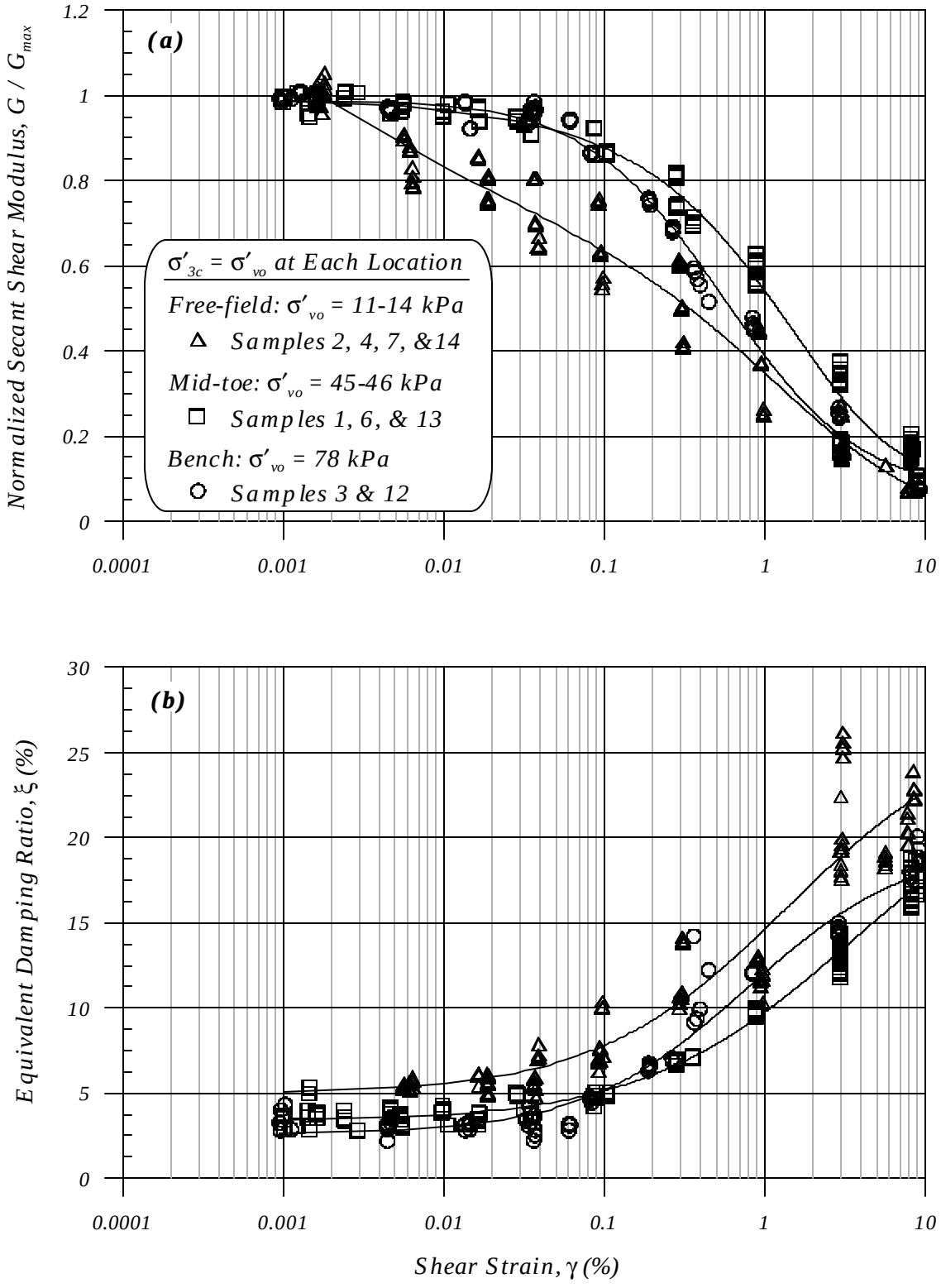

Figure 18: Summary of results for samples from the levee bench, levee mid-toe, and free-field consolidated to their in situ overburden stresses: (a) normalized secant shear modulus and (b) equivalent damping ratio

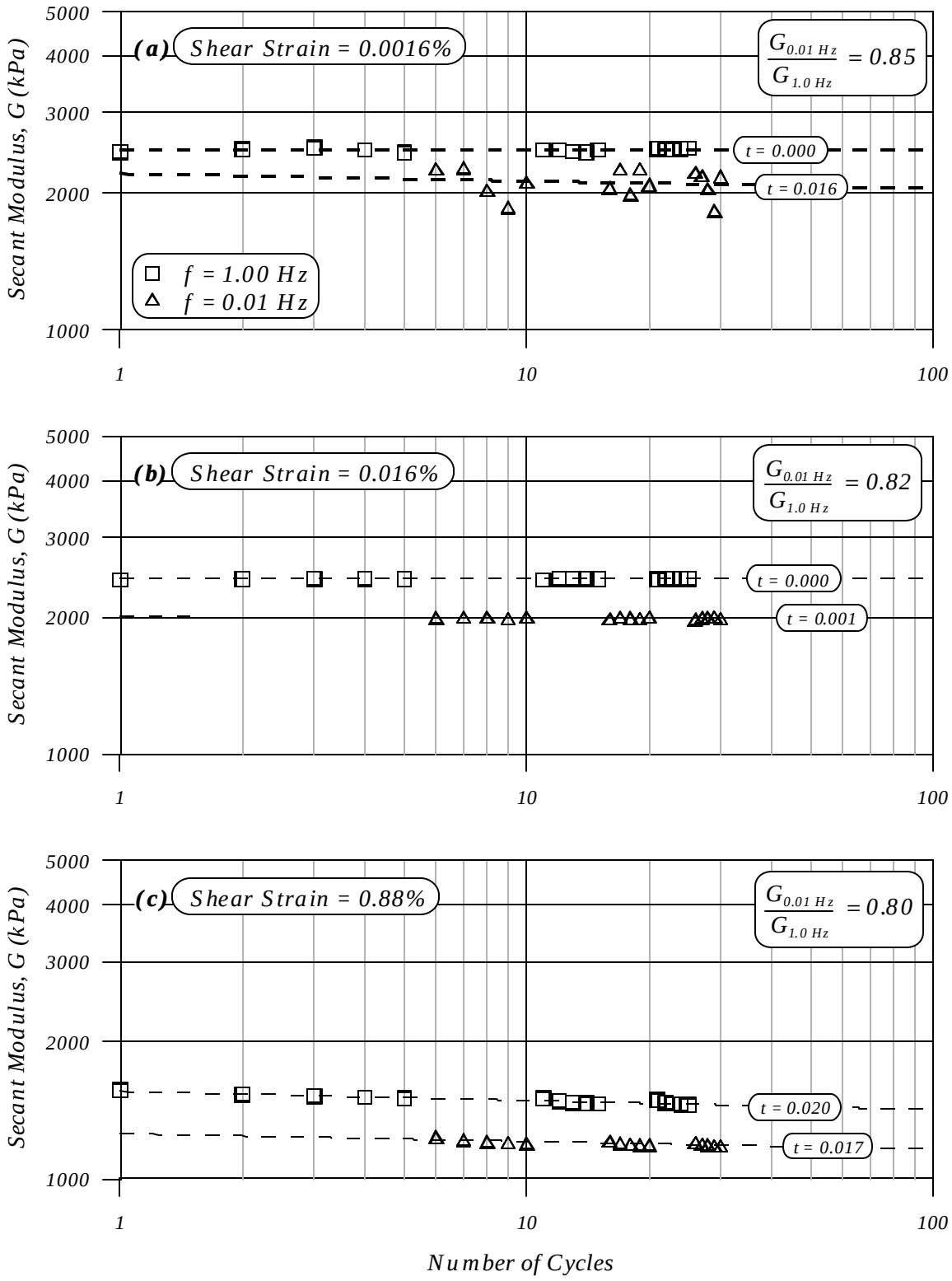

Figure 19: Effect of loading frequency on sample 6 from the mid-toe at three different shear strains: (a) 0.0016%, (b) 0.016%, and (c) 0.88%

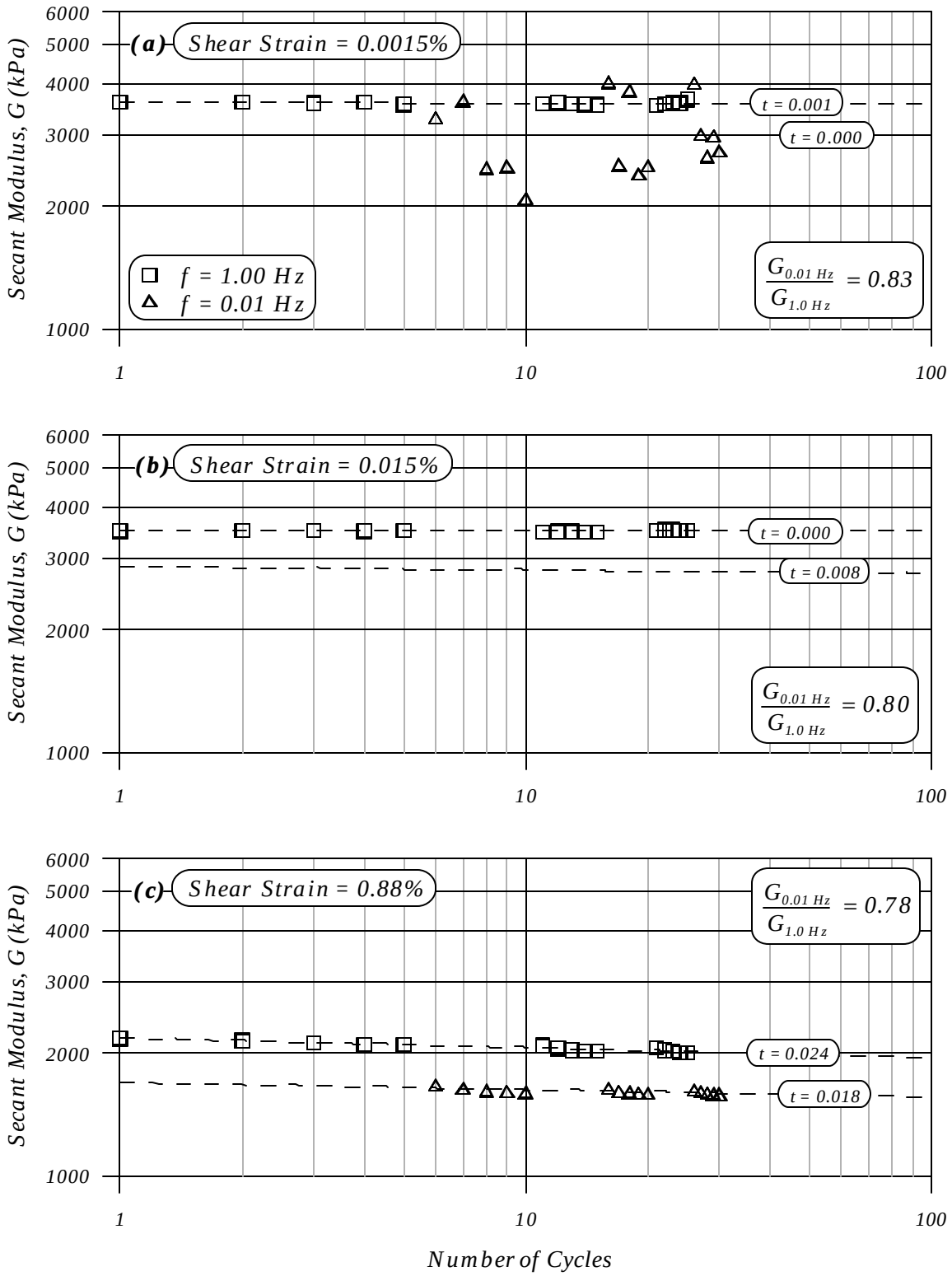

Figure 20: Effect of loading frequency on sample 9 from the mid-toe at three different shear strains: (a) 0.0015%, (b) 0.015%, and (c) 0.88%

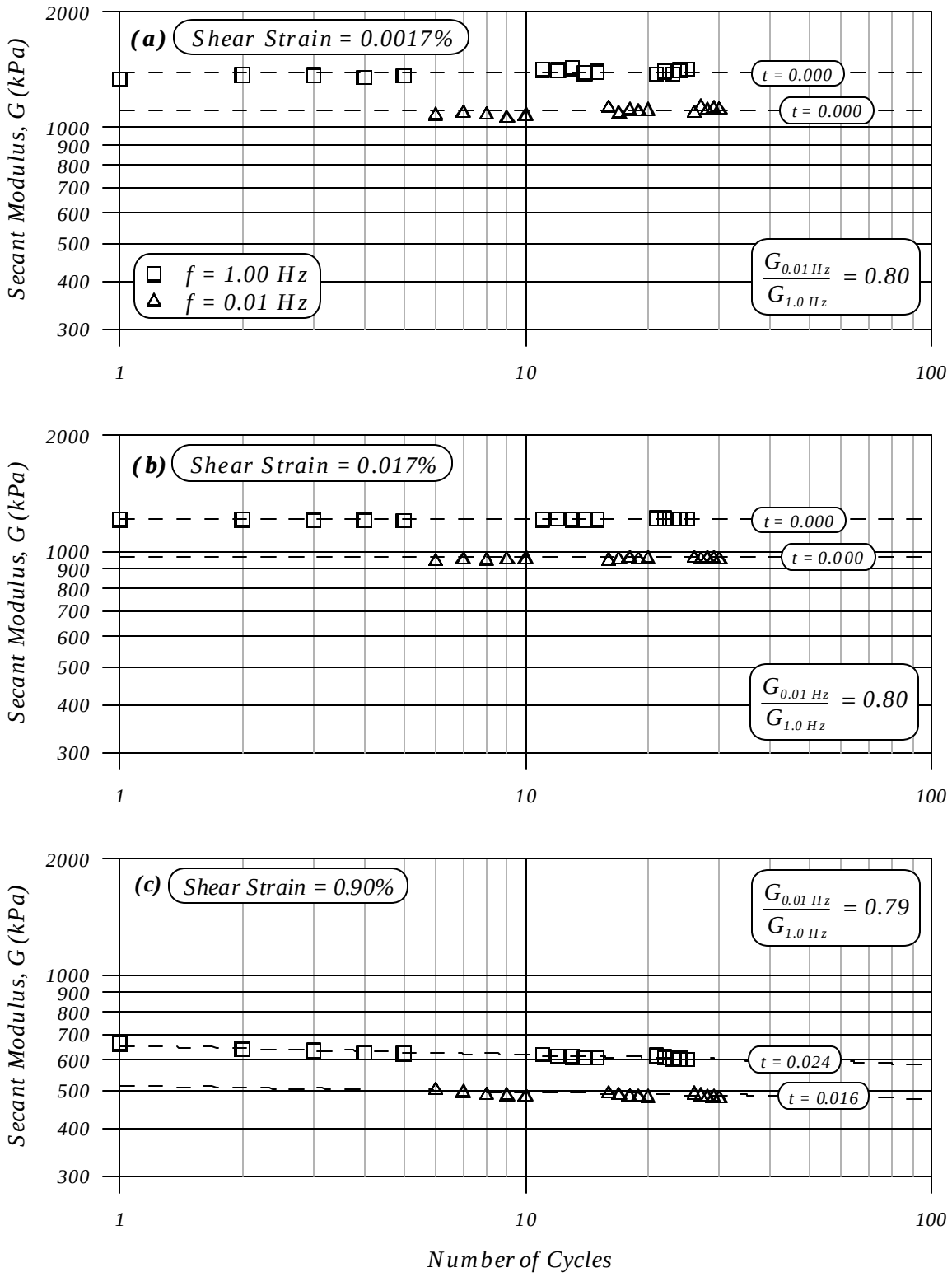

Figure 21: Effect of loading frequency on sample 11 from the free-field at three different shear strains: (a) 0.0017%, (b) 0.017%, and (c) 0.90%

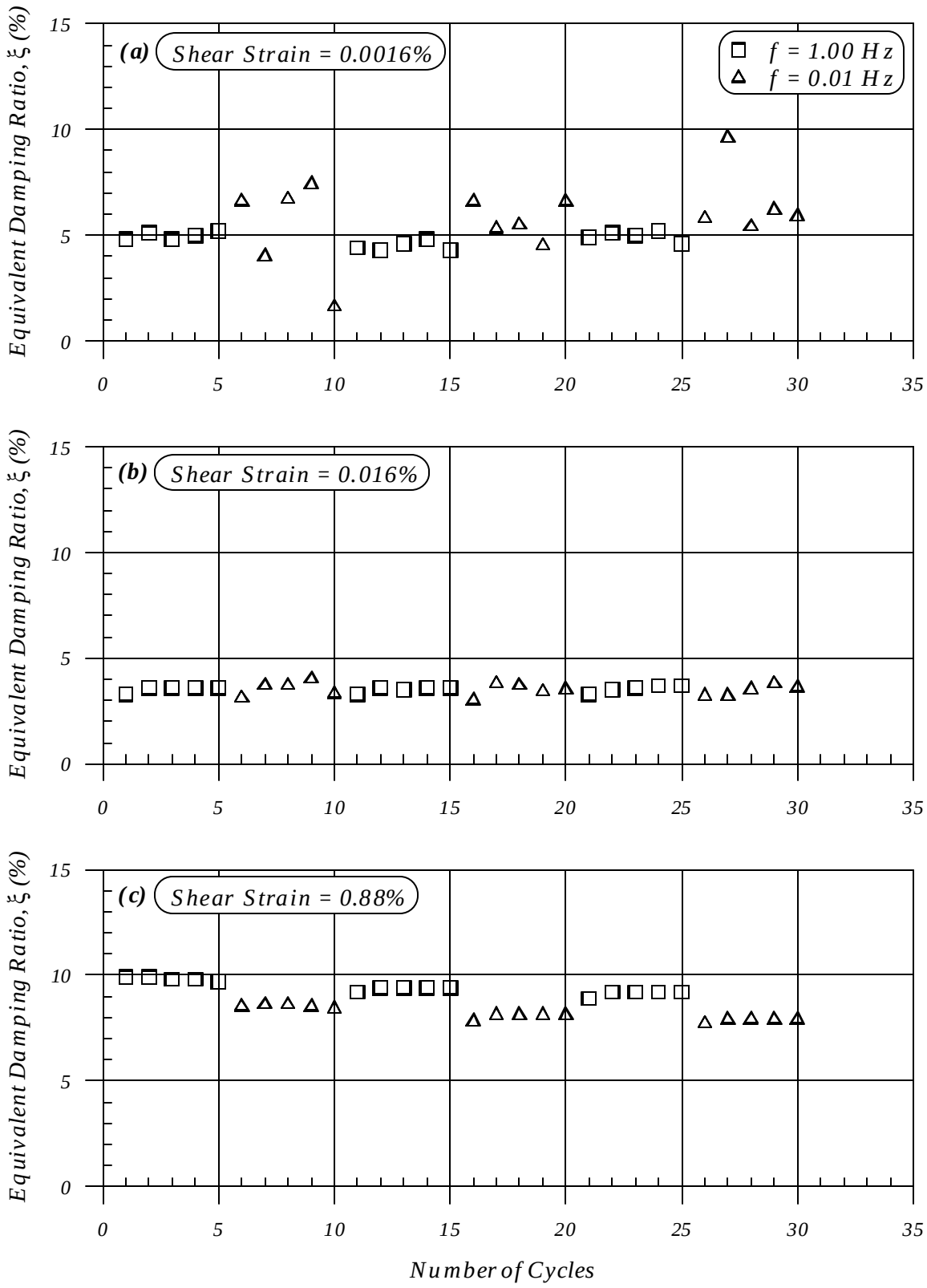

Figure 22: Effect of loading frequency on sample 6 from the mid-toe at three different shear strains: (a) 0.0016%, (b) 0.016%, and (c) 0.88%

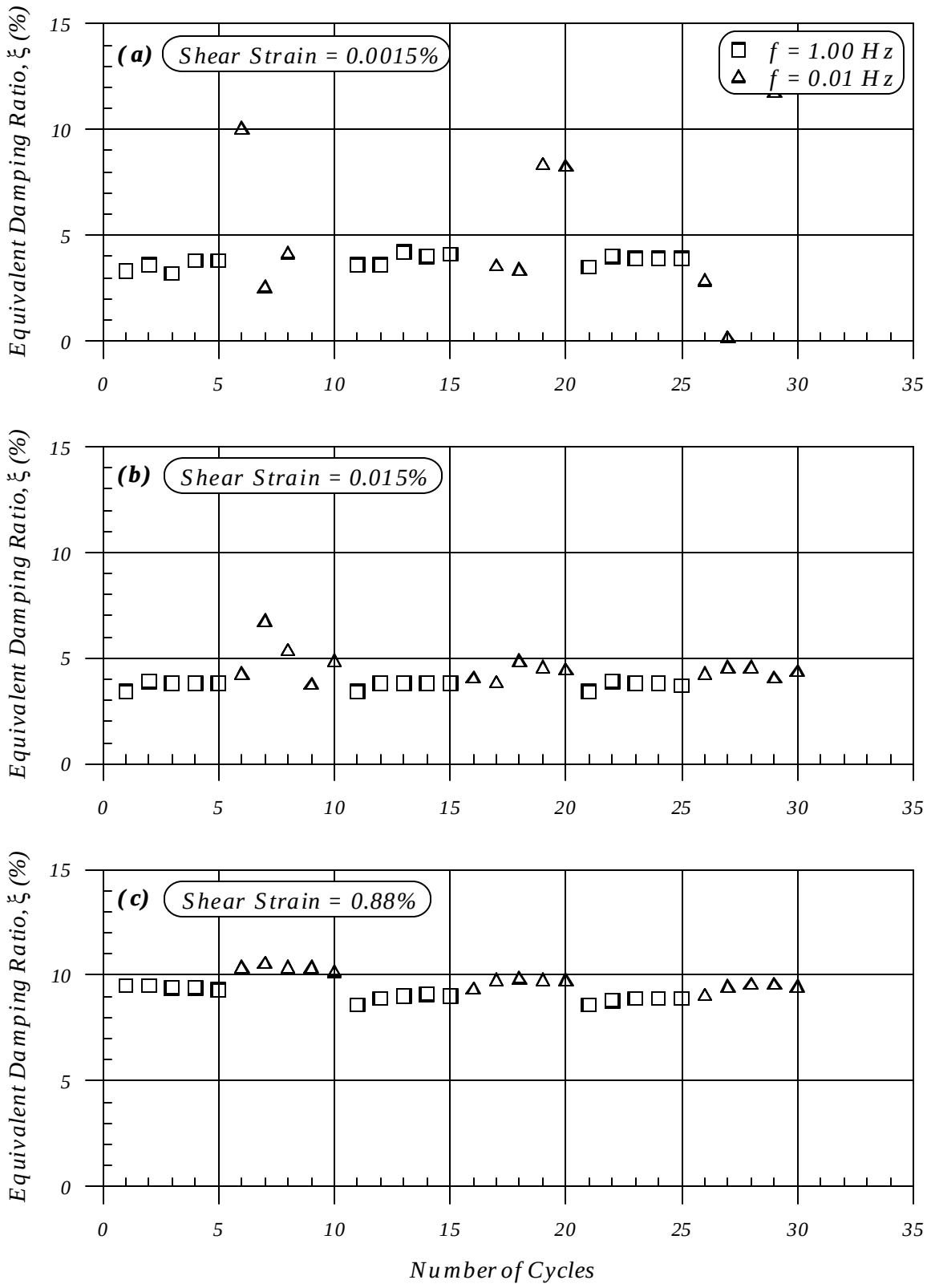

Figure 23: Effect of loading frequency on sample 9 from the mid-toe at three different shear strains: (a) 0.0015%, (b) 0.015%, and (c) 0.88%

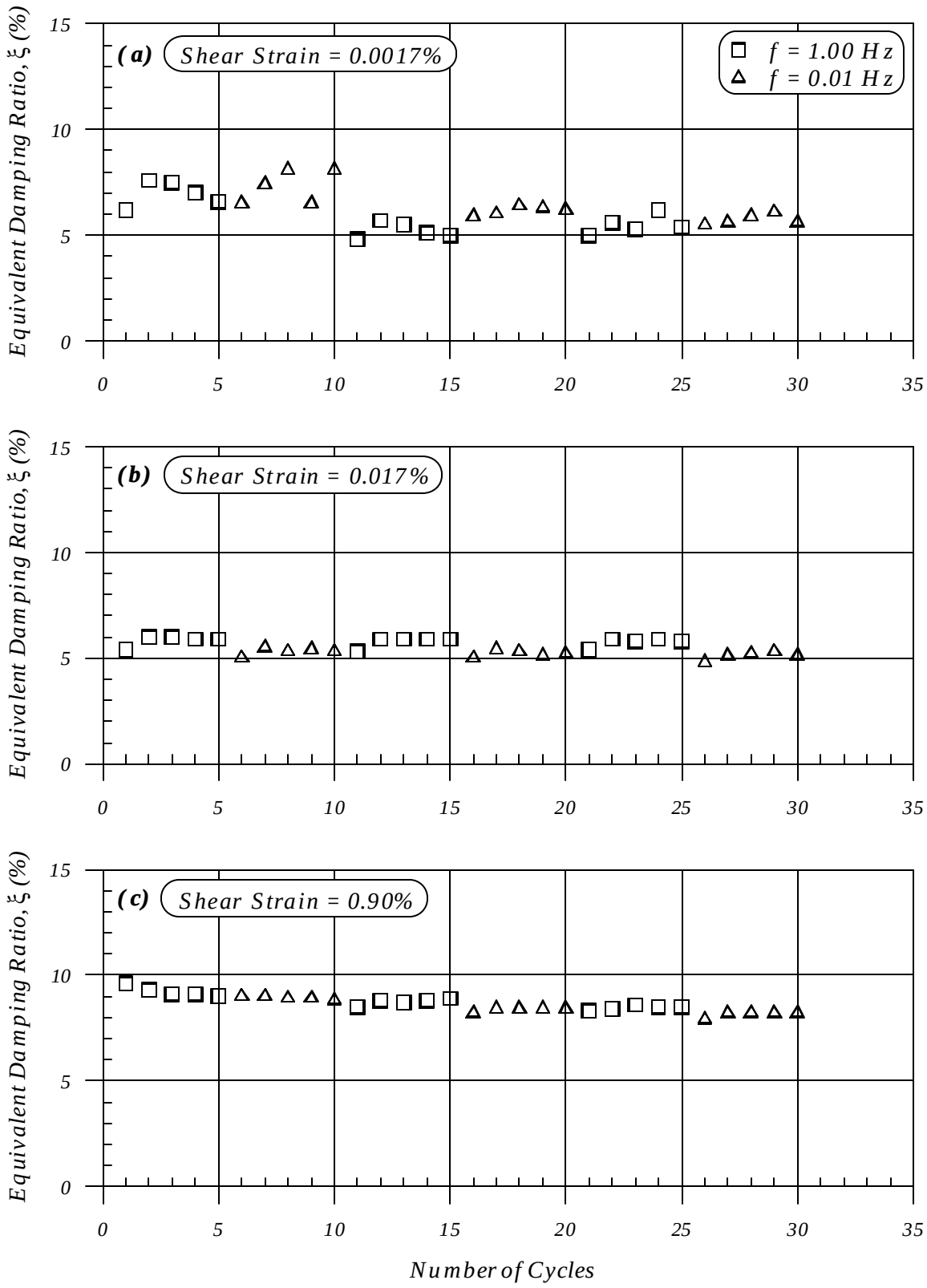

Figure 24: Effect of loading frequency on sample 11 from the free-field at three different shear strains: (a) 0.0017%, (b) 0.017%, and (c) 0.90%

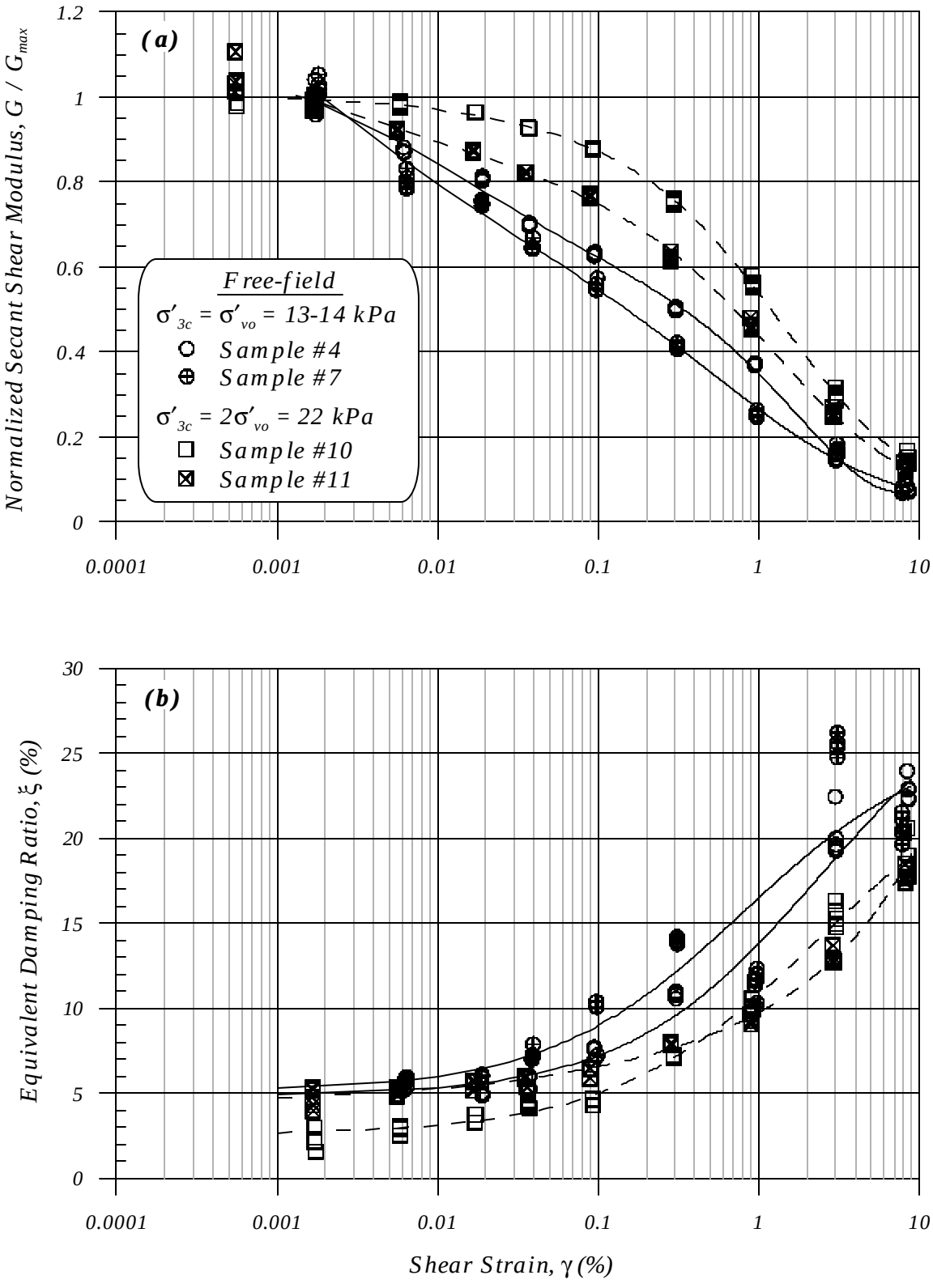

Figure 25: Effect of laboratory consolidation stress on samples from the free-field: (a) normalized secant shear modulus and (b) equivalent damping ratio

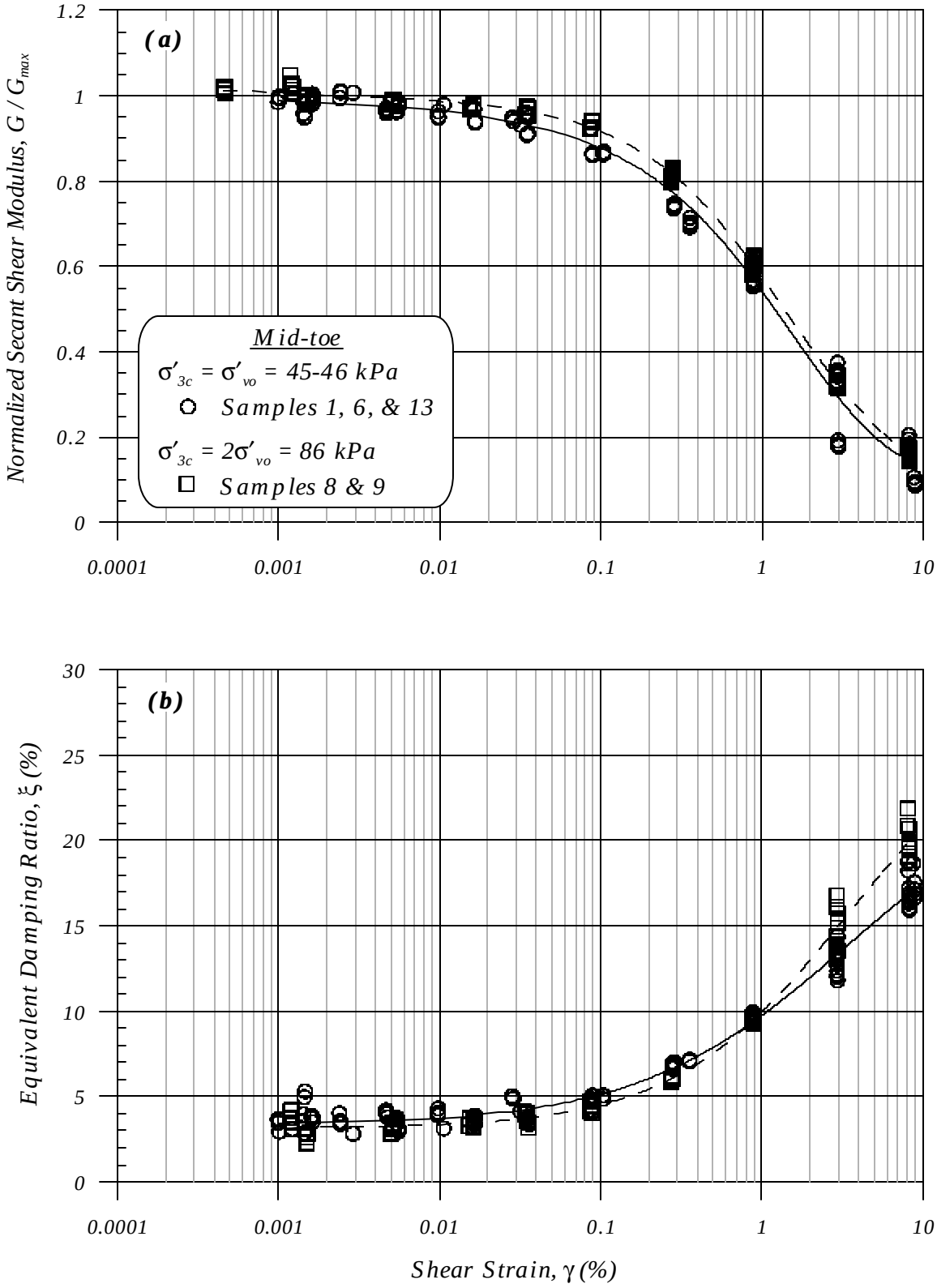

Figure 26: Effect of laboratory consolidation stress on samples from the mid-toe of the levee: (a) normalized secant shear modulus and (b) equivalent damping ratio

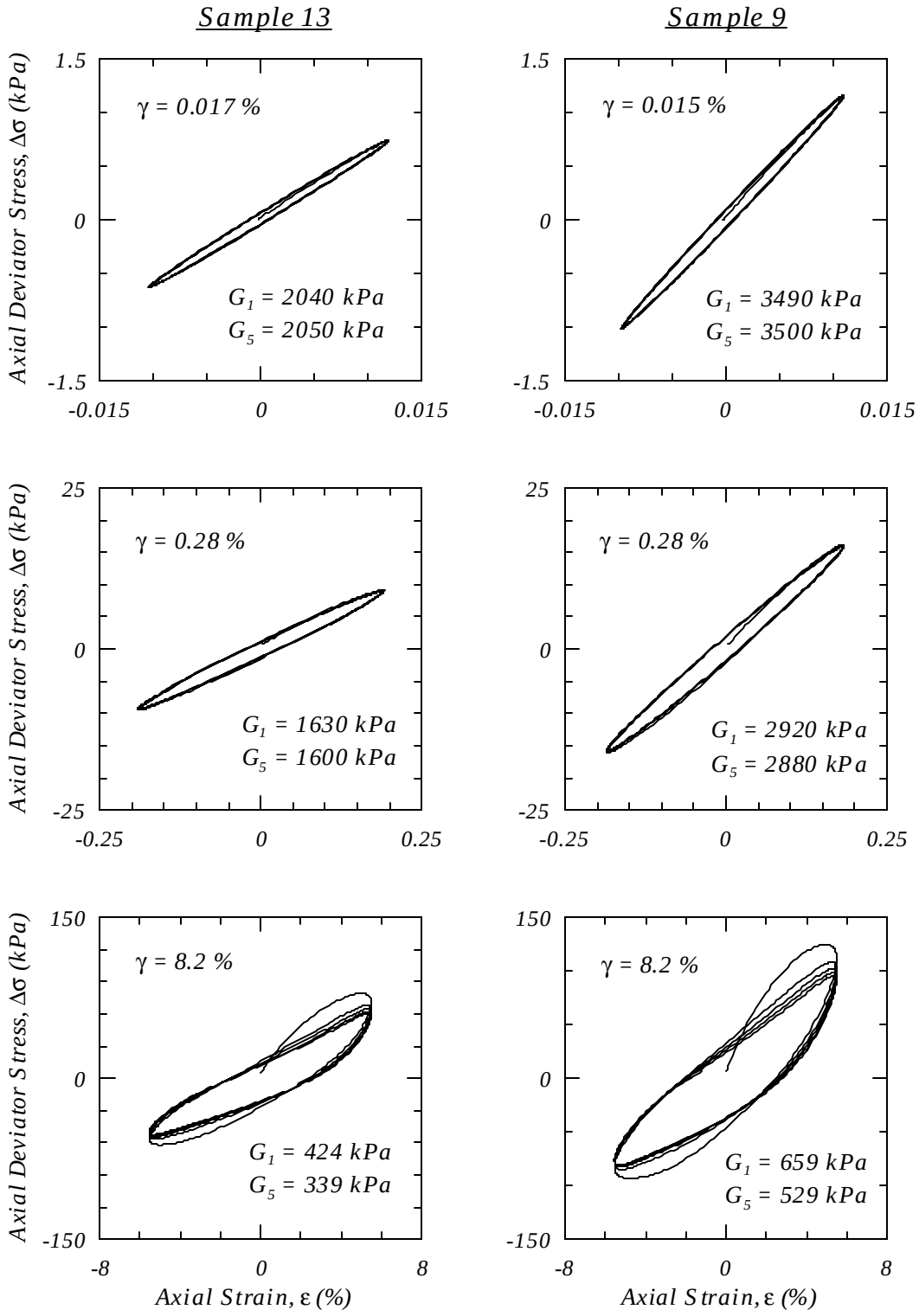

Figure 27: Stress-strain loops for two samples from the levee mid-toe: sample 13 is consolidated to in situ stresses; sample 9 is consolidated to twice its in situ stresses. Secant shear modulus is shown for the 1st and 5th cycles of each strain level.

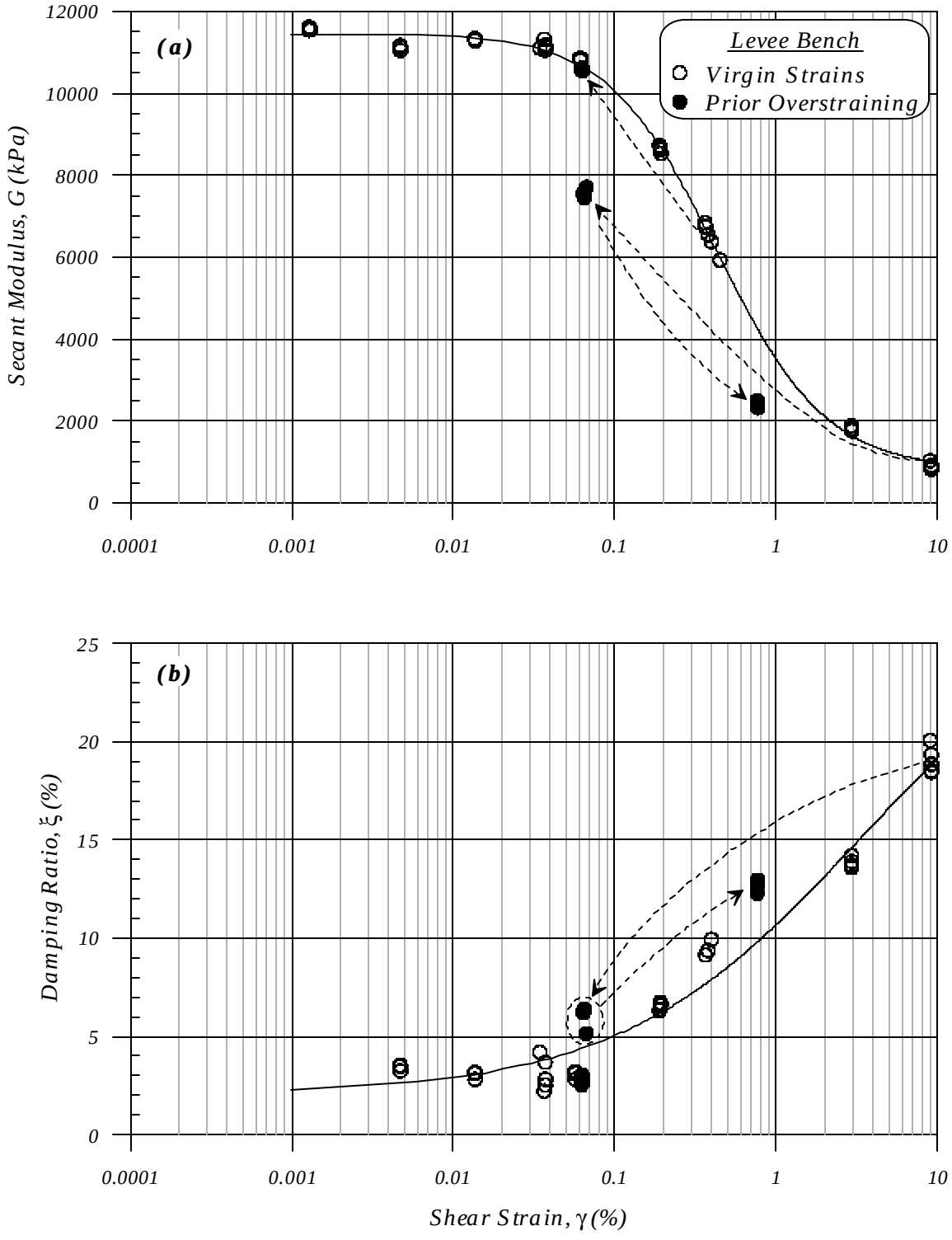

Figure 28: Effect of prior overstraining for sample 3 from the levee bench: (a) secant shear modulus and (b) equivalent damping ratio

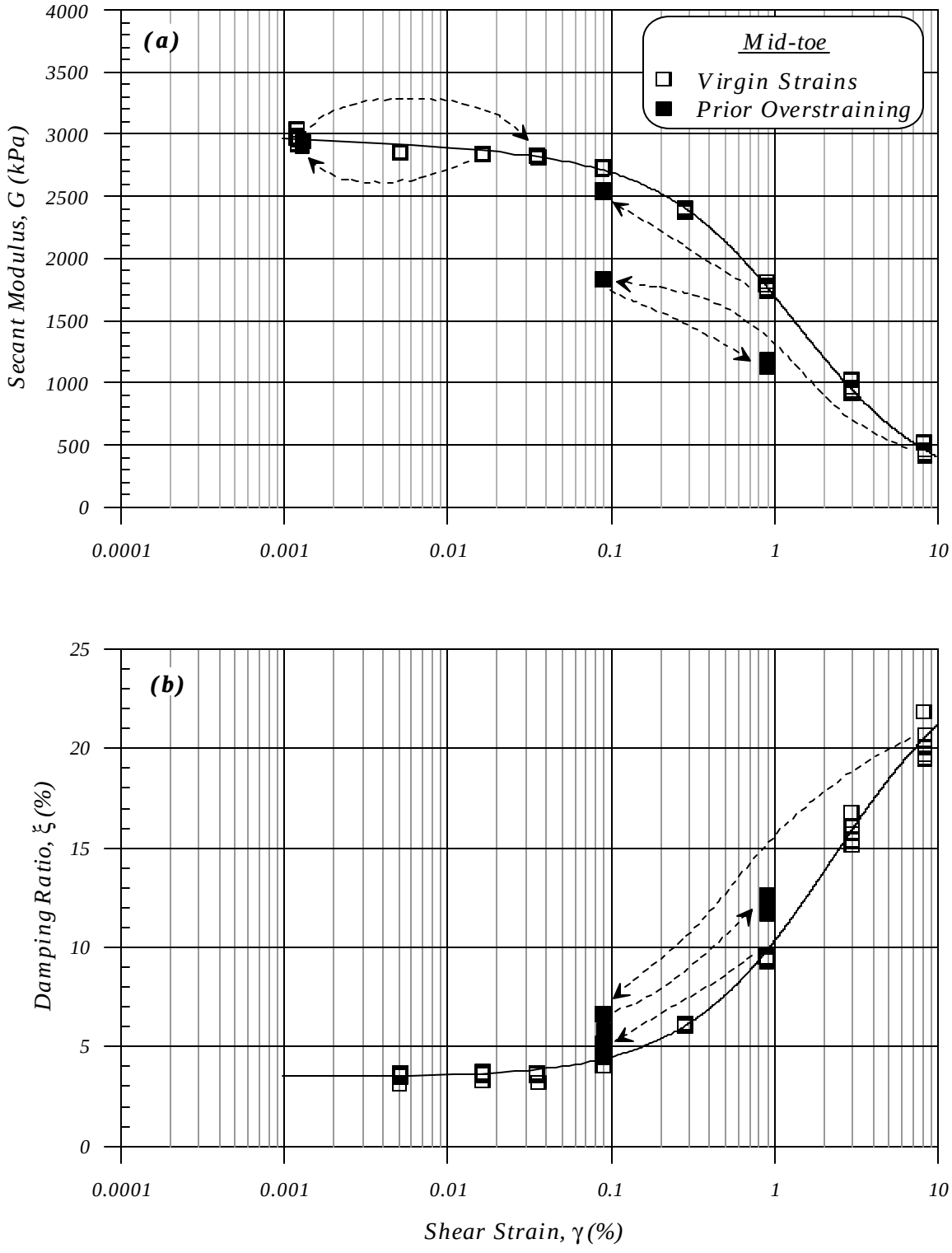

Figure 29: Effect of prior overstraining for sample 8 from the levee mid-toe: (a) secant shear modulus and (b) equivalent damping ratio

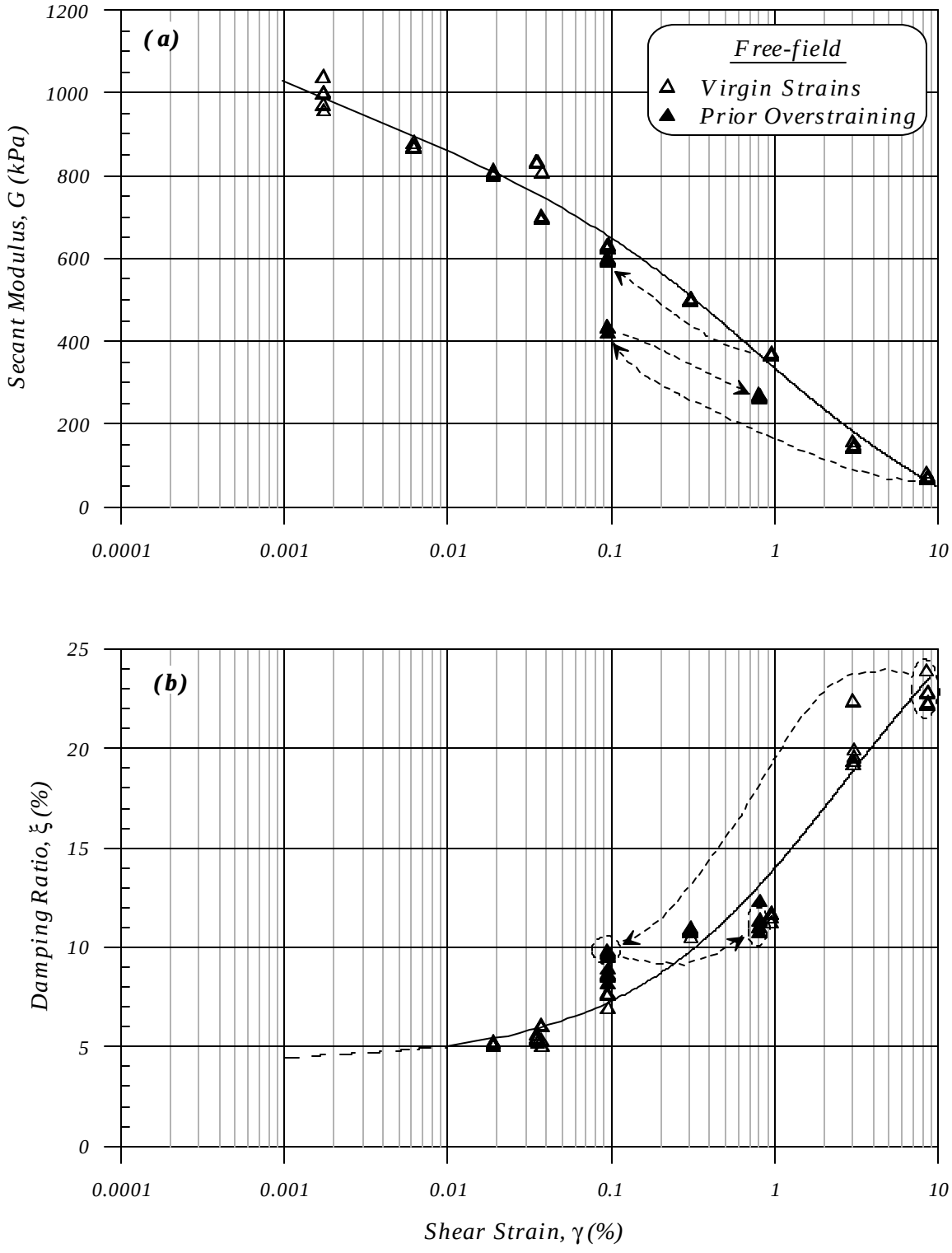

Figure 30: Effect of prior overstraining for sample 4 from the free-field: (a) secant shear modulus and (b) equivalent damping ratio

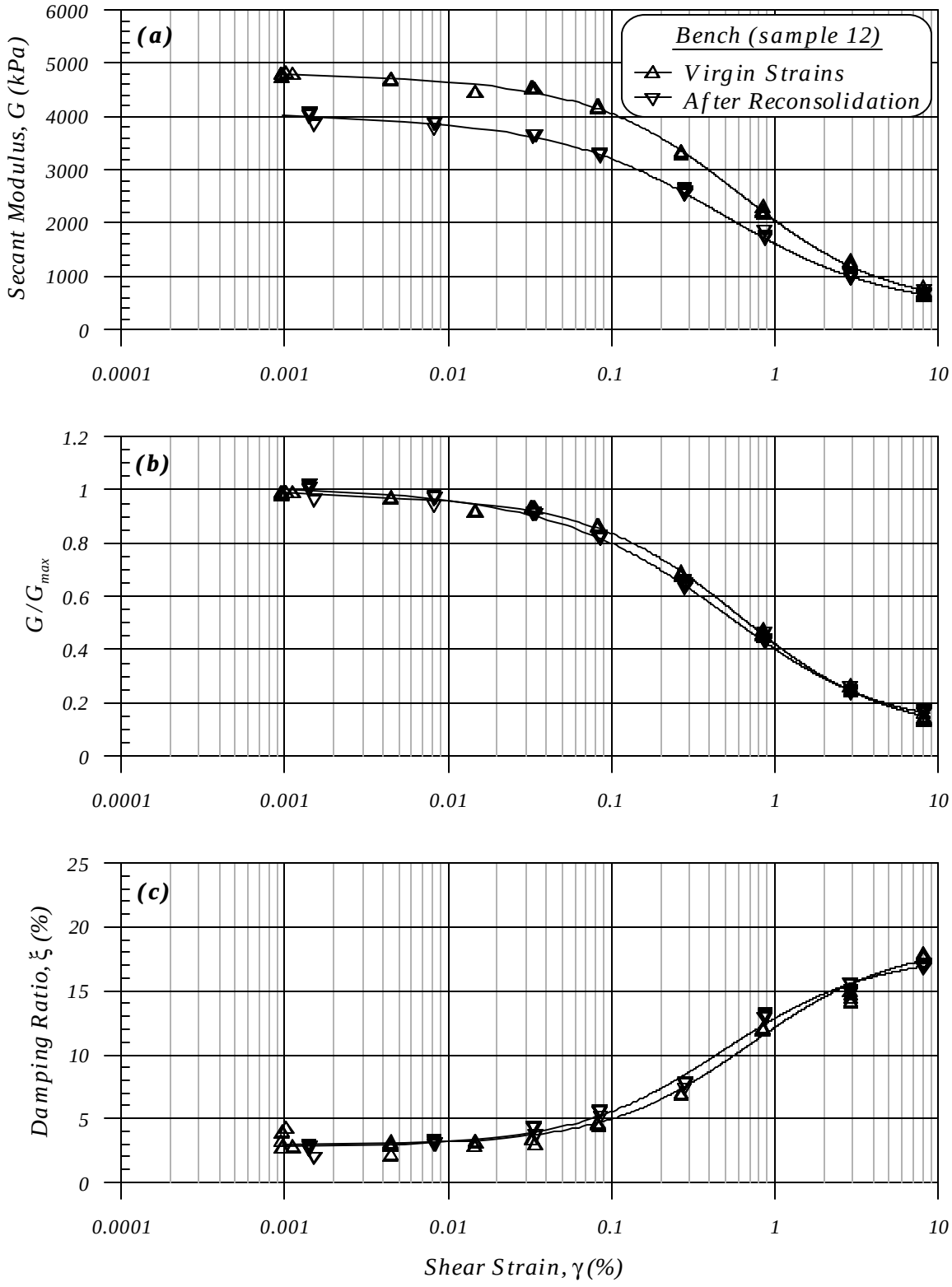

Figure 31: Effect of prior overstraining to a shear strain of 9% followed by reconsolidation for sample 12 from the levee bench: (a) secant shear modulus, (b) normalized secant shear modulus, and (c) equivalent damping ratio

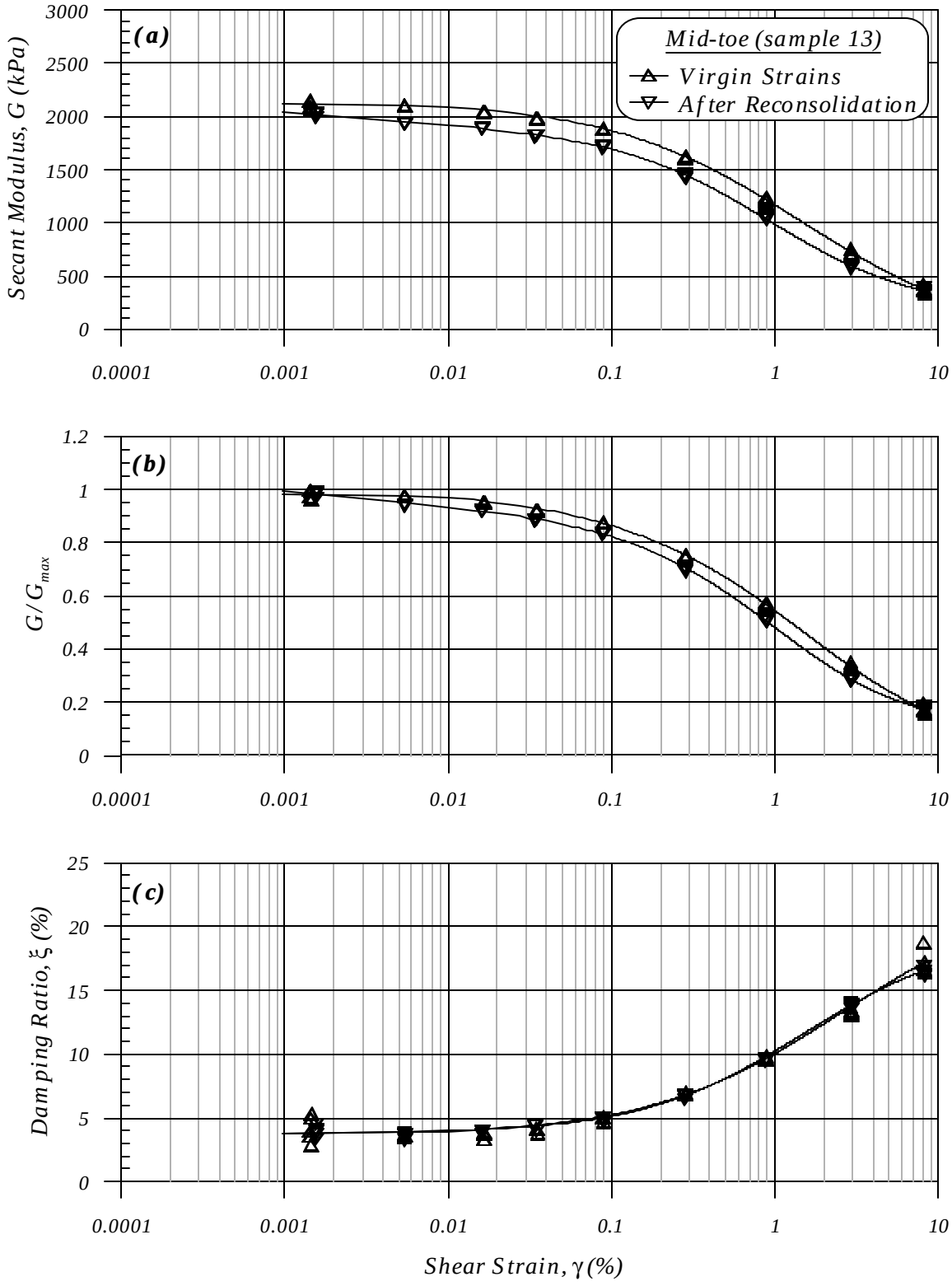

Figure 32: Effect of prior overstraining to a shear strain of 8% followed by reconsolidation for sample 13 from the levee mid-toe: (a) secant shear modulus, (b) normalized secant shear modulus, and (c) equivalent damping ratio

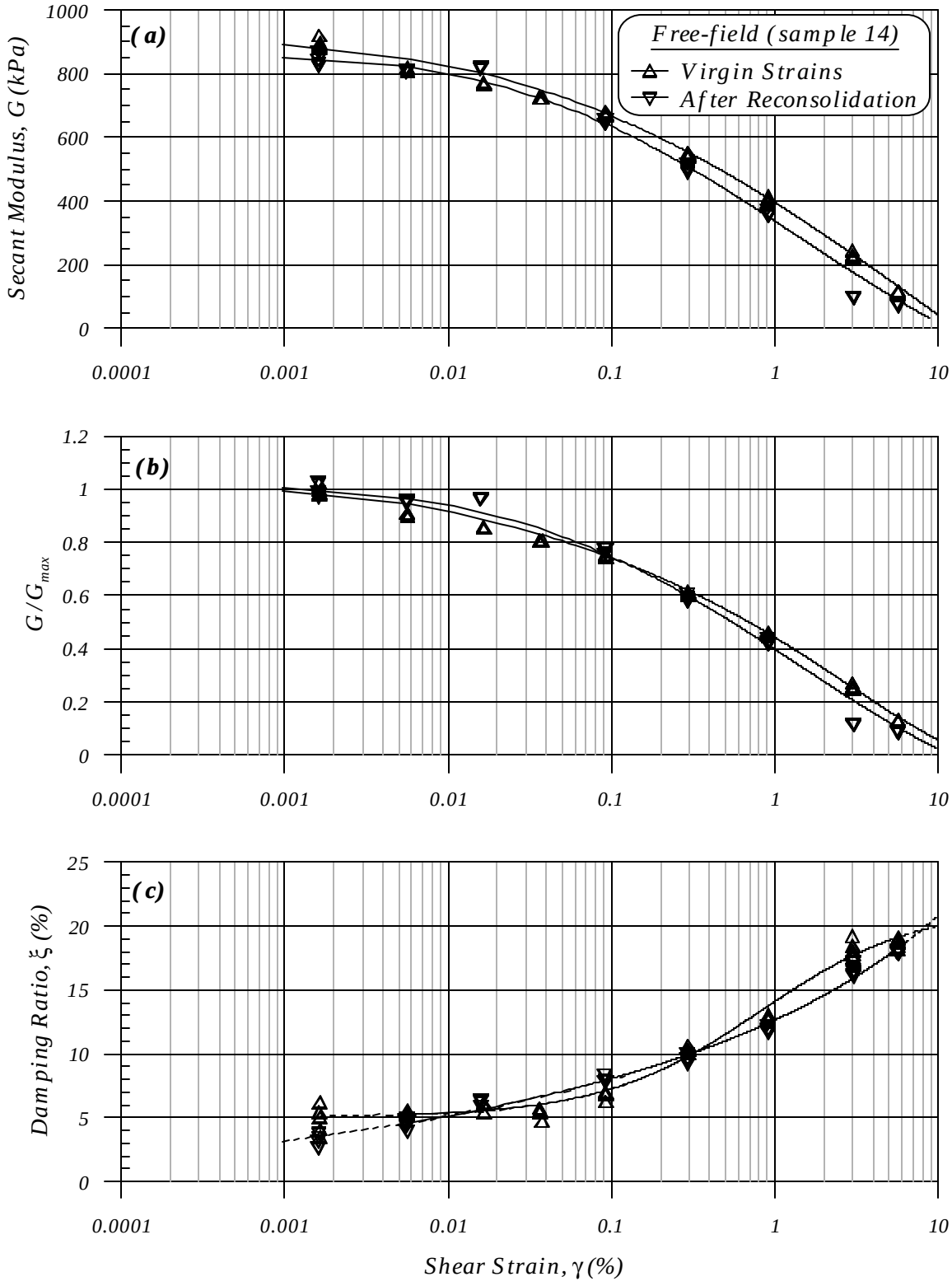

Figure 33: Effect of prior overstraining to a shear strain of 6% followed by reconsolidation for sample 14 from the free-field: (a) secant shear modulus, (b) normalized secant shear modulus, and (c) equivalent damping ratio

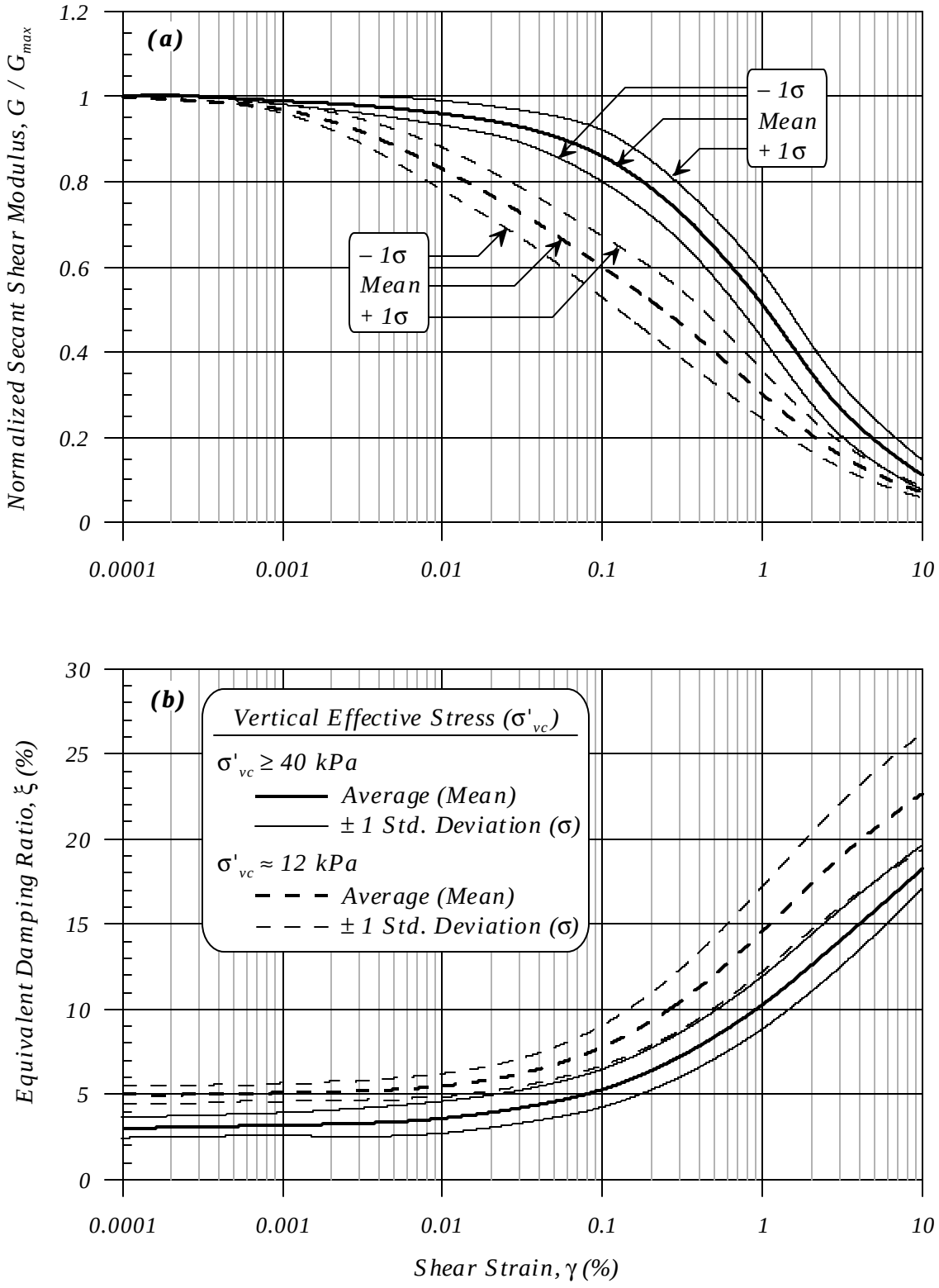

Figure 34: Summary of G/G_{max} and x data for different in situ vertical effective consolidation stress conditions

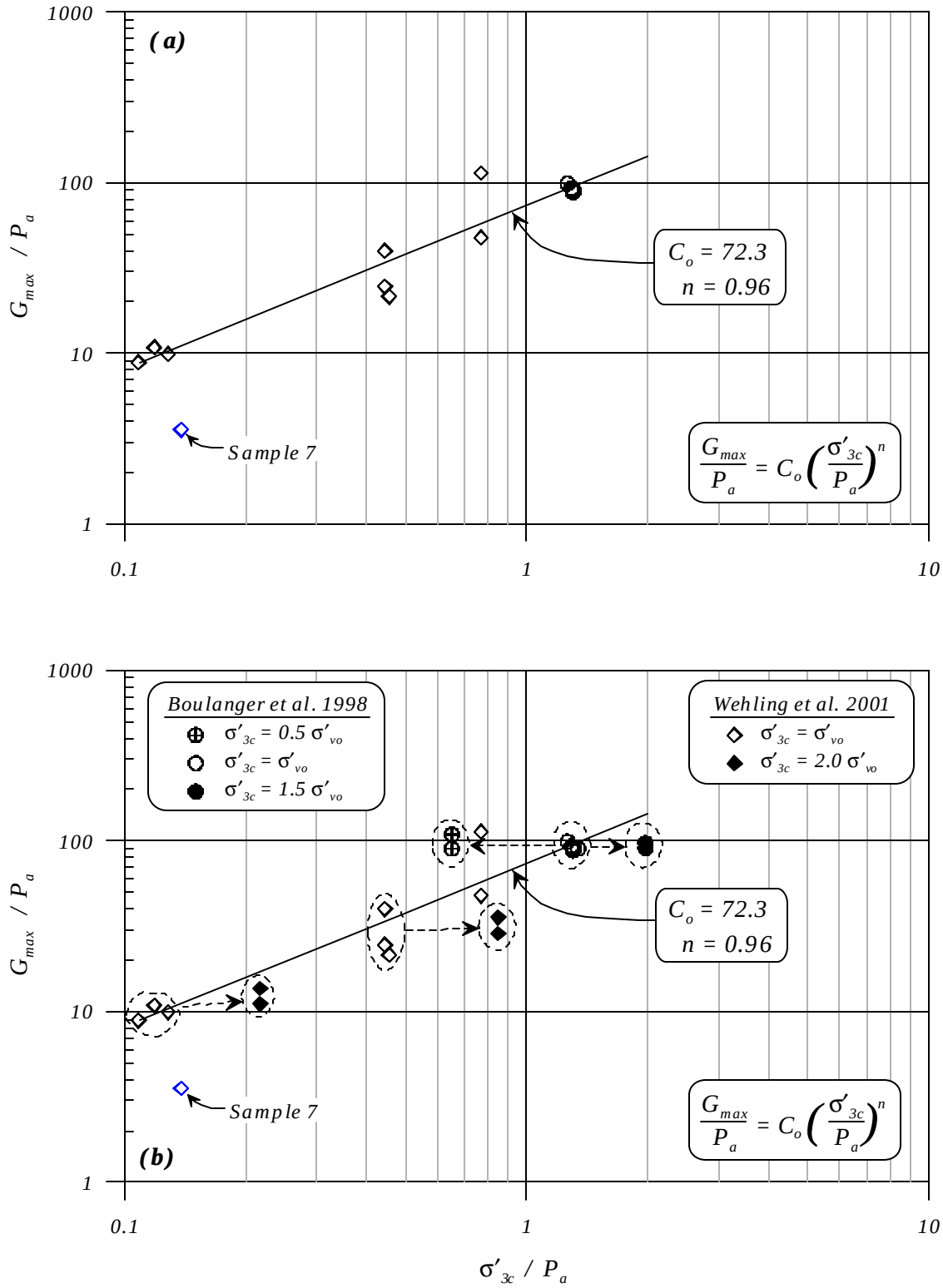

Figure 35: Maximum shear modulus versus consolidation stress for samples consolidated to (a) their in situ overburden stresses and (b) various stresses. Sample 7 is excluded from the regression content. (Includes data from Boulanger et al. 1998)

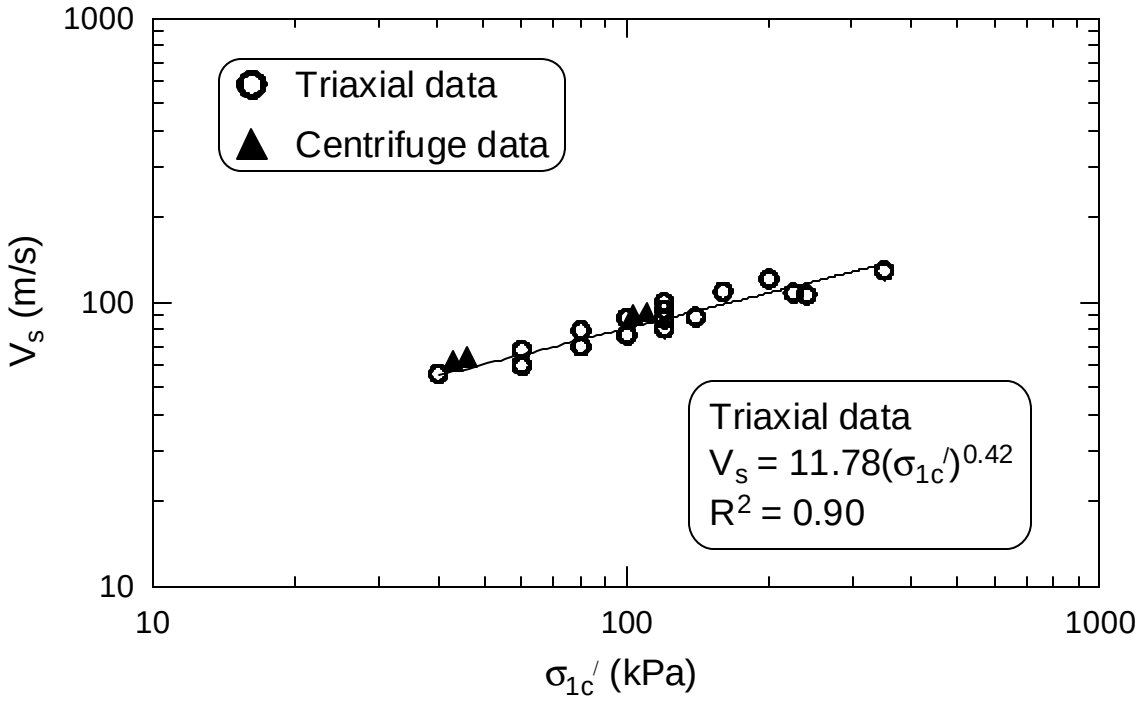

Figure 36: Summary of results for reconstituted Sherman Island peat from centrifuge tests and bender element tests on triaxial specimens (Arulnathan 2001)

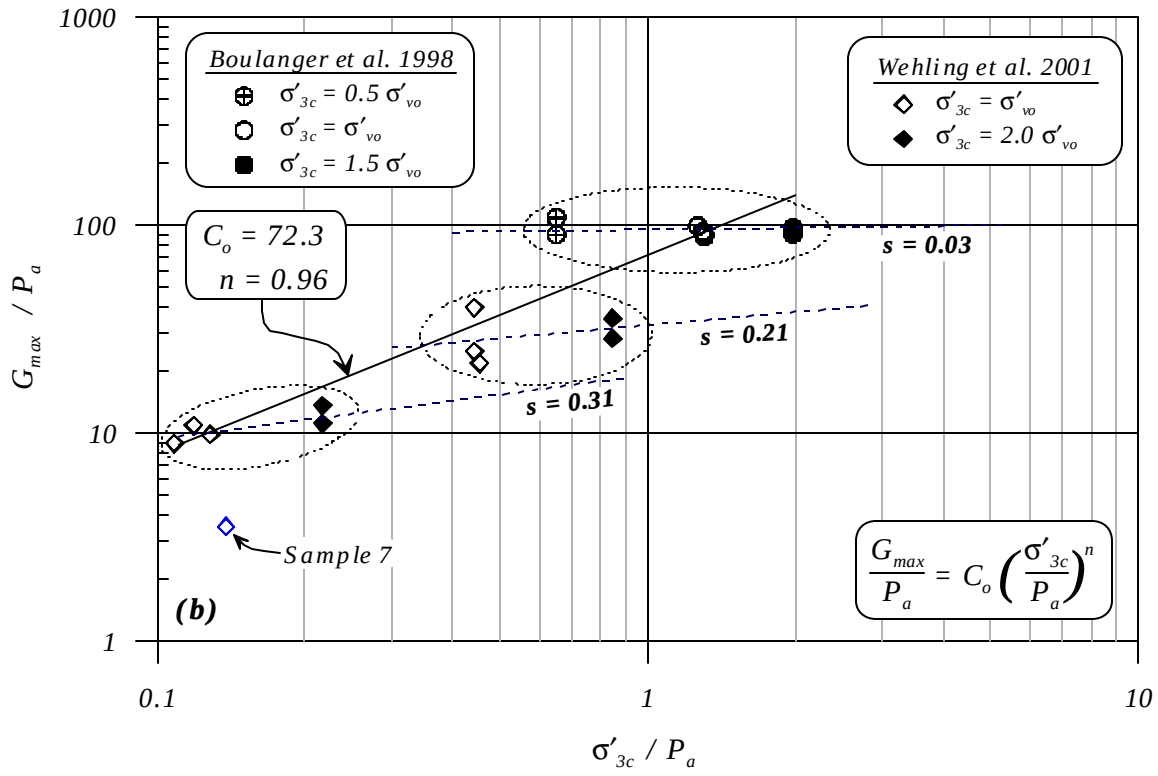

Figure 37: Maximum shear modulus versus consolidation stress for samples consolidated to various stresses. The approximate slope *s* corresponds to samples taken from the same location. Sample 7 is excluded from the regression content. (Includes data from Boulanger et al. 1998)

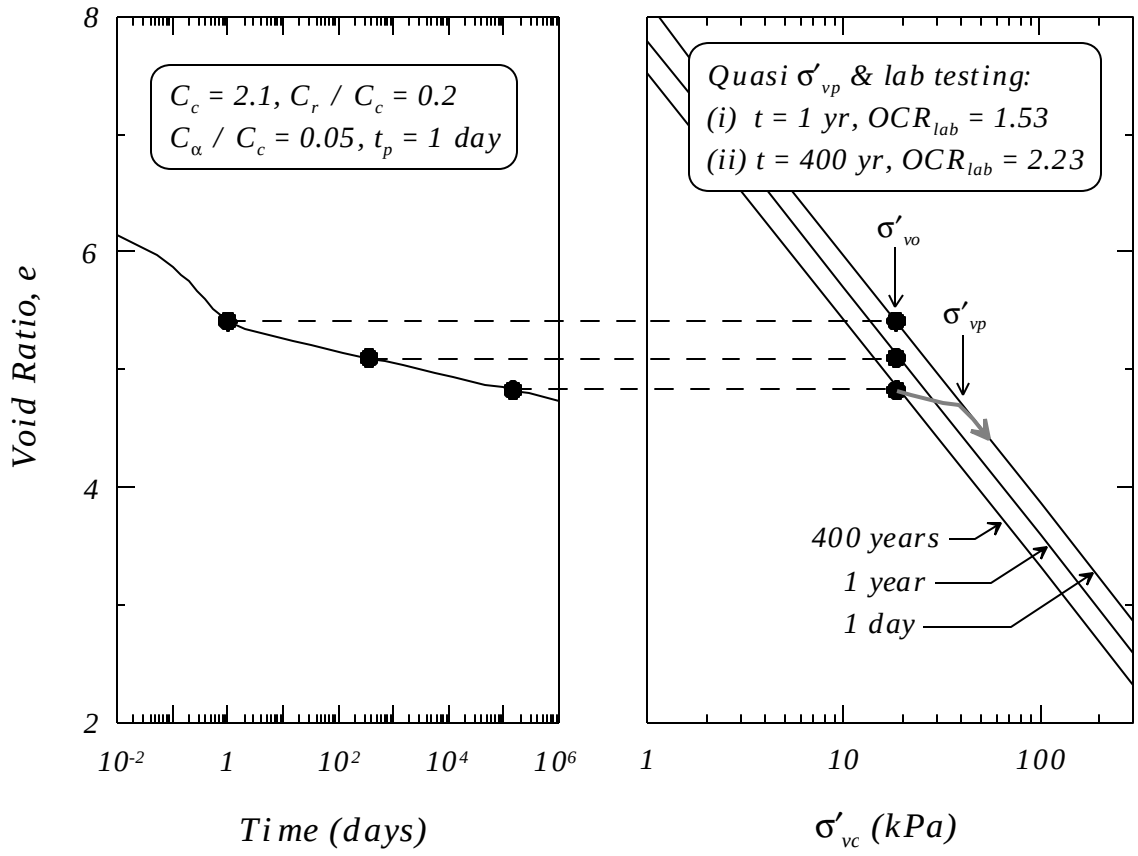

Figure 38: Concept of quasi-preconsolidation pressure applied to Sherman Island peat

Conclusions

This report summarizes the results of laboratory experiments evaluating the dynamic properties of a peaty organic soil ("peat") underlying the south levee of Sherman Island near the western side of the Delta. Standard and modified Shelby tubes were used to obtain high quality samples from this peat layer that is about 10.5 m thick in the free-field and about 7.5 m thick beneath the levee bench. The in situ effective consolidation stresses ranged from about 11 kPa to 14 kPa in the free-field to about 78 kPa beneath the levee bench. The samples were tested in undrained cyclic triaxial loading at staged levels of shear strain from about 5×10^{-4} % to 10%. This Phase II laboratory study complements the prior test results for samples from beneath the levee crest where in situ effective consolidation stresses were about 130 kPa (Boulanger et al. 1998).

The modulus reduction (G/G_{max}) and equivalent damping (x) relations for Sherman Island peat were shown to be dependent on the consolidation stress (s'_{vc}). The G/G_{max} behavior showed increasing linearity as s'_{vc} increased from about 10 kPa to about 40 kPa, after which further increases in s'_{vc} had no significant effect. Similarly, the x values decreased as s'_{vc} increased from about 10 kPa to about 40 kPa, after which further increases in s'_{vc} had no significant effect. These results are consistent with the trends observed by Kramer (2000) for Mercer Slough peat under consolidation stresses of 2 to 30 kPa. The mean relations for Sherman Island peat are compared to the results for Mercer Slough (Kramer 2000) and Queensboro Bridge (Stokoe et al. 1996) in Figure 39. Recommended G/G_{max} and x relations for evaluating seismic site response of Sherman Island peaty organic soil are summarized in Figure 40 and Table 2, including mean and ± 1 standard deviation relations.

The effect of sample disturbance on the G/G_{max} and x relations appears to be negligible for practical purposes, based on cyclic tests involving prior undrained overstraining. Prior undrained overstraining up to 1% shear strain had only a small effect on modulus and damping ratios that were subsequently measured at smaller shear strains. Furthermore, reconsolidation after undrained overstraining to 10% shear strain resulted in G/G_{max} and x relations that were essentially unchanged from those for virgin loading.

The effect of loading frequency on shear modulus and damping was investigated using loading frequencies of 0.01 Hz and 1 Hz. Generally, shear modulus increases by about 10% per log cycle increase in loading frequency, while damping showed no consistent differences between these two loading frequencies.

The in situ maximum shear modulus (G_{max}) of Sherman Island peat is reasonably represented by the expression:

$$\frac{G_{\max}}{P_a} = 72\left(\frac{s'_{vc}}{P_a}\right)^{0.96} \tag{10}$$

This relation is generally consistent with results obtained by Arulnathan (2000) for reconstituted, normally consolidated, peaty organic soil specimens. Further study is needed to determine how to best incorporate the effects of ongoing secondary compression (or age) and mechanical overconsolidation into this relation.

The results and conclusions presented herein for Sherman Island peaty organic soils provide guidance on how highly organic soils will respond during dynamic shaking. Additional laboratory testing is needed on samples from other sites in the Delta addressing other characteristics (e.g., ash content, fabric, level of decomposition, and stress-path effects). Extrapolation of the results presented in this report to other conditions must take into account these uncertainties.

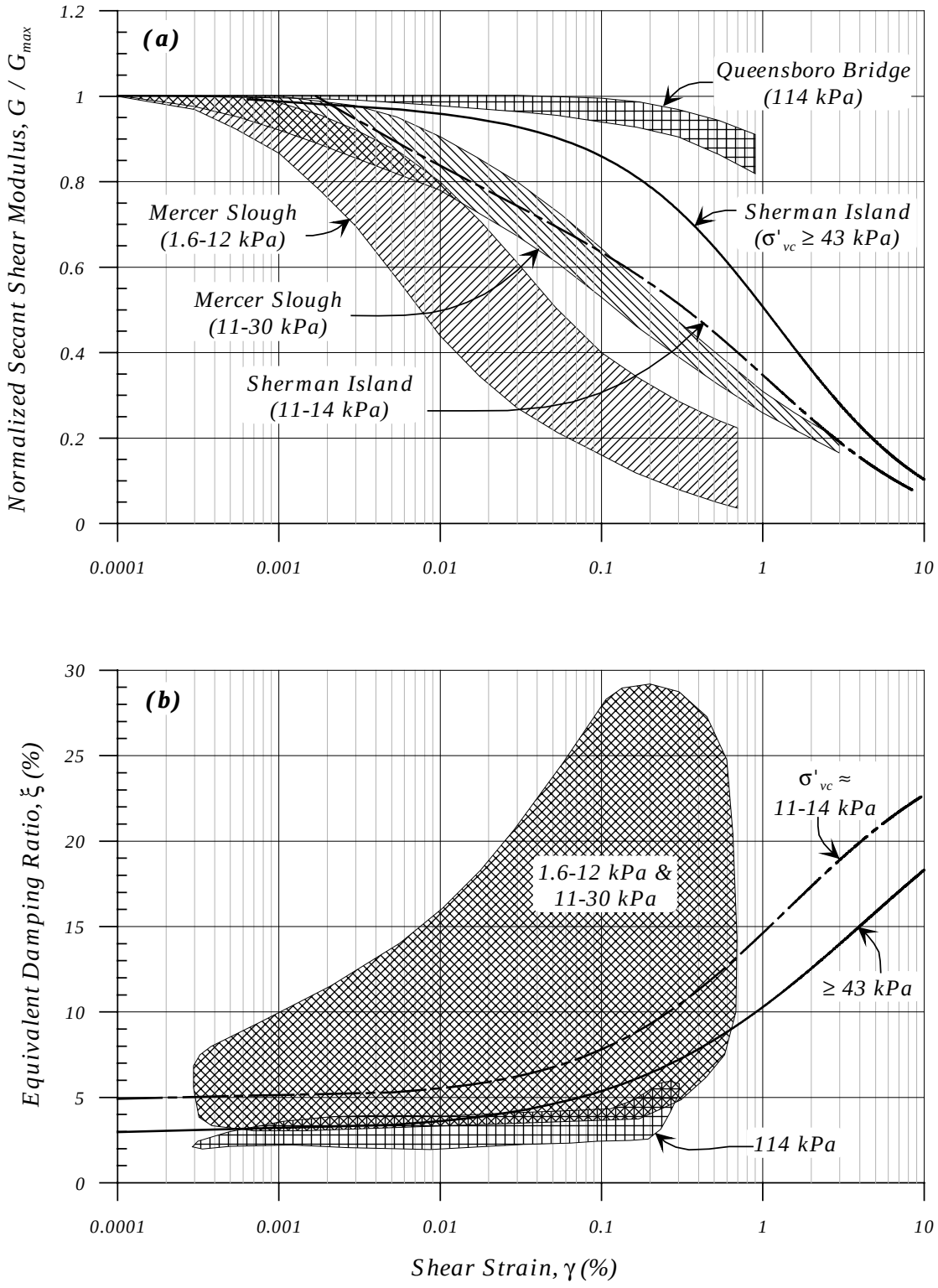

Figure 39: Effect of vertical effective consolidation stress on (a) modulus reduction and (b) damping for peat from Sherman Island (mean relations), Mercer Slough (Kramer 2000), and Queensboro Bridge (Stokoe et al. 1996) showing a possible "threshold" consolidation stress

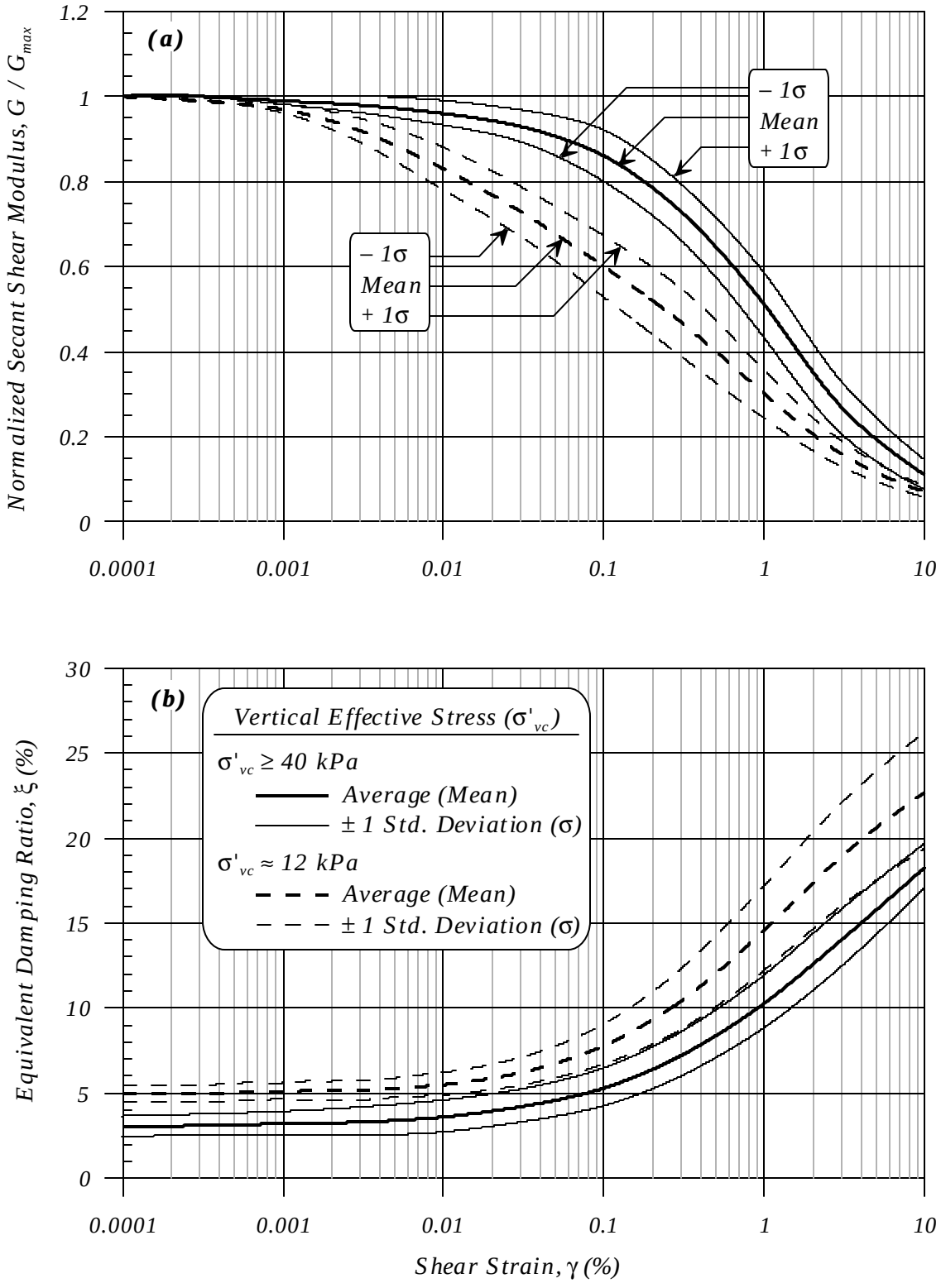

Figure 40: Recommended G/G_{max} and x relations for evaluating seismic site response of peat and peaty organic soil

Table 2: Recommended G/G_{max} and x relations for evaluating seismic site response of peat and peaty organic soil

	σ'_{vc} @ 12 kPa						σ'_{vc} > 40 kPa					
g	G/G_{max}			x (%)			G/G_{max}			x (%)		
(%)	Mean	+ 1σ	- 1σ	Mean	+ 1σ	- 1σ	Mean	+ 1σ	- 1σ	Mean	+ 1σ	- 1σ
0.0001	1.00	1.00	1.00	5.0	5.5	4.5	1.00	1.00	1.00	3.0	3.6	2.4
0.0003	0.99	0.99	0.99	5.0	5.5	4.5	1.00	1.00	1.00	3.1	3.7	2.5
0.001	0.97	0.98	0.96	5.1	5.6	4.6	0.99	1.00	0.98	3.2	3.9	2.5
0.003	0.92	0.95	0.89	5.2	5.8	4.6	0.98	1.00	0.96	3.3	4.1	2.5
0.01	0.83	0.88	0.78	5.5	6.2	4.8	0.96	0.99	0.93	3.6	4.5	2.7
0.03	0.73	0.79	0.67	6.2	7.0	5.4	0.93	0.97	0.89	4.2	5.2	3.2
0.1	0.60	0.67	0.53	7.8	9.0	6.6	0.86	0.92	0.80	5.3	6.4	4.2
0.3	0.47	0.55	0.39	10.4	12.2	8.6	0.73	0.80	0.66	7.2	8.5	5.9
1	0.30	0.36	0.24	14.6	17.1	12.1	0.51	0.59	0.43	10.3	11.8	8.8
3	0.16	0.19	0.13	18.9	21.9	15.9	0.27	0.33	0.21	14.0	15.7	12.3
10	0.07	0.08	0.06	22.7	26.1	19.3	0.11	0.15	0.07	18.3	19.6	17.0

References

Arulnathan, R., Boulanger, R. W., and Riemer, M. F. (1998). "Analysis of bender element tests." Geotechnical Testing Journal, GTJODJ, Vol. 21, No. 2, June 1998, pp.120-131.

Arulnathan, R. (2000). "Dynamic properties and site response of organic soils." Ph.D. thesis, Department of Civil and Environmental Engineering, University of California, Davis, 301 pp.

Arulnathan, R., Boulanger, R. W., Kutter, B. L., and Sluis, W. K. (2001). "New tool for shear wave velocity measurements in model tests." Geotechnical Testing Journal, GTJODJ, Vol. 23, No. 4, December, pp. 444-453.

ASTM (1996). "D 2974-87 (Reapproved 1995) – Standard test methods for moisture, ash, and organic matter of peat and other organic soils." Annual Book of ASTM Standards, American Society for Testing and Materials, Philadelphia, PA.

Boulanger, R. W., Arulnathan, R., Harder, L. F., Torres, R. A., and Driller, M. W. (1998). "Dynamic properties of Sherman Island peat." Journal of Geotechnical and Geoenvironmental Engineering, Vol. 124, No. 1, January 1998, pp. 12-20.

CDWR (1992). "Seismic stability evaluation f the Sacramento-San Joaquin Delta levees." Phase I Report: Preliminary Evaluations and Review of Previous Studies, Division of Design and Construction, Department of Water Resources (CDWR), The Resources Agency, State of California, August.

CDWR (1993). Sacramento San Joaquin Delta Atlas. California Department of Water Resources (CDWR), The Resources Agency, State of California, 122 pp.

Gookin, W. B., Riemer, M. F., Boulanger, R. W., and Bray, J. D. (1996). "Development of cyclic triaxial apparatus with broad frequency and strain ranges." Transportation Research Record 1548, TRB, National Research Council, Washington, D. C., pp.1-8.

Idriss, I. M. Dobry, R., and Singh, R. D. (1978). "Nonlinear behavior of soft clays during cyclic loading." Journal of Geotechnical Engineering Division, ASCE, 104(12), 1427-1447.

Kramer, S. L. (1993). "Seismic response – Foundations in soft soils." Final Research Report, Washington State Department of Transportation, 135 pp.

Kramer, S. L. (1996). "Dynamic response of peats." Final Research Report WA-RD 412.1, Washington State Transportation Center, University of Washington, Seattle, Washington, November.

Kramer, S. L. (1996a). *Geotechnical Earthquake Engineering*, Prentice-Hall, Inc., New Jersey.

Kramer, S. L. (2000). "Dynamic response of Mercer Slough Peat." Journal of Geotechnical and Geoenvironmental Engineering, Vol. 126, No. 6, June 2000, pp. 504-510.

Landva, A., Korpijaakko, E. O., and Pheeney, P. E. (1983). "Geotechnical classification of peats and organic soils." Testing of Peat and Organic Soils, ASTM STP 820, pp. 141-156.

Mesri, G. and Castro, A. (1987). "C_a / C_c concept and K_o during secondary compression." Journal of Geotechnical Engineering, ASCE, 113(3), 230-247.

Seed, H. B., and Idriss, I. M. (1970). "Analyses of ground motions at Union Bay, Seattle during earthquakes and distant nuclear blasts." Bulletin Seismological Society of America, 60(1), 125-136.

Stokoe, K. H. II, Bay, J. A., Rosenbald, B. L. Hwang, S. K., and Twede, M. R. (1996). "In situ seismic and dynamic laboratory measurements of geotechnical materials at Queensboro Bridge and Roosevelt Island." Geotechnical Engineering Report GR94-5, Civil Engineering Department, University of Texas at Austin, June.

Vucetic, M., and Dobry, R. (1991). "Effect of soil plasticity on cyclic response." Journal of Geotechnical Engineering, ASCE, 117(1), 89-107.

Winterkorn, Hans F. (1975) Foundation engineering handbook, edited by Hans F. Winterkorn and Hsai-Yang Fang. Van Nostrand Reinhold, New York, xvi, pp. 183-185.

Leonards, G. A. and Altschaeffl, A. G. (1964), "Compressibility of clay", Journal of the Soil Mechanics and Foundations Division, ASCE 90, No. SM5.

Appendix A: Summary Sheets for Cyclic Triaxial Tests

General Information of Tested Sample:

Borehole:	DHP - 5I1
Shelby Tube Number:	S-3
Sample Number:	1
Location of Borehole:	Mid-slope of levee
Depth below Surface:	23.7' - 24.2'
Date Sampled:	5/19/00
Date Tested:	06/26/00
Visual Description:	Dark brown silty peat: long yellowish-brown grassy fibers
Average Ash Content:	64%
Initial Density:	1.10 Mg/m^3

Water Content (%) immediately above and below the triaxial specimen at time of extrusion:

Above: (not available)
Below: 391%

Average Water Content (%) over length of sample after triaxial testing:

Average: 254%

Initial Water Content (%) back-calculated from final water content and change in volume:

Initial: 265%

Stresses on Triaxial Specimen:	σ_{vo} (kPa)	σ'_{vo} (kPa)	u (kPa)
Estimated In-situ:	100	45	55
Consolidation in Lab:	100	45	55

Average shear wave velocity measured prior to triaxial testing by means of bender elements:

Vs = 41 m/s

Summary of Test Data for Shear Strain g, Shear Modulus G, and Damping Ratio x:

1st cycle			2nd cycle			3rd cycle		
g (%)	G (kPa)	x (%)	g (%)	G (kPa)	x (%)	g (%)	G (kPa)	x (%)
0.00123	4070	3.1	0.00101	4024	2.9	0.00102	4034	3.6
0.00291	4079	2.8	0.00240	4030	4.0	0.00243	4092	3.6
0.00557	3990	3.2	0.00476	3909	3.8	0.00469	3883	4.0
0.01058	3964	3.1	0.00984	3841	4.3	0.00987	3846	4.1
0.03178	3775	4.1	0.02878	3809	4.9	0.02835	3838	5.0
0.10416	3518	4.9	0.10404	3510	5.1	0.10365	3507	5.1
0.35764	2891	7.1	0.35672	2849	7.1	0.35669	2828	7.1
2.96450	778	14.4	2.98440	744	13.8	2.98440	733	13.5
8.74710	428	18.6	8.86710	386	17.5	8.89110	368	17.1

4th cycle			5th cycle		
g (%)	G (kPa)	x (%)	g (%)	G (kPa)	x (%)
0.00099	3990	3.7	0.00100	4040	3.5
0.00241	4029	3.4	0.00243	4081	3.4
0.00468	3907	4.0	0.00467	3932	4.2
0.00983	3857	4.0	0.00980	3902	3.9
0.02831	3845	5.0	0.02861	3808	4.9
0.10337	3504	5.0	0.10381	3494	5.1
0.35670	2818	7.1	0.35660	2805	7.1
2.98410	725	13.4	2.98270	720	13.3
8.89040	359	16.9	8.88750	353	16.7

Modulus Reduction Curve

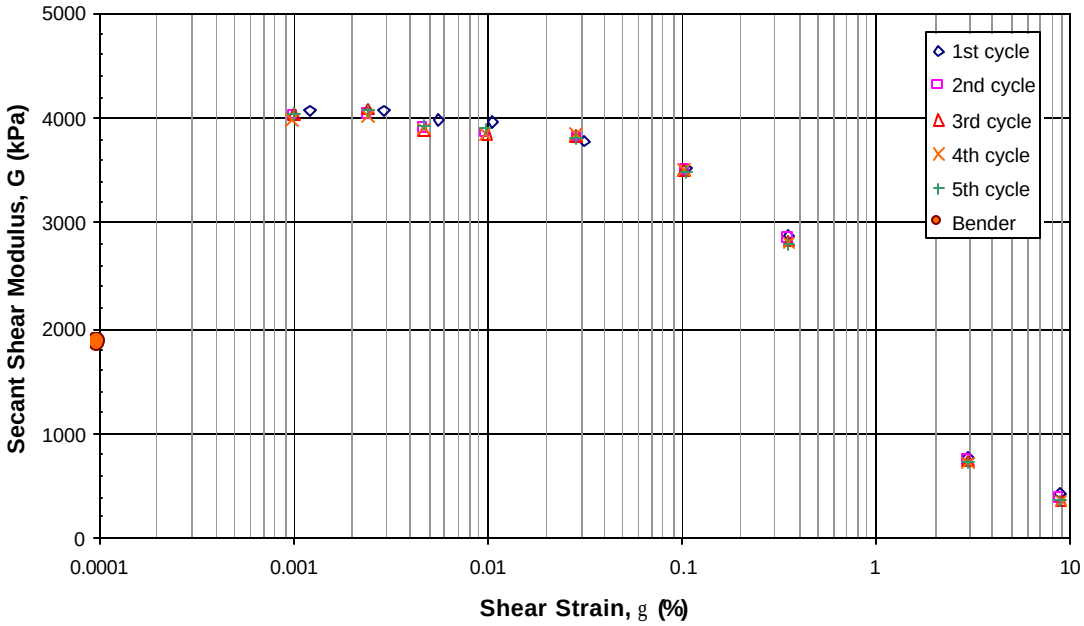

Damping Ratio Curve

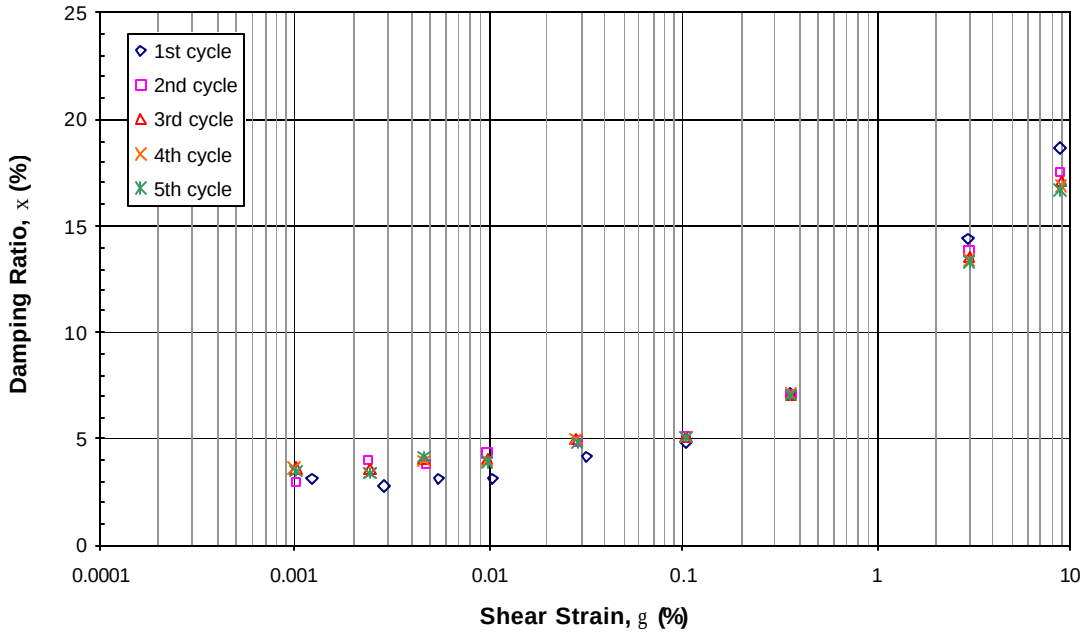

General Information of Tested Sample:

Borehole:	DHP - 5J1
Shelby Tube Number:	S-6
Sample Number:	2
Location of Borehole:	Free-field
Depth below Surface:	19.6' - 20.2'
Date Sampled:	5/19/00
Date Tested:	07/03/00
Visual Description:	Soft, spongy dark brown peat; long yellowish-brown fibers
Average Ash Content:	66%
Initial Density:	1.145 Mg/m^3

Water Content (%) immediately above and below the triaxial specimen at time of extrusion:

Above: 492%
Below: 357%

Average Water Content (%) over length of sample after triaxial testing:

Average: 376%

Initial Water Content (%) back-calculated from final water content and change in volume:

Initial: 430%

Stresses on Triaxial Specimen:	σ_{vo} (kPa)	σ'_{vo} (kPa)	u (kPa)
Estimated In-situ:	63	12	51
Consolidation in Lab:	63	12	51

Average shear wave velocity measured prior to triaxial testing by means of bender elements:

Vs = 21 m/s

Summary of Test Data for Shear Strain γ, Shear Modulus G, and Damping Ratio χ:

1st cycle			2nd cycle			3rd cycle		
γ (%)	G (kPa)	χ (%)	γ (%)	G (kPa)	χ (%)	γ (%)	G (kPa)	χ (%)
0.00148	843	9.1	0.00132	991	8.2	0.00135	962	10.3
0.00782	654	14.6	0.00723	776	11.9	0.00755	772	10.6

4th cycle			5th cycle		
γ (%)	G (kPa)	χ (%)	γ (%)	G (kPa)	χ (%)
0.00142	997	4.7	0.00149	1031	5.4
0.00802	773	9.8	0.00837	756	9.8

Modulus Reduction Curve

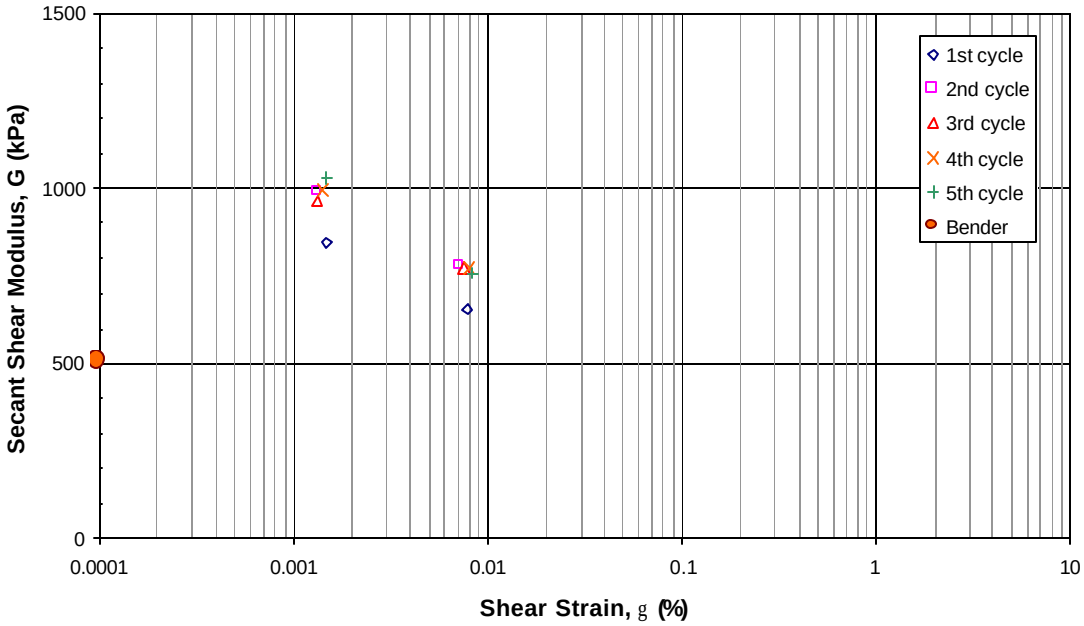

Damping Ratio Curve

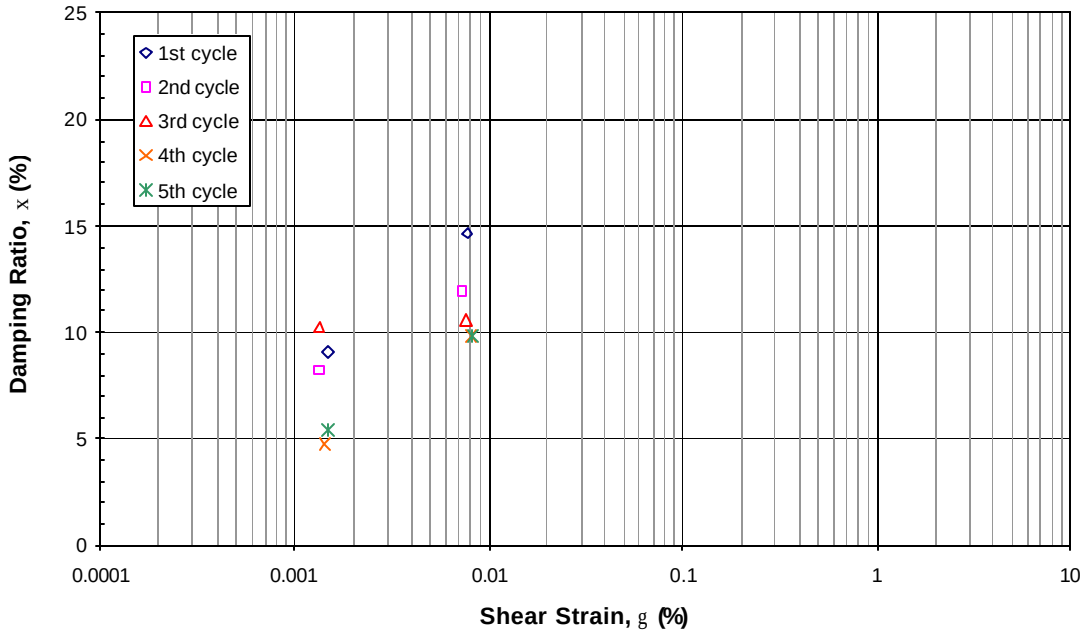

General Information of Tested Sample:

Borehole:	DHP - 5H3
Shelby Tube Number:	S-2
Sample Number:	3
Location of Borehole:	Levee bench
Depth below Surface:	39.1' - 39.7'
Date Sampled:	5/18/00
Date Tested:	7/6/00
Visual Description:	Dark brown, med-stiff, silty peat; yellow-brown woody fibers
Average Ash Content:	62%
Initial Density:	1.198 Mg/m^3

Water Content (%) immediately above and below the triaxial specimen at time of extrusion:

Above: 204%

Below: 218%

Average Water Content (%) over length of sample after triaxial testing:

Average: 178%

Initial Water Content (%) back-calculated from final water content and change in volume:

Initial: 185%

Stresses on Triaxial Specimen:	σ_{vo} (kPa)	σ'_{vo} (kPa)	u (kPa)
Estimated In-situ:	177	78	98
Consolidation in Lab:	177	78	98

Average shear wave velocity measured prior to triaxial testing by means of bender elements:

Vs = 95 m/s

Summary of Test Data for Shear Strain g, Shear Modulus G, and Damping Ratio x:

1st cycle			2nd cycle			3rd cycle		
g (%)	G (kPa)	x (%)	g (%)	G (kPa)	x (%)	g (%)	G (kPa)	x (%)
0.00128	11546	--	0.00130	11590	--	0.00128	11615	--
0.00470	11048	3.3	0.00469	11144	3.5	0.00468	11170	3.5
0.01365	11281	2.8	0.01360	11333	3.2	0.01358	11333	3.1
0.03655	11323	2.2	0.03723	11133	2.8	0.03444	11101	4.2
0.06043	10847	2.8	0.06167	10853	3.1	0.06049	10851	3.1
0.19295	8538	6.6	0.19071	8623	6.7	0.19095	8663	6.6
0.44857	5931	12.2	0.36208	6841	14.2	0.39607	6381	9.9
0.06201	10606	3.0	0.06202	10608	2.5	0.06251	10598	2.7
2.91680	1880	13.6	2.92550	1815	14.2	2.92620	1790	13.9
8.97450	1028	20.1	9.11990	911	19.3	9.11720	872	18.9
0.06650	7701	5.2	0.06368	7549	6.2	0.06406	7513	6.3
0.76177	2496	12.3	0.76498	2394	12.9	0.76501	2366	12.9

4th cycle			5th cycle		
g (%)	G (kPa)	x (%)	g (%)	G (kPa)	x (%)
0.00130	11550	--	0.00128	11589	--
0.00468	11154	3.5	0.00469	11130	3.6
0.01359	11330	3.2	0.01360	11334	3.2
0.03705	11186	3.7	0.03718	11053	2.5
0.06073	10847	3.2	0.06119	10798	3.1
0.19051	8696	6.4	0.18857	8726	6.3
0.37860	6543	9.4	0.36419	6740	9.1
0.06265	10589	2.7	0.06270	10545	2.8
2.92610	1770	13.7	2.92410	1759	13.6
9.11620	847	18.5	9.11260	823	18.5
0.06443	7481	6.3	0.06484	7453	6.4
0.76706	2337	12.8	0.76718	2321	12.8

Modulus Reduction Curve

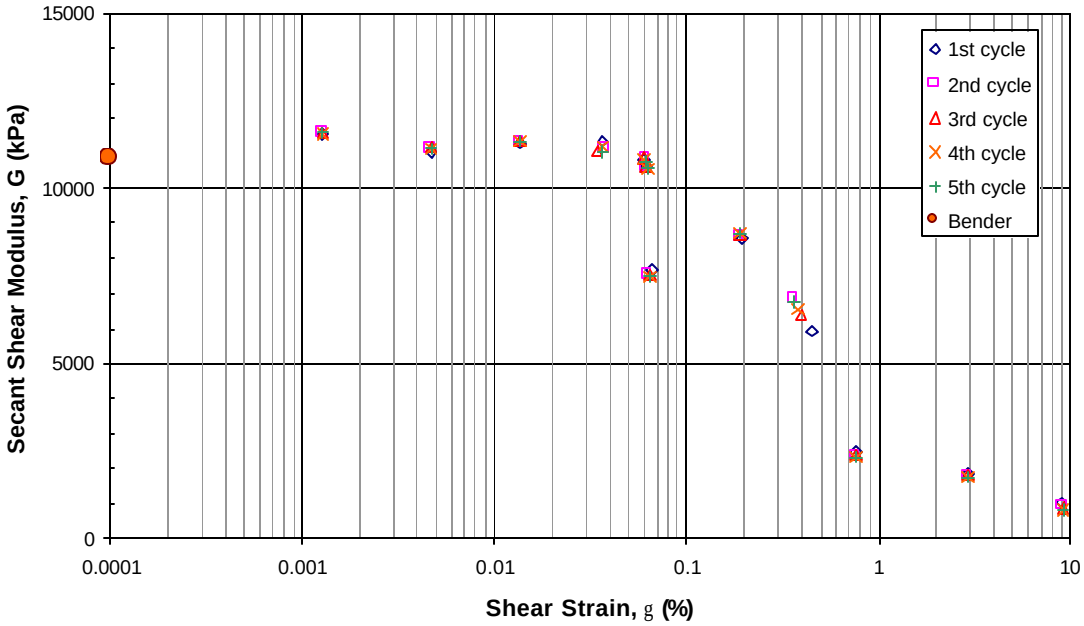

Damping Ratio Curve

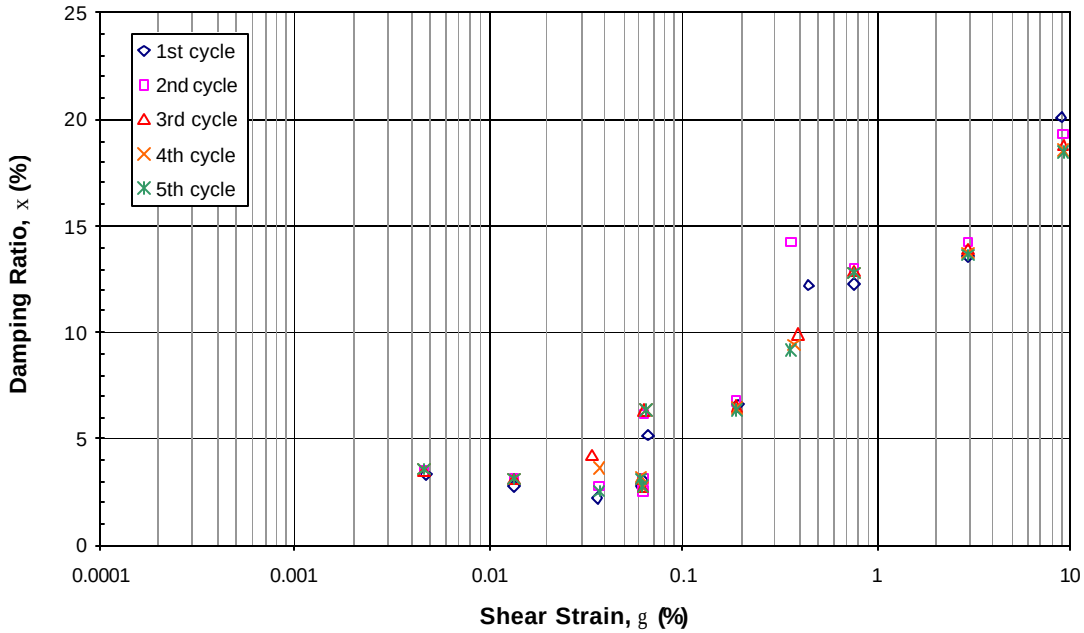

General Information of Tested Sample:

Borehole:	DHP - 5J1
Shelby Tube Number:	S-7
Sample Number:	4
Location of Borehole:	Free-field
Depth below Surface:	22.7' - 23.2'
Date Sampled:	5/19/00
Date Tested:	07/11/00
Visual Description:	Soft, spongy dark brown peat; long yellowish-brown fibers
Average Ash Content:	63%
Initial Density:	1.116 Mg/m^3

Water Content (%) immediately above and below the triaxial specimen at time of extrusion:

Above: 472%

Below: 576%

Average Water Content (%) over length of sample after triaxial testing:

Average: 396%

Initial Water Content (%) back-calculated from final water content and change in volume:

Initial: 442%

Stresses on Triaxial Specimen:	σ_{vo} (kPa)	σ'_{vo} (kPa)	u (kPa)
Estimated In-situ:	73	13	60
Consolidation in Lab:	73	13	60

Average shear wave velocity measured prior to triaxial testing by means of bender elements:

Vs = 23 m/s

Summary of Test Data for Shear Strain g, Shear Modulus G, and Damping Ratio x:

1st cycle			2nd cycle			3rd cycle		
g (%)	G (kPa)	x (%)	g (%)	G (kPa)	x (%)	g (%)	G (kPa)	x (%)
0.00175	959	--	0.00173	1041	--	0.00173	974	--
0.00620	871	5.6	0.00615	869	5.2	0.00616	881	5.6
0.01898	808	4.8	0.01896	802	5.0	0.01895	807	5.0
0.03740	703	5.2	0.03710	702	5.9	0.03728	698	6.0
0.09517	635	6.9	0.09476	633	7.6	0.09466	630	7.6
0.30533	507	10.6	0.30474	503	10.9	0.30483	500	11.0
0.95053	374	11.7	0.94979	370	11.7	0.94865	368	11.3
0.09486	604	8.2	0.09464	601	8.6	0.09471	599	8.7
2.99650	159	22.4	3.02900	151	20.0	3.02730	148	19.4
8.41830	84	23.9	8.55240	77	22.9	8.57340	73	22.9
0.09530	423	8.9	0.09436	434	9.8	0.09443	436	9.7
0.80467	266	12.4	0.80372	270	11.4	0.80254	269	11.1

4th cycle			5th cycle		
g (%)	G (kPa)	x (%)	g (%)	G (kPa)	x (%)
0.00172	1001	--	0.00173	1003	--
0.00615	872	5.3	0.00616	872	5.7
0.01894	812	5.0	0.01894	814	5.0
0.03712	697	6.0	0.03711	697	5.9
0.09461	627	7.7	0.09450	626	7.7
0.30468	499	10.8	0.30470	497	10.8
0.94740	369	11.6	0.94467	371	11.7
0.09472	597	8.5	0.09469	595	8.6
3.02880	146	19.6	3.02760	145	19.2
8.55080	72	22.4	8.57180	70	22.3
0.09455	437	9.7	0.09445	435	9.5
0.79909	272	11.0	0.79713	274	10.8

Modulus Reduction Curve

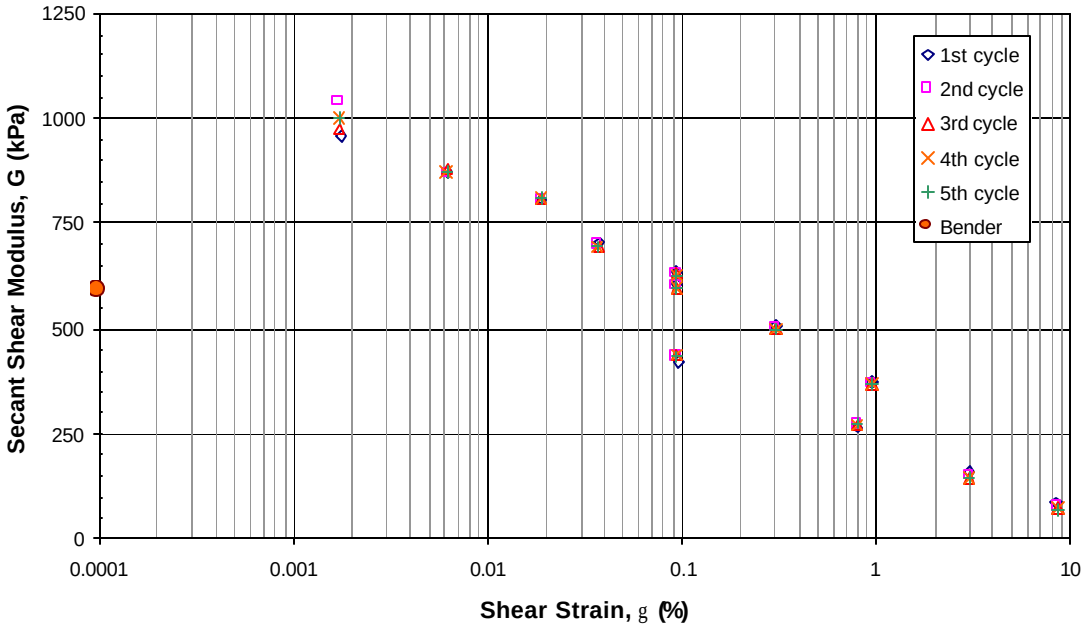

Damping Ratio Curve

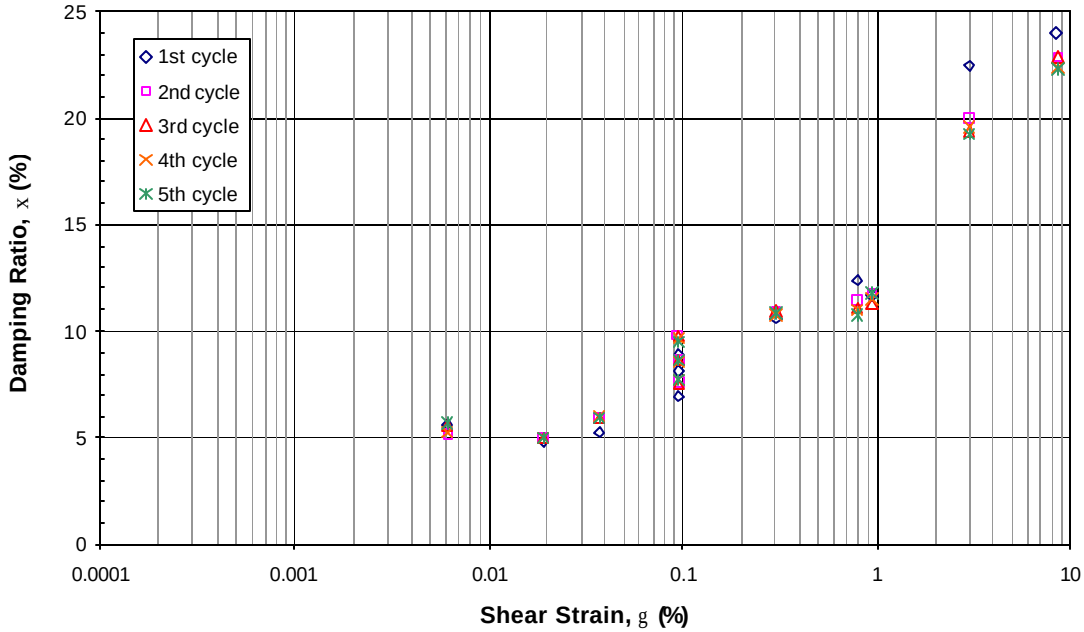

General Information of Tested Sample:

Borehole:	DHP - 5I1
Shelby Tube Number:	S-3
Sample Number:	6
Location of Borehole:	Mid-slope of levee
Depth below Surface:	22.5' - 23.0'
Date Sampled:	5/19/00
Date Tested:	07/29/00
Visual Description:	Firm, dark brown silty peat; brown, hairlike fibers with some yellowish-brown grassy fibers; 1-mm-thick sloping band of grey silt or clay at 2.5 cm from bottom of sample.
Average Ash Content:	49%
Initial Density:	1.102 Mg/m^3

Water Content (%) immediately above and below the triaxial specimen at time of extrusion:

Above: 510%

Below: 310%

Average Water Content (%) over length of sample after triaxial testing:

Average: 316%

Initial Water Content (%) back-calculated from final water content and change in volume:

Initial: 334%

Stresses on Triaxial Specimen:	σ_{vo} (kPa)	σ'_{vo} (kPa)	u (kPa)
Estimated In-situ:	100	45	55
Consolidation in Lab:	100	45	55

Average shear wave velocity measured prior to triaxial testing by means of bender elements:

Vs = (Not measurable)

Summary of Test Data for Shear Strain γ, Shear Modulus G, and Damping Ratio χ:

1st cycle			2nd cycle			3rd cycle		
γ (%)	G (kPa)	χ (%)	γ (%)	G (kPa)	χ (%)	γ (%)	G (kPa)	χ (%)
0.00163	2457	3.5	0.00163	2492	3.8	0.00162	2511	3.5
0.00558	2450	3.0	0.00556	2447	3.1	0.00555	2439	3.1
0.01638	2418	3.2	0.01632	2428	3.5	0.01630	2431	3.5
0.03595	2375	3.4	0.03463	2395	3.7	0.03476	2398	3.7
0.08691	2305	4.2	0.08676	2312	4.9	0.08660	2311	4.9
0.27968	2048	6.6	0.27931	2041	6.9	0.27912	2035	6.9
0.87624	1567	9.9	0.87778	1533	9.9	0.87868	1521	9.8
2.93340	936	12.7	2.94610	890	12.4	2.94620	876	12.1
8.14170	512	18.2	8.24270	459	16.9	8.25660	441	16.4

4th cycle			5th cycle		
γ (%)	G (kPa)	χ (%)	γ (%)	G (kPa)	χ (%)
0.00162	2482	3.7	0.00161	2449	3.9
0.00556	2438	3.1	0.00557	2445	3.1
0.01630	2431	3.4	0.01637	2428	3.4
0.03480	2398	3.7	0.03468	2399	3.7
0.08657	2311	4.8	0.08667	2306	4.8
0.27919	2029	6.9	0.27964	2019	6.9
0.87922	1509	9.8	0.87960	1504	9.7
2.94580	867	12.0	2.95080	856	11.8
8.25580	430	16.1	8.26850	420	15.9

Summary of Test Data for Different Loading Frequencies:

***Shear Strain* = 0.0016%**

cycle	G (kPa)
1	2457
2	2492
3	2511
4	2482
5	2449

cycle	G (kPa)
6	2263
7	2269
8	2030
9	1856
10	2112

cycle	G (kPa)
11	2488
12	2486
13	2466
14	2454
15	2482

cycle	G (kPa)
16	2052
17	2252
18	1987
19	2262
20	2085

cycle	G (kPa)
21	2496
22	2481
23	2494
24	2496
25	2505

cycle	G (kPa)
26	2216
27	2180
28	2039
29	1826
30	2173

***Shear Strain* = 0.016 %**

cycle	G (kPa)
1	2418
2	2428
3	2431
4	2431
5	2428

cycle	G (kPa)
6	1999
7	2002
8	2003
9	1988
10	2005

cycle	G (kPa)
11	2420
12	2429
13	2434
14	2431
15	2427

cycle	G (kPa)
16	1987
17	2001
18	1993
19	1992
20	2007

cycle	G (kPa)
21	2423
22	2436
23	2431
24	2429
25	2428

cycle	G (kPa)
26	1980
27	1997
28	2001
29	2009
30	1989

***Shear Strain* = 0.88 %**

cycle	G (kPa)
1	1567
2	1533
3	1521
4	1509
5	1504

cycle	G (kPa)
6	1236
7	1219
8	1207
9	1203
10	1197

cycle	G (kPa)
11	1502
12	1482
13	1471
14	1465
15	1461

cycle	G (kPa)
16	1210
17	1197
18	1192
19	1188
20	1186

cycle	G (kPa)
21	1491
22	1469
23	1462
24	1457
25	1454

cycle	G (kPa)
26	1205
27	1193
28	1188
29	1185
30	1183

Modulus Reduction Curve

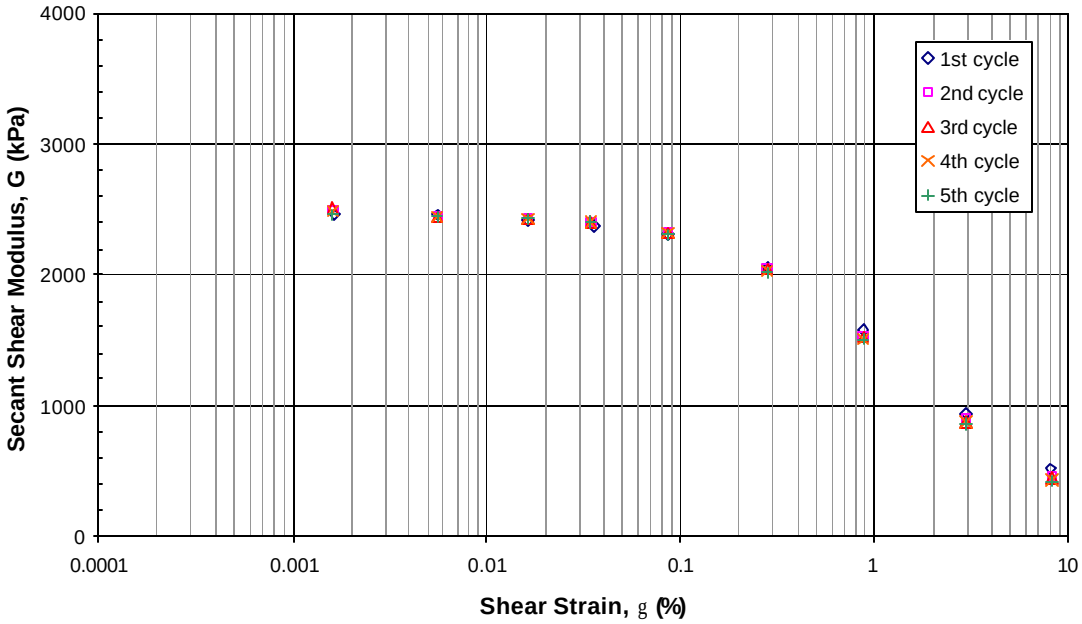

Damping Ratio Curve

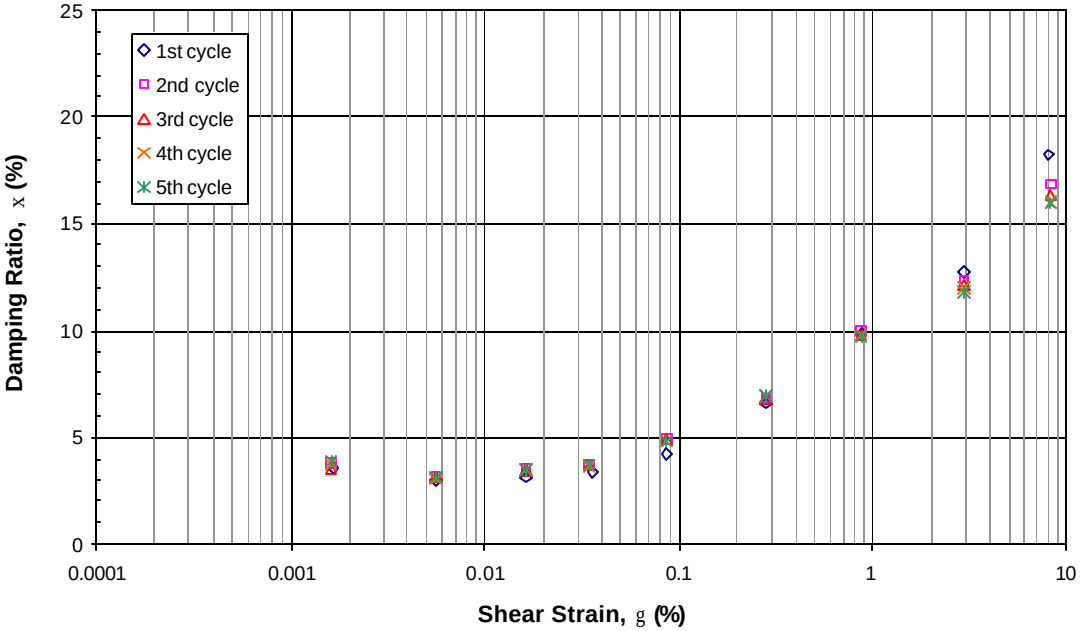

Effect of Loading Frequency on Secant Modulus

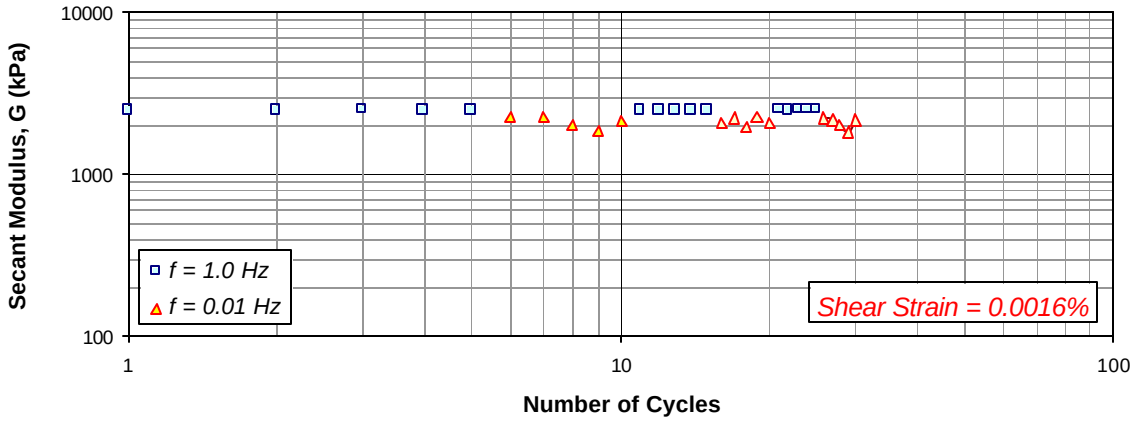

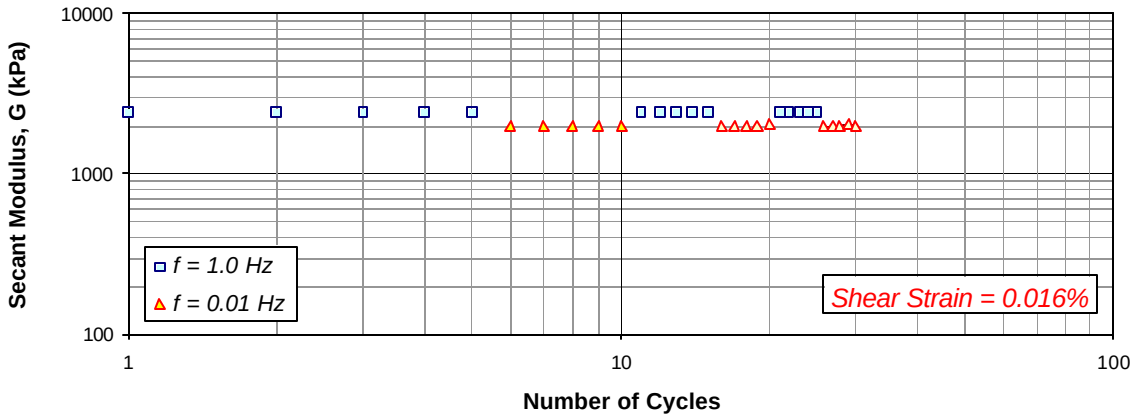

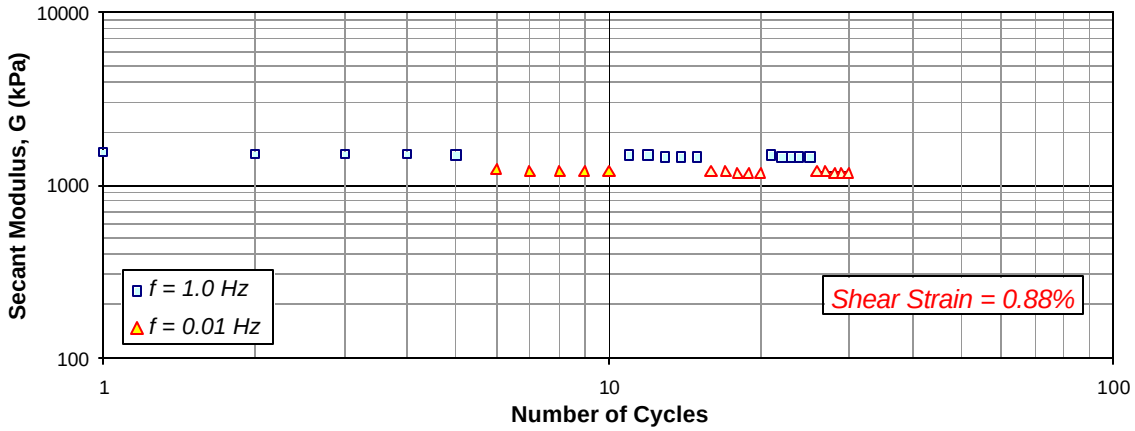

General Information of Tested Sample:

Borehole:	DHP - 5J1
Shelby Tube Number:	S-9
Sample Number:	7
Location of Borehole:	Free-field
Depth below Surface:	29.2' - 29.7'
Date Sampled:	5/19/00
Date Tested:	08/01/00
Visual Description:	Very soft, peaty silt; many large patches of grey silt or clay; fine brown fibers w/ some yellowish brown grassy fibers mixed within. Few patches of dense, dark brown peat.
Average Ash Content:	79%
Initial Density:	1.197 Mg/m^3

Water Content (%) immediately above and below the triaxial specimen at time of extrusion:

Above: 244%

Below: 281%

Average Water Content (%) over length of sample after triaxial testing:

Average: 226%

Initial Water Content (%) back-calculated from final water content and change in volume:

Initial: 236%

Stresses on Triaxial Specimen:	σ_{vo} (kPa)	σ'_{vo} (kPa)	u (kPa)
Estimated In-situ:	92	14	78
Consolidation in Lab:	92	14	78

Average shear wave velocity measured prior to triaxial testing by means of bender elements:

Vs = (Not Measurable)

Summary of Test Data for Shear Strain γ, Shear Modulus G, and Damping Ratio λ:

1st cycle			2nd cycle			3rd cycle		
γ (%)	G (kPa)	λ (%)	γ (%)	G (kPa)	λ (%)	γ (%)	G (kPa)	λ (%)
0.00181	379	--	0.00180	361	--	0.00182	371	--
0.00646	292	5.4	0.00639	299	5.9	0.00643	283	5.8
0.01888	273	5.6	0.01886	271	5.6	0.01886	273	6.1
0.00189	355	--	0.00186	366	--	0.00188	359	--
0.01886	270	5.6	0.01882	273	5.9	0.01882	271	6.1
0.03939	241	7.9	0.03908	233	7.2	0.03894	232	7.1
0.09898	207	7.2	0.09762	201	10.1	0.09748	197	10.4
0.31081	152	14.0	0.31083	149	13.9	0.31080	148	14.0
0.97921	95	10.3	0.97650	91	12.0	0.97646	91	11.7
0.09804	175	10.8	0.09774	171	12.1	0.09777	170	12.0
3.07570	66	25.3	3.08010	62	25.3	3.09090	59	25.6
7.79580	29	21.5	7.82260	26	21.2	7.82180	26	20.4
0.09766	119	11.8	0.09733	117	13.5	0.09764	116	13.6
0.96260	58	20.0	0.97546	51	16.2	0.97387	53	14.5
7.82390	27	18.8	7.84430	25	19.5	7.82310	25	18.8

4th cycle			5th cycle		
γ (%)	G (kPa)	λ (%)	γ (%)	G (kPa)	λ (%)
0.00182	366	--	0.00182	362	--
0.00639	287	5.7	0.00642	284	5.9
0.01886	268	5.9	0.01893	269	6.0
0.00188	340	--	0.00187	330	--
0.01882	273	5.7	0.01889	271	6.1
0.03857	232	7.0	0.03903	231	7.1
0.09741	197	10.4	0.09783	197	10.1
0.31027	146	14.2	0.31201	146	13.8
0.97563	89	11.9	0.97835	89	12.3
0.09765	169	12.2	0.09791	169	12.1
3.09100	58	24.7	3.09390	57	26.2
7.84260	25	20.3	7.85200	25	19.6
0.09705	112	15.0	0.09727	110	15.8
0.97592	51	17.3	0.98035	52	14.5
7.84140	24	18.7	7.85040	24	18.5

Modulus Reduction Curve

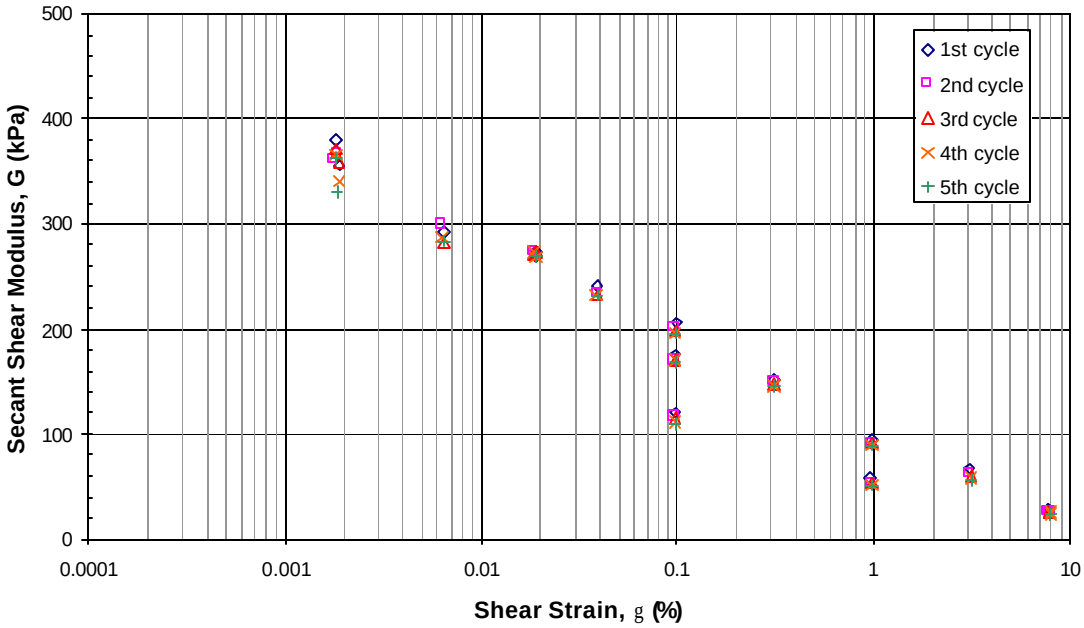

Damping Ratio Curve

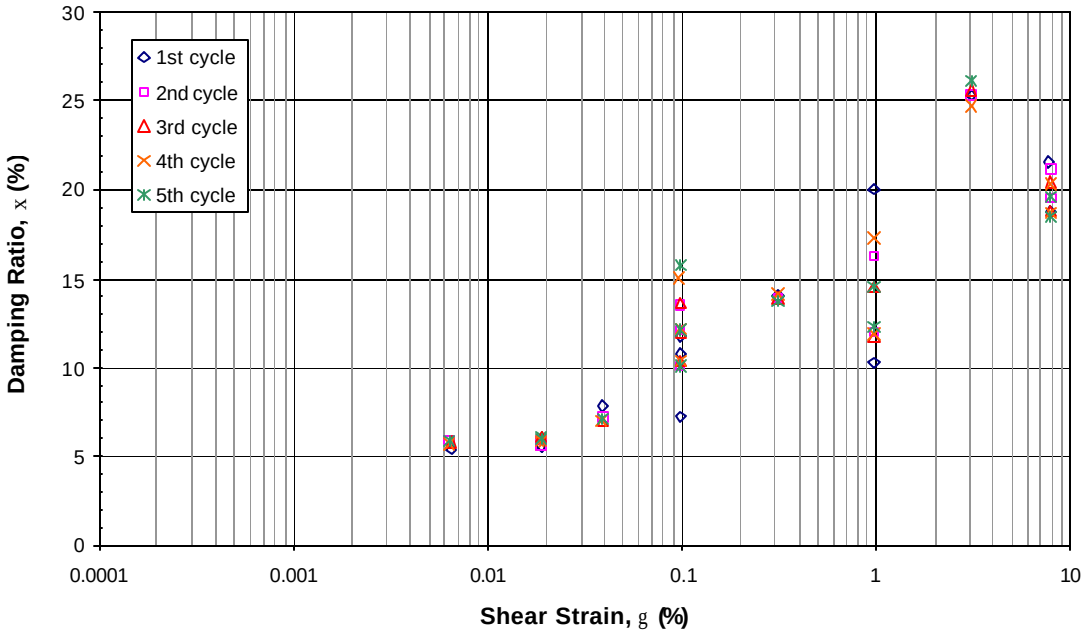

General Information of Tested Sample:

Borehole:	DHP - 5I1
Shelby Tube Number:	S-2
Sample Number:	8
Location of Borehole:	Mid-slope of levee
Depth below Surface:	20.6' - 21.2'
Date Sampled:	5/19/00
Date Tested:	08/03/00
Visual Description:	Firm, dense, dark brown peat w/ few fines. Mostly fine, horizontally laid, dark brown fibers with very few yellowish-brown grassy fibers. Few specks of black coal/ash.
Average Ash Content:	52%
Initial Density:	1.079 Mg/m^3

Water Content (%) immediately above and below the triaxial specimen at time of extrusion:

Above: 382%

Below: 376%

Average Water Content (%) over length of sample after triaxial testing:

Average: 348%

Initial Water Content (%) back-calculated from final water content and change in volume:

Initial: 409%

Stresses on Triaxial Specimen:	σ_{vo} (kPa)	σ'_{vo} (kPa)	u (kPa)
Estimated In-situ:	86	43	43
Consolidation in Lab:	172	86	86

Average shear wave velocity measured prior to triaxial testing by means of bender elements:

Vs = 58 m/s

Summary of Test Data for Shear Strain γ, Shear Modulus G, and Damping Ratio χ:

1st cycle			2nd cycle			3rd cycle		
γ (%)	G (kPa)	χ (%)	γ (%)	G (kPa)	χ (%)	γ (%)	G (kPa)	χ (%)
0.00123	2962	3.5	0.00119	2970	4.2	0.00121	2922	4.2
0.00507	2852	2.9	0.00506	2856	3.4	0.00507	2856	3.3
0.01622	2834	3.2	0.01621	2844	3.6	0.01623	2843	3.6
0.00132	2942	3.2	0.00129	2923	3.3	0.00129	2906	3.5
0.03573	2813	3.2	0.03495	2828	3.5	0.03490	2830	3.6
0.08898	2735	4.0	0.08813	2735	4.4	0.08774	2731	4.5
0.28156	2408	6.0	0.28165	2394	6.2	0.28170	2383	6.2
0.88579	1811	9.5	0.88596	1789	9.5	0.88828	1764	9.4
0.08839	2550	4.5	0.08802	2546	5.0	0.08802	2542	5.1
2.92880	1022	16.8	2.94570	965	16.1	2.95170	940	15.7
8.11860	519	21.9	8.25630	458	20.7	8.27370	437	20.1
0.08932	1832	5.8	0.08893	1831	6.6	0.08897	1829	6.6
0.89632	1181	11.7	0.89851	1148	12.4	0.89862	1138	12.6

4th cycle			5th cycle		
γ (%)	G (kPa)	χ (%)	γ (%)	G (kPa)	χ (%)
0.00119	3036	3.7	0.00120	2983	3.1
0.00509	2855	3.3	0.00512	2855	3.4
0.01626	2844	3.6	0.01632	2847	3.5
0.00129	2941	3.0	0.00128	2923	3.5
0.03490	2826	3.7	0.03486	2824	3.6
0.08771	2729	4.5	0.08779	2724	4.5
0.28164	2374	6.2	0.28184	2368	6.1
0.88876	1751	9.3	0.88941	1743	9.3
0.08803	2539	5.1	0.08809	2534	5.1
2.95200	924	15.4	2.95760	912	15.1
8.27230	426	19.7	8.28820	415	19.5
0.08894	1826	6.7	0.08907	1826	6.6
0.89885	1129	12.6	0.89921	1126	12.6

Modulus Reduction Curve

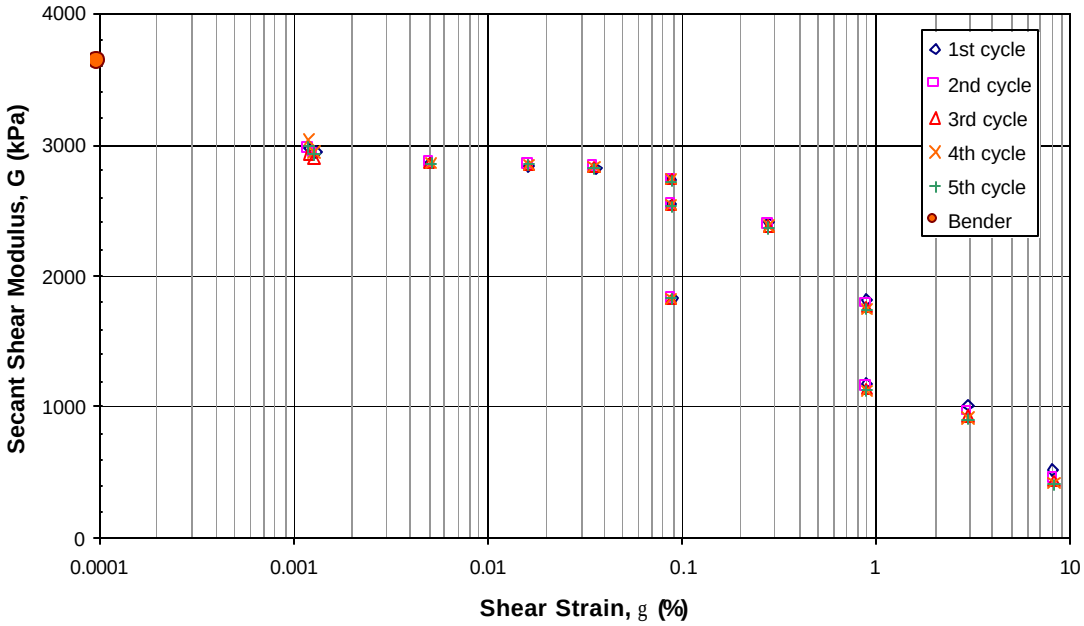

Damping Ratio Curve

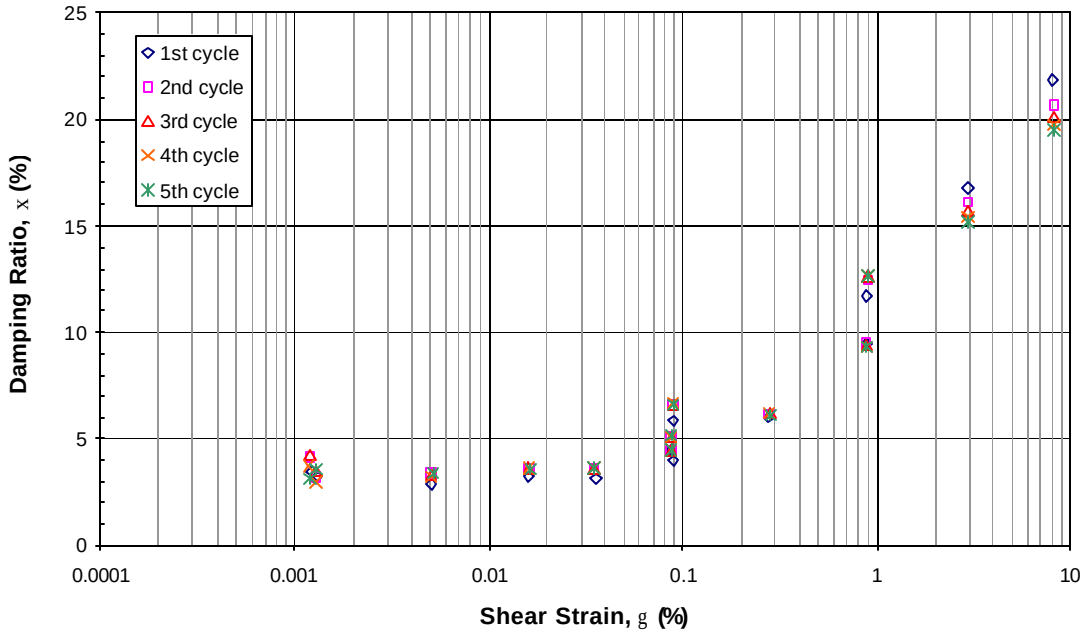

General Information of Tested Sample:

Borehole:	DHP - 5I1
Shelby Tube Number:	S-2
Sample Number:	9
Location of Borehole:	Mid-slope of levee
Depth below Surface:	19.9' - 20.5'
Date Sampled:	5/19/00
Date Tested:	08/09/00
Visual Description:	Firm, dense, dark brown peat with some fines; brown, thin, hairlike fibers; very homogeneous except for a small vein of black ash/coal.
Average Ash Content:	53%
Initial Density:	1.168 Mg/m^3

Water Content (%) immediately above and below the triaxial specimen at time of extrusion:

Above: 372%

Below: 376%

Average Water Content (%) over length of sample after triaxial testing:

Average: 321%

Initial Water Content (%) back-calculated from final water content and change in volume:

Initial: 406%

Stresses on Triaxial Specimen:	σ_{vo} (kPa)	σ'_{vo} (kPa)	u (kPa)
Estimated In-situ:	86	43	43
Consolidation in Lab:	172	86	86

Average shear wave velocity measured prior to triaxial testing by means of bender elements:

Vs = (Not measured)

Summary of Test Data for Shear Strain γ, Shear Modulus G, and Damping Ratio λ:

1st cycle			2nd cycle			3rd cycle		
γ (%)	G (kPa)	λ (%)	γ (%)	G (kPa)	λ (%)	γ (%)	G (kPa)	λ (%)
0.00046	3648	--	0.00046	3677	--	0.00047	3627	--
0.00151	3598	2.3	0.00149	3608	2.6	0.00150	3579	2.2
0.00501	3533	2.8	0.00513	3564	3.2	0.00516	3561	3.1
0.01530	3489	3.3	0.01539	3502	3.8	0.01545	3495	3.7
0.03560	3436	3.4	0.03446	3445	4.0	0.03450	3445	4.0
0.08651	3331	4.2	0.08585	3332	4.7	0.08571	3325	4.7
0.27557	2923	5.8	0.27510	2904	6.0	0.27519	2889	6.0
0.87900	2174	9.5	0.87574	2146	9.5	0.87526	2124	9.4
2.90060	1271	14.4	2.92320	1199	14.1	2.92350	1174	14.0
8.04070	659	20.9	8.19440	579	19.7	8.19490	556	19.1

4th cycle			5th cycle		
γ (%)	G (kPa)	λ (%)	γ (%)	G (kPa)	λ (%)
0.00046	3669	--	0.00047	3615	--
0.00151	3599	2.8	0.00151	3556	2.8
0.00517	3560	3.1	0.00519	3556	3.2
0.01549	3492	3.7	0.01554	3497	3.7
0.03383	3448	4.0	0.03372	3451	4.0
0.08556	3328	4.7	0.08573	3323	4.7
0.27526	2882	6.0	0.27539	2876	5.9
0.87601	2102	9.4	0.87627	2092	9.3
2.92920	1155	13.8	2.92930	1142	13.7
8.19450	542	18.8	8.21060	529	18.6

Summary of Test Data for Different Loading Frequencies:

***Shear Strain* = 0.0015%**

cycle	G (kPa)
1	3598
2	3608
3	3579
4	3599
5	3556

cycle	G (kPa)
6	3297
7	3633
8	2480
9	2504
10	2093

cycle	G (kPa)
11	3565
12	3588
13	3563
14	3553
15	3549

cycle	G (kPa)
16	4024
17	2530
18	3847
19	2397
20	2510

cycle	G (kPa)
21	3535
22	3573
23	3599
24	3577
25	3659

cycle	G (kPa)
26	4009
27	3003
28	2652
29	2985
30	2732

***Shear Strain* = 0.015 %**

cycle	G (kPa)
1	3489
2	3502
3	3495
4	3492
5	3497

cycle	G (kPa)
6	2852
7	2828
8	2842
9	2712
10	2784

cycle	G (kPa)
11	3466
12	3480
13	3482
14	3476
15	3475

cycle	G (kPa)
16	2849
17	2825
18	2717
19	2710
20	2783

cycle	G (kPa)
21	3508
22	3512
23	3510
24	3509
25	3509

cycle	G (kPa)
26	2785
27	2769
28	2844
29	2764
30	2792

***Shear Strain* = 0.88 %**

cycle	G (kPa)
1	2174
2	2146
3	2124
4	2102
5	2092

cycle	G (kPa)
6	1673
7	1641
8	1621
9	1612
10	1603

cycle	G (kPa)
11	2088
12	2055
13	2033
14	2024
15	2020

cycle	G (kPa)
16	1640
17	1615
18	1603
19	1597
20	1595

cycle	G (kPa)
21	2064
22	2033
23	2025
24	2008
25	2004

cycle	G (kPa)
26	1624
27	1607
28	1599
29	1592
30	1589

Modulus Reduction Curve

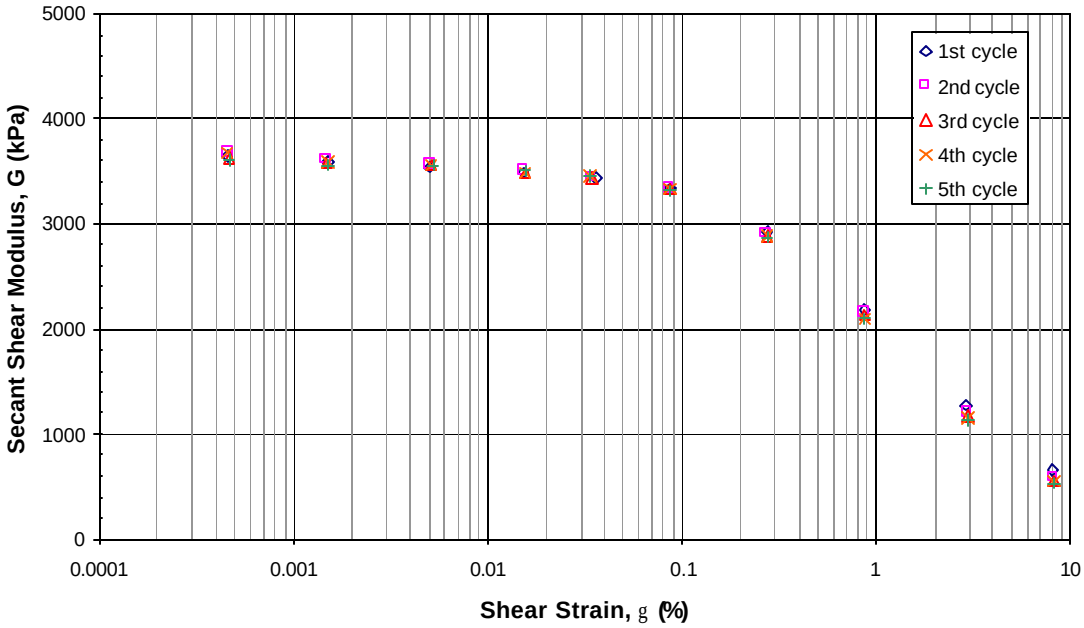

Damping Ratio Curve

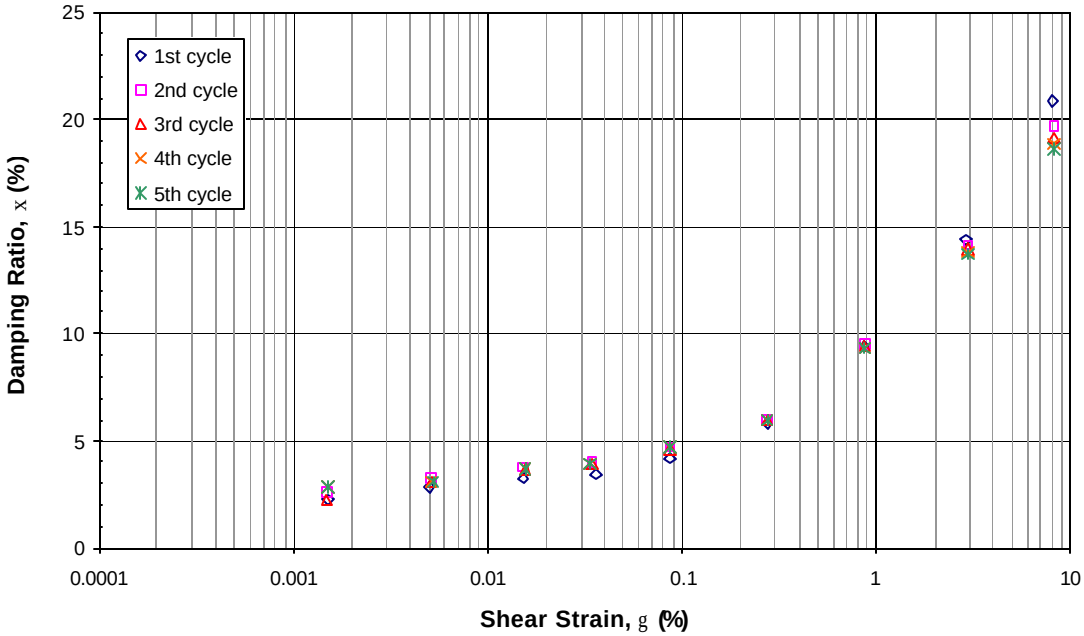

Effect of Loading Frequency on Secant Modulus

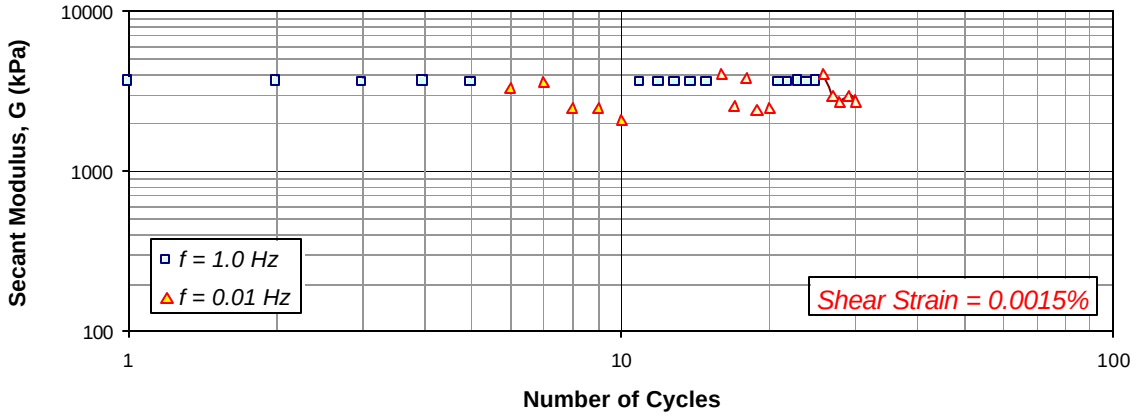

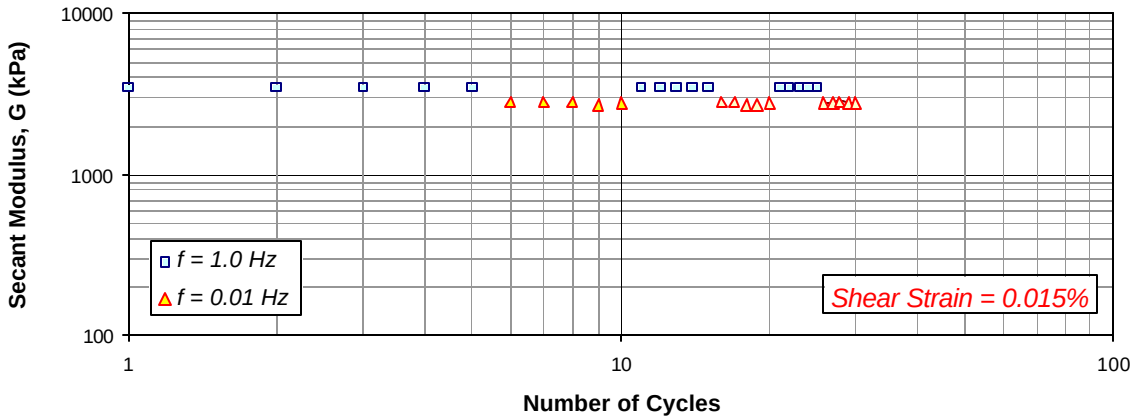

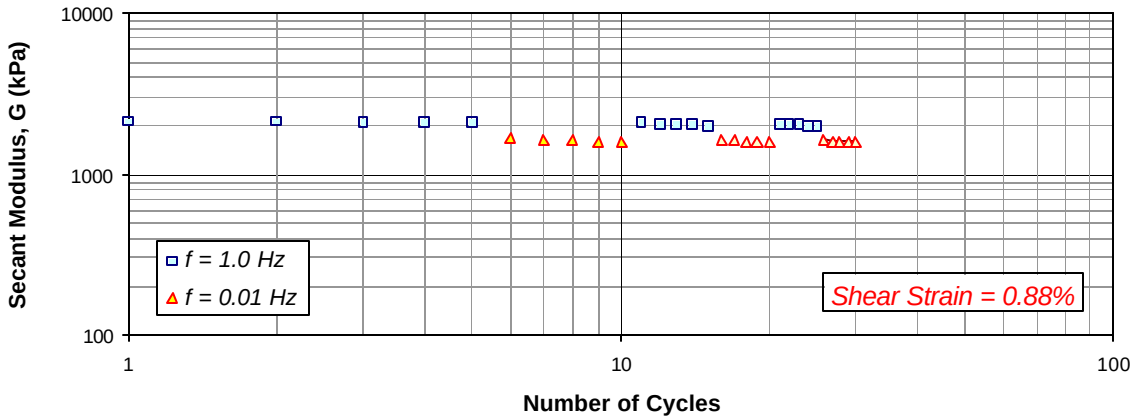

General Information of Tested Sample:

Borehole:	DHP - 5J1
Shelby Tube Number:	S-4
Sample Number:	10
Location of Borehole:	Free-field
Depth below Surface:	13.6' - 14.1'
Date Sampled:	5/19/00
Date Tested:	08/22/00
Visual Description:	Soft, dark brown silty peat; fibers mostly dark brown and fine; large 2.4-in diameter highly decomposed woody knot in center of sample.
Average Ash Content:	57%
Ash Content of Woody Knot:	42%
Ash Content of Homogeneous Portion:	60%
Initial Density:	1.095 Mg/m^3

Water Content (%) immediately above and below the triaxial specimen at time of extrusion:

Above: 498%

Below: 505%

Average Water Content (%) over length of sample after triaxial testing:

Average: 377%

Initial Water Content (%) back-calculated from final water content and change in volume:

Initial: 433%

Stresses on Triaxial Specimen:	σ_{vo} (kPa)	σ'_{vo} (kPa)	u (kPa)
Estimated In-situ:	44	11	33
Consolidation in Lab:	88	22	66

Average shear wave velocity measured prior to triaxial testing by means of bender elements:

Vs = (Not Measurable)

Summary of Test Data for Shear Strain γ, Shear Modulus G, and Damping Ratio λ:

1st cycle			2nd cycle			3rd cycle		
γ (%)	G (kPa)	λ (%)	γ (%)	G (kPa)	λ (%)	γ (%)	G (kPa)	λ (%)
0.00056	1109	--	0.00056	1099	--	0.00056	1171	--
0.00174	1102	1.6	0.00172	1130	2.1	0.00172	1119	2.2
0.00175	1110	1.9	0.00174	1109	2.1	0.00174	1136	2.7
0.00179	1118	0.8	0.00176	1123	0.7	0.00177	1106	1.7
0.00174	1068	1.5	0.00172	1080	2.3	0.00172	1119	1.7
0.00583	1105	2.5	0.00583	1112	2.9	0.00584	1103	2.9
0.01715	1085	3.3	0.01715	1086	3.7	0.01718	1085	3.7
0.00178	1113	2.4	0.00176	1144	2.1	0.00177	1151	2.4
0.03721	1042	4.1	0.03688	1046	4.5	0.03676	1046	4.3
0.09332	992	4.3	0.09251	988	4.6	0.09260	985	4.7
0.29423	857	7.2	0.29449	852	7.1	0.29440	847	7.1
0.91394	651	10.6	0.91790	636	10.1	0.91810	628	10.0
0.09239	913	5.3	0.09222	912	5.7	0.09198	911	5.7
3.01030	358	16.3	3.03610	340	15.7	3.04190	332	15.2
8.42710	189	20.6	8.54170	170	19.0	8.55940	163	18.3
0.09147	700	7.2	0.09147	698	8.1	0.09158	695	8.1
0.91679	418	13.5	0.92297	401	13.5	0.92573	394	13.4

4th cycle			5th cycle		
γ (%)	G (kPa)	λ (%)	γ (%)	G (kPa)	λ (%)
0.00056	1138	--	0.00056	1166	--
0.00173	1091	3.0	0.00172	1108	3.0
0.00174	1133	2.4	0.00175	1131	1.8
0.00177	1091	1.7	0.00178	1106	1.9
0.00172	1132	2.2	0.00173	1129	2.4
0.00585	1096	2.8	0.00585	1108	3.0
0.01719	1084	3.7	0.01726	1085	3.7
0.00177	1121	2.4	0.00177	1118	2.0
0.03669	1044	4.4	0.03690	1044	4.2
0.09245	985	4.6	0.09257	984	4.6
0.29445	846	7.0	0.29466	841	7.0
0.91877	622	9.9	0.91758	620	10.1
0.09203	910	5.7	0.09194	909	5.7
3.04930	327	15.0	3.04740	323	14.8
8.55790	159	17.9	8.56710	155	17.7
0.09160	693	8.0	0.09163	692	8.0
0.92635	392	13.1	0.92704	390	13.1

Modulus Reduction Curve

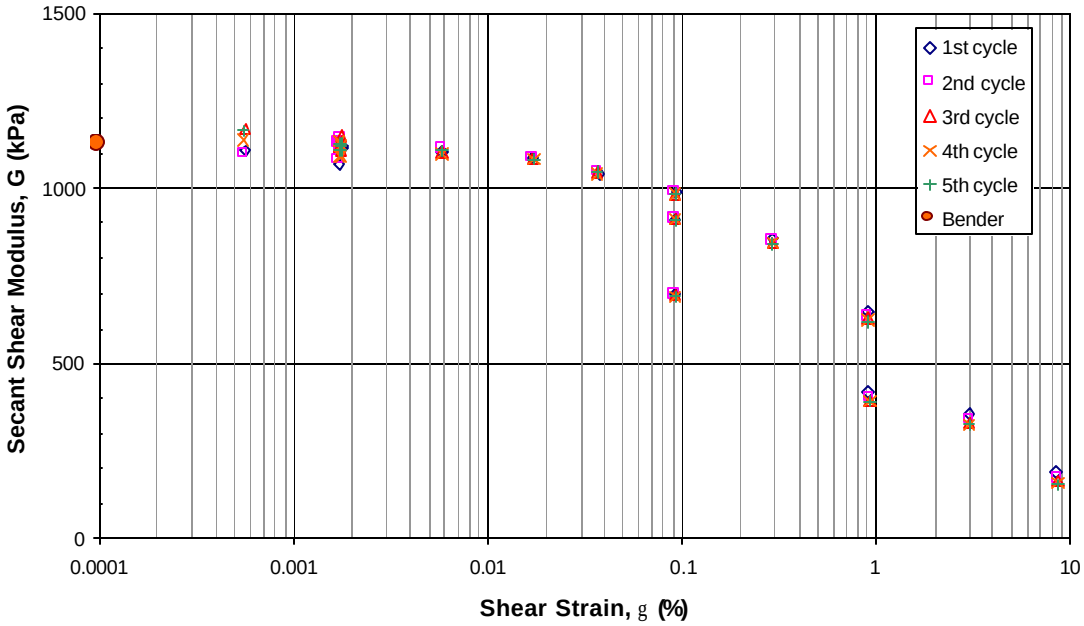

Damping Ratio Curve

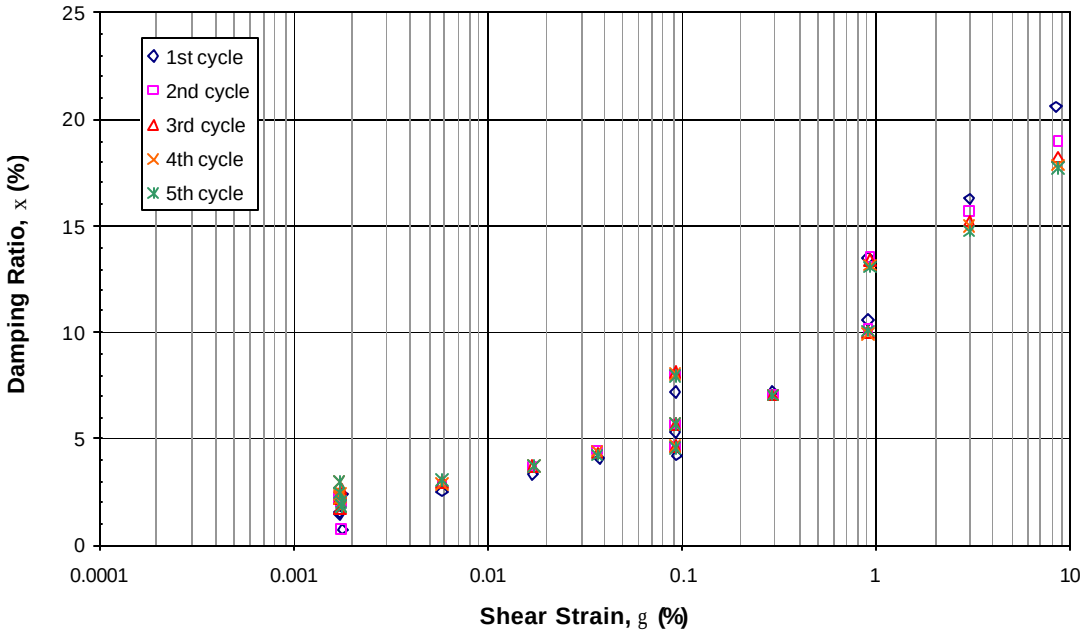

General Information of Tested Sample:

Borehole:	DHP - 5J1
Shelby Tube Number:	S-4
Sample Number:	11
Location of Borehole:	Free-field
Depth below Surface:	13.0' - 13.5'
Date Sampled:	5/19/00
Date Tested:	08/24/00
Visual Description:	The top half of the sample is a uniform, dark yellowish brown peaty silt. Below the midsection of the sample, the color gradually darkens to black. Here, the fines are less abundant, the fibers are larger, and the compressibility is higher.
Average Ash Content:	48%
Initial Density:	1.066 Mg/m^3

Water Content (%) immediately above and below the triaxial specimen at time of extrusion:

Above: 481%

Below: 642%

Average Water Content (%) over length of sample after triaxial testing:

Average: 495%

Initial Water Content (%) back-calculated from final water content and change in volume:

Initial: 588%

Stresses on Triaxial Specimen:	σ_{vo} (kPa)	σ'_{vo} (kPa)	u (kPa)
Estimated In-situ:	41	11	30
Consolidation in Lab:	82	22	60

Average shear wave velocity measured prior to triaxial testing by means of bender elements:

Vs = (Not measurable)

Summary of Test Data for Shear Strain γ, Shear Modulus G, and Damping Ratio λ:

1st cycle			2nd cycle			3rd cycle		
γ (%)	G (kPa)	λ (%)	γ (%)	G (kPa)	λ (%)	γ (%)	G (kPa)	λ (%)
0.00054	1398	--	0.00055	1434	--	0.00055	1529	--
0.00168	1335	4.0	0.00166	1369	5.3	0.00167	1369	5.2
0.00564	1270	4.8	0.00560	1273	5.4	0.00560	1269	5.2
0.01669	1208	5.2	0.01668	1209	5.7	0.01669	1205	5.7
0.03606	1135	5.4	0.03522	1136	6.0	0.03516	1137	6.0
0.08903	1065	5.9	0.08863	1061	6.5	0.08858	1058	6.4
0.28513	878	8.0	0.28595	865	8.0	0.28618	858	7.8
0.89301	662	9.6	0.89773	641	9.3	0.89740	635	9.1
2.89860	374	13.7	2.91800	356	13.0	2.92280	348	12.7
7.98420	196	20.3	8.15840	176	18.5	8.17490	170	17.8

4th cycle			5th cycle		
γ (%)	G (kPa)	λ (%)	γ (%)	G (kPa)	λ (%)
0.00055	1426	--	0.00055	1525	--
0.00166	1349	4.8	0.00167	1362	4.3
0.00560	1272	5.1	0.00563	1280	4.9
0.01667	1205	5.6	0.01673	1201	5.6
0.03508	1136	5.9	0.03514	1135	5.9
0.08905	1056	6.4	0.08875	1053	6.4
0.28626	853	7.8	0.28640	848	7.8
0.89871	627	9.1	0.89840	624	9.0
2.92740	343	12.8	2.92580	340	12.6
8.17310	166	17.6	8.18300	162	17.4

Summary of Test Data for Different Loading Frequencies:

***Shear Strain* = 0.00167%**

cycle	G (kPa)
1	1335
2	1369
3	1369
4	1349
5	1362

cycle	G (kPa)
6	1088
7	1105
8	1094
9	1070
10	1086

cycle	G (kPa)
11	1412
12	1409
13	1429
14	1386
15	1395

cycle	G (kPa)
16	1138
17	1098
18	1122
19	1113
20	1118

cycle	G (kPa)
21	1379
22	1398
23	1379
24	1409
25	1418

cycle	G (kPa)
26	1106
27	1146
28	1123
29	1132
30	1127

***Shear Strain* = 0.0167 %**

cycle	G (kPa)
1	1208
2	1209
3	1205
4	1205
5	1201

cycle	G (kPa)
6	952
7	961
8	957
9	964
10	965

cycle	G (kPa)
11	1209
12	1212
13	1208
14	1206
15	1209

cycle	G (kPa)
16	956
17	963
18	970
19	962
20	967

cycle	G (kPa)
21	1215
22	1215
23	1215
24	1214
25	1212

cycle	G (kPa)
26	969
27	964
28	971
29	968
30	963

***Shear Strain* = 0.90 %**

cycle	G (kPa)
1	662
2	641
3	635
4	627
5	624

cycle	G (kPa)
6	507
7	500
8	494
9	491
10	489

cycle	G (kPa)
11	620
12	615
13	612
14	609
15	607

cycle	G (kPa)
16	497
17	492
18	489
19	487
20	485

cycle	G (kPa)
21	616
22	610
23	607
24	605
25	604

cycle	G (kPa)
26	494
27	490
28	487
29	486
30	484

Modulus Reduction Curve

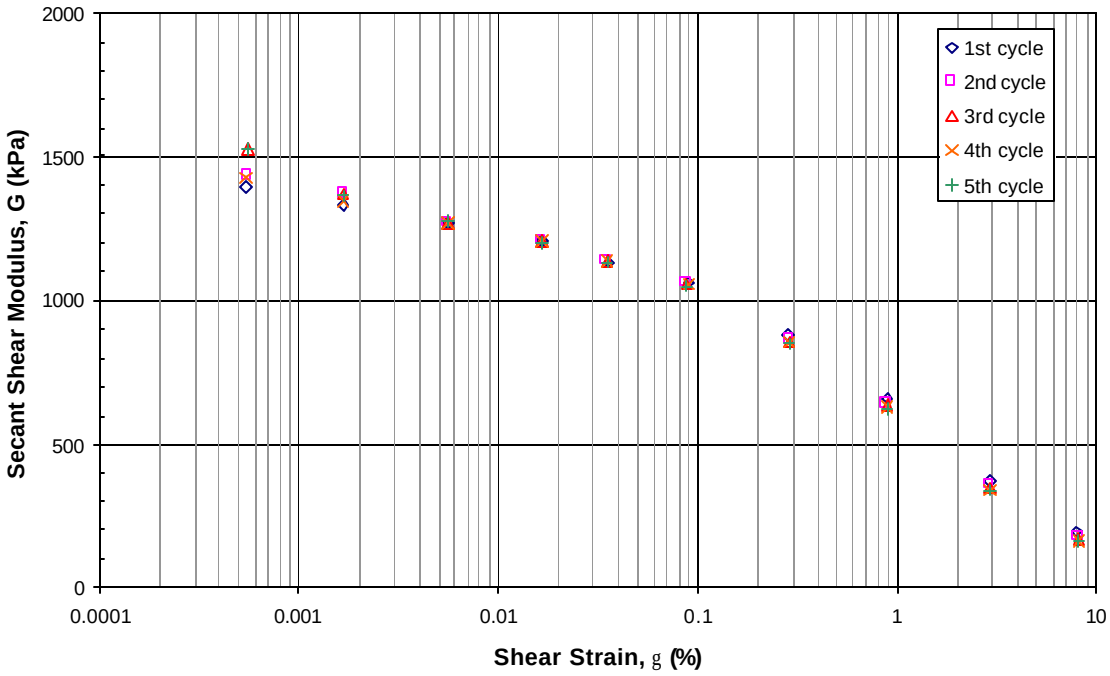

Damping Ratio Curve

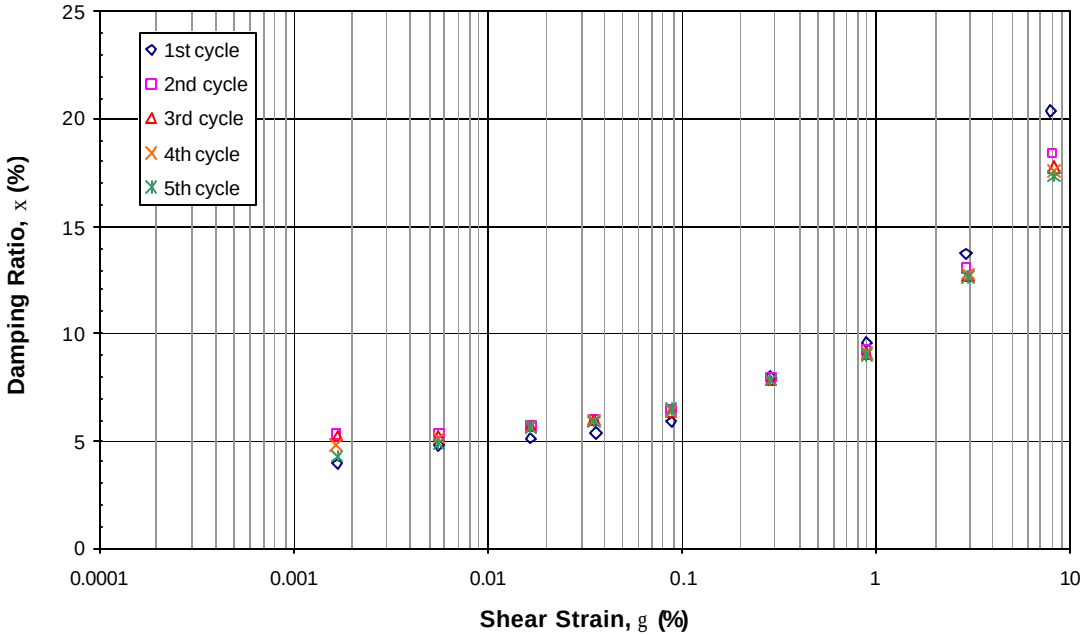

Effect of Loading Frequency on Secant Modulus

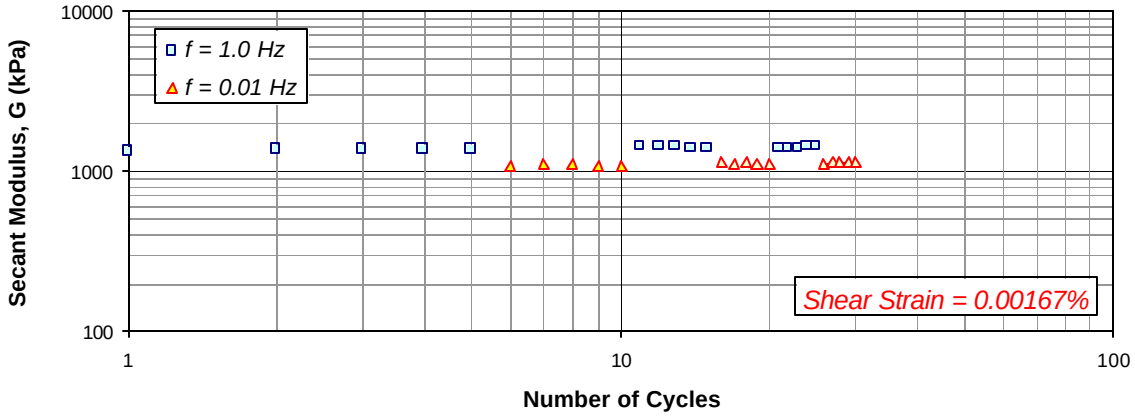

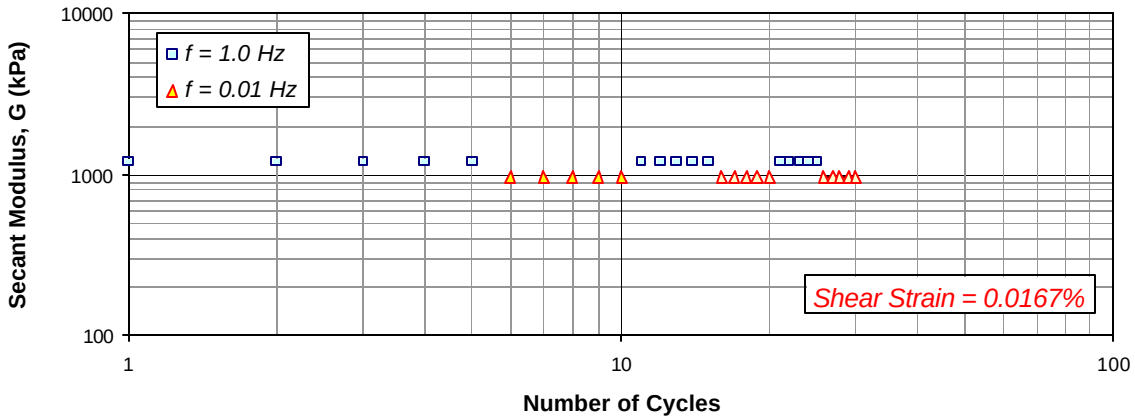

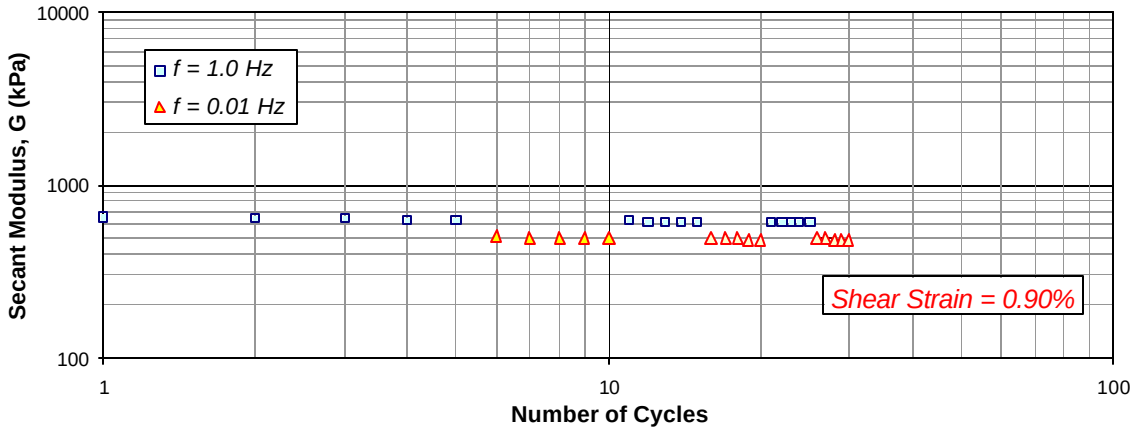

General Information of Tested Sample:

Borehole:	DHP - 5H3
Shelby Tube Number:	S-3
Sample Number:	12
Location of Borehole:	Levee Bench
Depth below Surface:	41.5' - 42.0'
Date Sampled:	5/18/00
Date Tested:	08/16/00
Visual Description:	Very firm, stiff, dark brown silty peat or peaty silt; fibrous and silty layers at a dip angle of about 20 degrees; fibers are very fine and not very abundant.
Average Ash Content:	68%
Initial Density:	1.236 Mg/m^3

Water Content (%) immediately above and below the triaxial specimen at time of extrusion:

Above: 222%

Below: 140%

Average Water Content (%) over length of sample after triaxial testing:

Average: 165%

Initial Water Content (%) back-calculated from final water content and change in volume:

Initial: 171%

Stresses on Triaxial Specimen:	σ_{vo} (kPa)	σ'_{vo} (kPa)	u (kPa)
Estimated In-situ:	177	78	98
Consolidation in Lab:	177	78	98

Average shear wave velocity measured prior to triaxial testing by means of bender elements:

Vs = 72 m/s

Summary of Test Data for Shear Strain γ, Shear Modulus G, and Damping Ratio λ:

1st cycle			2nd cycle			3rd cycle		
γ (%)	G (kPa)	λ (%)	γ (%)	G (kPa)	λ (%)	γ (%)	G (kPa)	λ (%)
0.00113	4811	2.9	0.00103	4826	4.3	0.00097	4802	4.0
0.00103	4708	2.1	0.00097	4778	2.5	0.00098	4804	3.1
0.00107	4756	3.0	0.00106	4704	3.1	0.00107	4773	3.4
0.00105	4760	3.8	0.00105	4800	3.7	0.00107	4709	3.3
0.00448	4698	2.2	0.00446	4703	3.2	0.00446	4716	2.9
0.01460	4471	2.9	0.01463	4474	3.3	0.01466	4474	3.3
0.03402	4538	3.1	0.03268	4550	3.5	0.03295	4544	3.4
0.08359	4203	4.4	0.08243	4202	4.7	0.08230	4199	4.7
0.26693	3358	6.9	0.26541	3353	7.0	0.26541	3328	7.0
0.84036	2317	12.0	0.84298	2249	12.1	0.84534	2212	12.1
2.88840	1293	15.0	2.89570	1234	14.7	2.89580	1212	14.5
8.06920	806	18.0	8.13060	726	17.9	8.12970	694	17.7
0.00152	3836	1.9	0.00141	4076	2.8	0.00141	3995	2.5
0.00836	3871	3.0	0.00822	3751	2.9	0.00820	3868	3.2
0.03427	3634	3.6	0.03346	3642	4.2	0.03335	3630	4.3
0.08523	3298	5.1	0.08452	3287	5.5	0.08458	3276	5.5
0.27978	2627	7.3	0.28060	2574	7.7	0.28102	2550	7.7
0.86056	1835	12.9	0.86786	1747	13.1	0.86975	1718	13.0
2.88190	1029	15.5	2.89600	977	15.4	2.89600	961	15.1
8.11300	714	16.7	8.13440	669	17.0	8.13410	651	17.0

4th cycle			5th cycle		
γ (%)	G (kPa)	λ (%)	γ (%)	G (kPa)	λ (%)
0.00095	4813	3.3	0.00096	4769	2.8
0.00099	4756	3.0	0.00101	4719	2.6
0.00107	4709	2.4	0.00108	4742	3.0
0.00107	4864	4.1	0.00107	4982	3.9
0.00447	4718	3.1	0.00448	4716	2.9
0.01468	4476	3.3	0.01474	4471	3.2
0.03262	4542	3.4	0.03263	4541	3.4
0.08235	4189	4.7	0.08246	4182	4.7
0.26557	3313	7.0	0.26615	3296	7.0
0.84630	2195	12.1	0.84742	2181	12.1
2.90150	1191	14.3	2.90160	1181	14.2
8.12940	671	17.7	8.12890	654	17.7
0.00141	4060	2.9	0.00143	4020	2.7
0.00819	3868	3.1	0.00822	3883	3.3
0.03317	3626	4.3	0.03315	3623	4.3
0.08470	3264	5.5	0.08477	3254	5.5
0.28139	2534	7.7	0.28169	2515	7.7
0.87100	1703	12.9	0.87174	1692	12.8
2.90210	947	14.9	2.90710	936	14.8
8.13150	639	17.0	8.12950	628	17.1

Modulus Reduction Curve

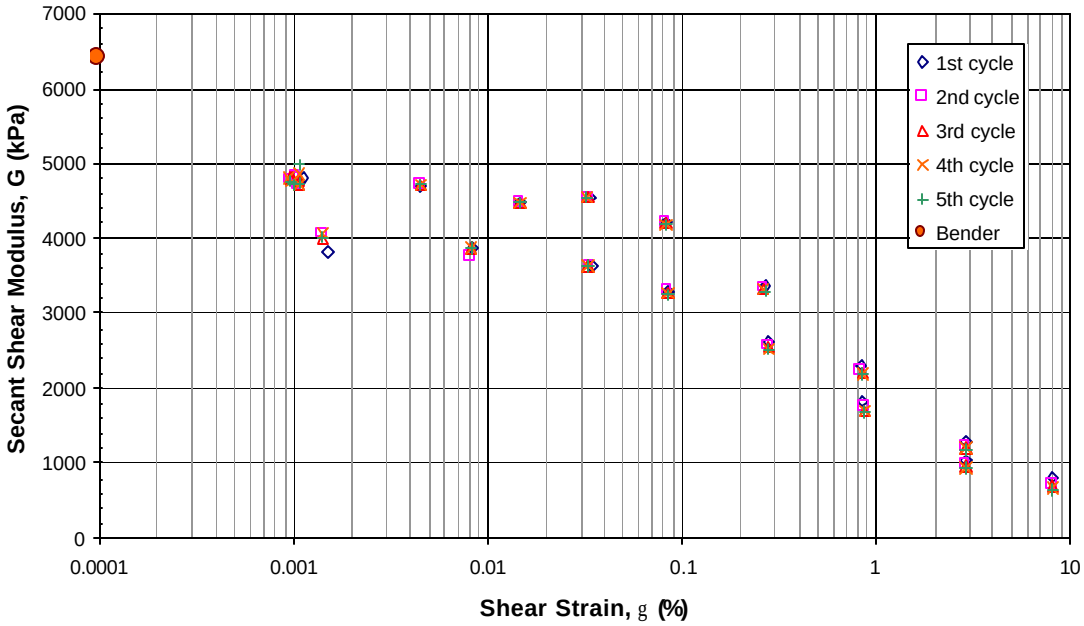

Damping Ratio Curve

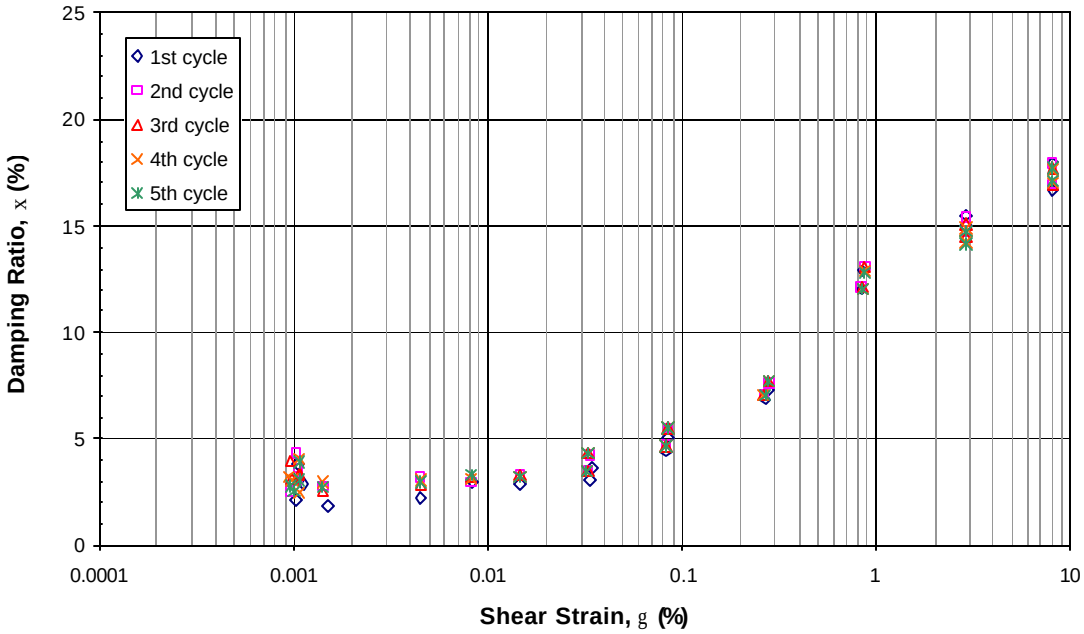

General Information of Tested Sample:

Borehole:	DHP - 5I1
Shelby Tube Number:	S-4
Sample Number:	13
Location of Borehole:	Mid-slope of levee
Depth below Surface:	25.5' - 26.0'
Date Sampled:	5/19/00
Date Tested:	08/31/00
Visual Description:	Dark brown silty peat or peaty silt; contains hairlike fibers and bands of grassy yellowish brown fibers; some small spots of black organic matter.
Average Ash Content:	69%
Initial Density:	1.119 Mg/m^3

Water Content (%) immediately above and below the triaxial specimen at time of extrusion:

Above: 270%

Below: 231%

Average Water Content (%) over length of sample after triaxial testing:

Average: 269%

Initial Water Content (%) back-calculated from final water content and change in volume:

Initial: 279%

Stresses on Triaxial Specimen:	σ_{vo} (kPa)	σ'_{vo} (kPa)	u (kPa)
Estimated In-situ:	105	46	59
Consolidation in Lab:	105	46	59

Average shear wave velocity measured prior to triaxial testing by means of bender elements:

Vs = (Not measurable)

Summary of Test Data for Shear Strain g, Shear Modulus G, and Damping Ratio x:

1st cycle			2nd cycle			3rd cycle		
g (%)	G (kPa)	x (%)	g (%)	G (kPa)	x (%)	g (%)	G (kPa)	x (%)
0.00143	2088	4.0	0.00143	2147	3.6	0.00145	2069	2.9
0.00152	2138	3.1	0.00148	2131	3.4	0.00147	2180	4.0
0.00148	2204	3.6	0.00149	2211	3.3	0.00149	2187	3.4
0.00149	2261	3.0	0.00149	2248	2.3	0.00151	2263	2.2
0.00543	2097	3.4	0.00542	2104	3.8	0.00543	2100	3.6
0.01661	2042	3.4	0.01662	2047	3.9	0.01663	2049	3.9
0.03538	1987	3.8	0.03492	1982	4.1	0.03480	1983	4.1
0.08941	1882	4.7	0.08870	1886	5.0	0.08884	1881	5.1
0.28454	1628	7.0	0.28393	1621	6.9	0.28361	1614	6.8
0.88128	1240	9.8	0.88135	1225	9.7	0.88093	1217	9.6
2.91580	755	13.7	2.92350	723	13.4	2.92290	711	13.3
8.09580	424	18.8	8.19040	376	17.2	8.20740	358	16.7
0.00156	2014	3.3	0.00156	2017	4.5	0.00156	1984	3.7
0.00544	1924	3.2	0.00544	1932	3.7	0.00542	1933	3.7
0.01615	1883	3.7	0.01616	1886	4.0	0.01618	1883	3.9
0.03496	1817	4.0	0.03392	1818	4.5	0.03412	1812	4.4
0.09053	1714	4.7	0.08844	1715	4.9	0.08787	1709	4.9
0.28123	1452	6.4	0.28194	1438	6.8	0.28305	1429	6.7
0.87613	1074	9.5	0.88055	1048	9.6	0.88258	1038	9.5
2.91930	611	14.0	2.92950	585	13.9	2.92930	577	13.8
8.17510	383	16.8	8.21320	357	16.5	8.20990	348	16.2

4th cycle			5th cycle		
g (%)	G (kPa)	x (%)	g (%)	G (kPa)	x (%)
0.00145	2136	5.0	0.00146	2072	5.3
0.00148	2155	3.8	0.00148	2134	3.5
0.00150	2194	3.6	0.00150	2199	4.0
0.00150	2248	2.4	0.00151	2224	2.7
0.00543	2100	3.6	0.00545	2102	3.7
0.01665	2049	3.8	0.01671	2045	3.8
0.03486	1982	4.1	0.03483	1980	4.2
0.08892	1877	5.0	0.08889	1877	5.0
0.28357	1607	6.8	0.28347	1603	6.8
0.88087	1213	9.6	0.88290	1204	9.5
2.92850	700	13.1	2.92870	695	13.0
8.21980	346	16.5	8.21820	339	16.3
0.00156	2034	4.1	0.00157	2030	3.9
0.00543	1925	3.8	0.00544	1924	3.6
0.01617	1889	4.0	0.01623	1883	3.9
0.03405	1811	4.3	0.03415	1810	4.3
0.08788	1705	5.0	0.08799	1703	4.9
0.28327	1423	6.7	0.28370	1417	6.7
0.88299	1032	9.5	0.88325	1027	9.5
2.92900	574	13.6	2.92960	570	13.5
8.22350	339	16.2	8.22200	334	16.1

Modulus Reduction Curve

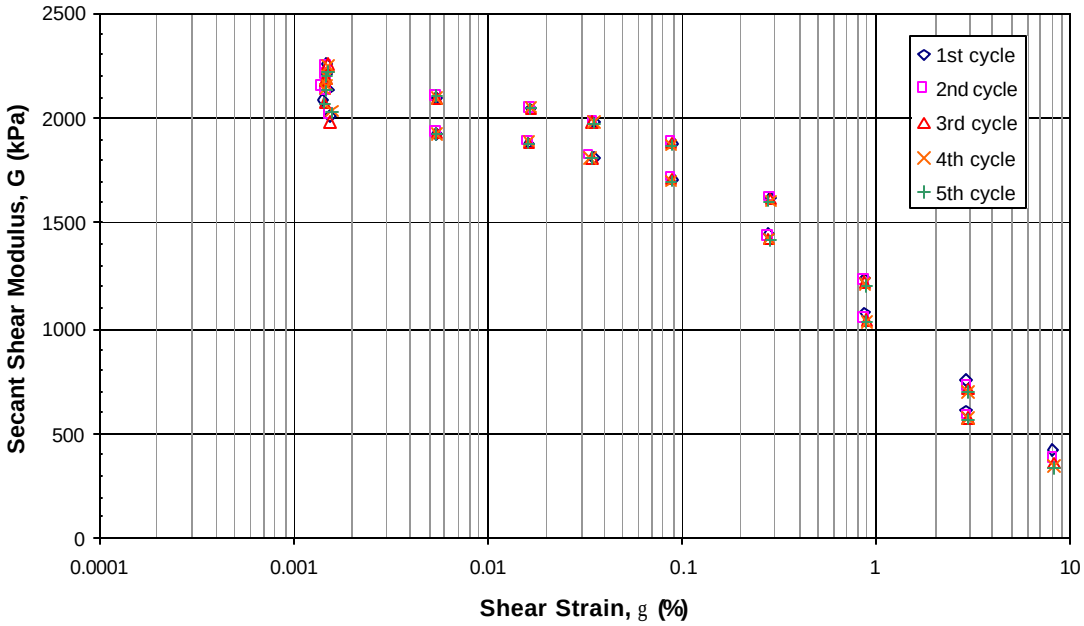

Damping Ratio Curve

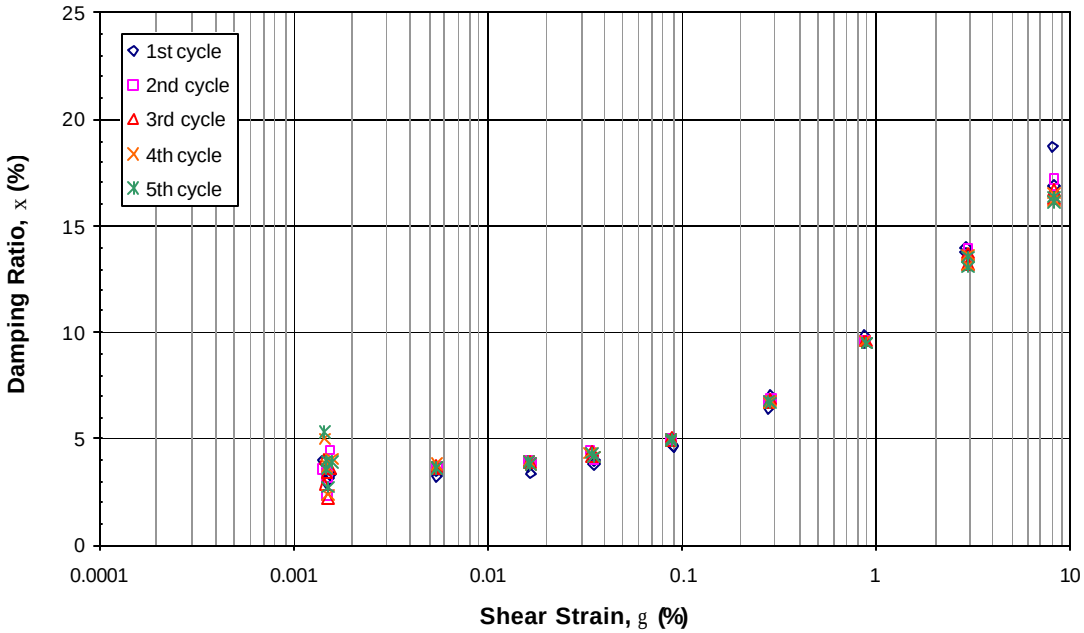

General Information of Tested Sample:

Borehole: DHP - 5J1
Shelby Tube Number: S-3
Sample Number: 14
Location of Borehole: Free-field
Depth below Surface: 8.6' - 9.1'
Date Sampled: 5/19/00
Date Tested: 12/05/00
Visual Description: Soft, dark brown silty peat. Mostly interwoven, hairlike fibers with horizontal preferential separation. Some flat, wide, fiber blades (laid horizontally) up to 10 mm wide. Few thin veins and lenses of black, highly decomposed, organic matter.

Average Ash Content: 63%
Initial Density: 1.062 Mg/m^3

Water Content (%) immediately above and below the triaxial specimen at time of extrusion:
Above: 350%
Below: 498%

Average Water Content (%) over length of sample after triaxial testing:
Average: 475%

Initial Water Content (%) back-calculated from final water content and change in volume:
Initial: 512%

Stresses on Triaxial Specimen:	σ_{vo} (kPa)	σ'_{vo} (kPa)	u (kPa)
Estimated In-situ:	25	10	15
Consolidation in Lab:	25	10	15

Average shear wave velocity measured prior to triaxial testing by means of bender elements:
Vs = (Not measurable)

Summary of Test Data for Shear Strain γ, Shear Modulus G, and Damping Ratio χ:

1st cycle			2nd cycle			3rd cycle		
γ (%)	G (kPa)	χ (%)	γ (%)	G (kPa)	χ (%)	γ (%)	G (kPa)	χ (%)
0.00165	898	--	0.00164	922	--	0.00164	887	--
0.00567	807	5.3	0.00564	819	5.6	0.00565	817	5.4
0.01657	767	5.5	0.01649	773	6.1	0.01651	772	6.1
0.03770	726	4.8	0.03668	726	5.6	0.03636	724	5.8
0.09282	682	6.3	0.09189	676	7.0	0.09234	672	7.0
0.29412	554	10.7	0.29421	550	10.3	0.29401	546	10.3
0.90822	415	13.1	0.91214	407	12.7	0.91315	404	13.1
2.96090	245	19.2	2.99850	232	18.5	2.99840	227	18.1
5.63200	119	18.9	5.66450	119	19.2	5.66410	118	18.7
0.00161	864	--	0.00161	870	--	0.00161	829	--
0.00562	809	3.9	0.00558	812	4.3	0.00558	812	4.5
0.01582	814	5.9	0.01582	818	6.3	0.01585	819	6.3
0.09253	656	7.8	0.09117	656	8.3	0.09162	645	8.0
0.29104	516	10.0	0.29146	503	9.6	0.29156	498	9.4
0.89929	372	12.2	0.90620	359	11.9	0.90725	355	11.7
3.01640	99	17.2	3.02680	96	16.4	3.02960	95	16.3
5.61310	76	17.9	5.65530	72	18.1	5.66410	71	17.8

4th cycle			5th cycle		
γ (%)	G (kPa)	χ (%)	γ (%)	G (kPa)	χ (%)
0.00164	879	--	0.00165	888	--
0.00564	817	5.3	0.00567	815	5.4
0.01651	769	6.1	0.01656	770	6.2
0.03644	725	5.5	0.03656	724	5.6
0.09232	672	6.9	0.09229	670	6.8
0.29417	542	10.3	0.29426	539	10.0
0.91429	400	12.9	0.91358	399	12.9
2.99850	225	17.8	3.00430	223	17.6
5.66350	118	18.4	5.66070	117	18.2
0.00161	842	--	0.00161	822	--
0.00559	804	4.6	0.00562	807	4.9
0.01586	816	6.4	0.01592	815	6.2
0.09125	643	7.8	0.09133	641	7.8
0.29170	493	9.3	0.29224	488	9.2
0.90708	354	11.7	0.90884	351	11.6
3.02580	95	16.2	3.02760	94	16.0
5.66410	70	17.7	5.66050	69	17.9

Modulus Reduction Curve

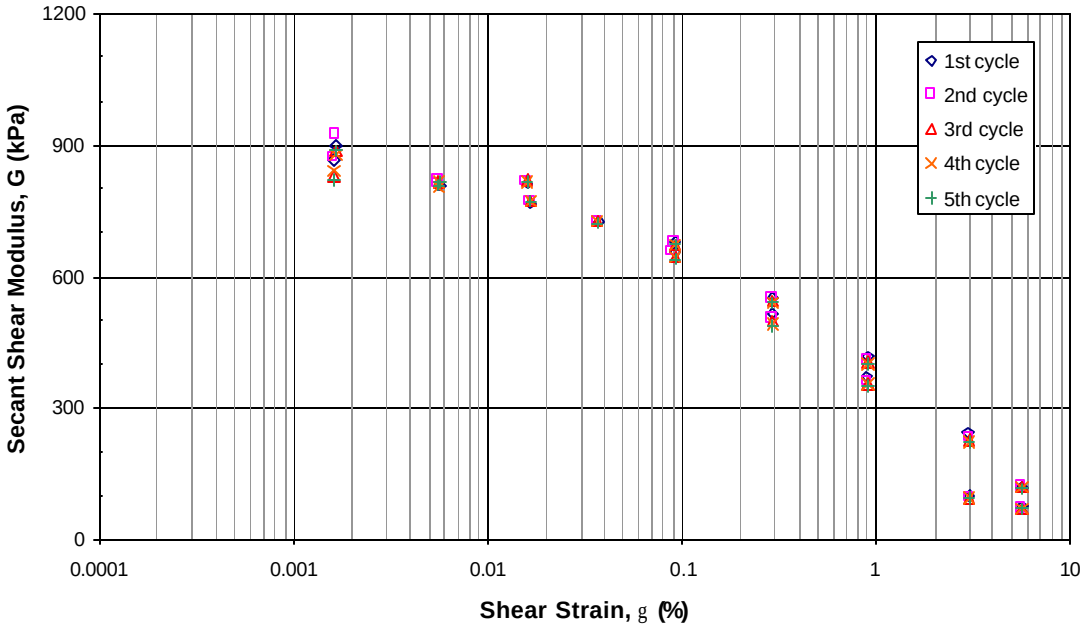

Damping Ratio Curve

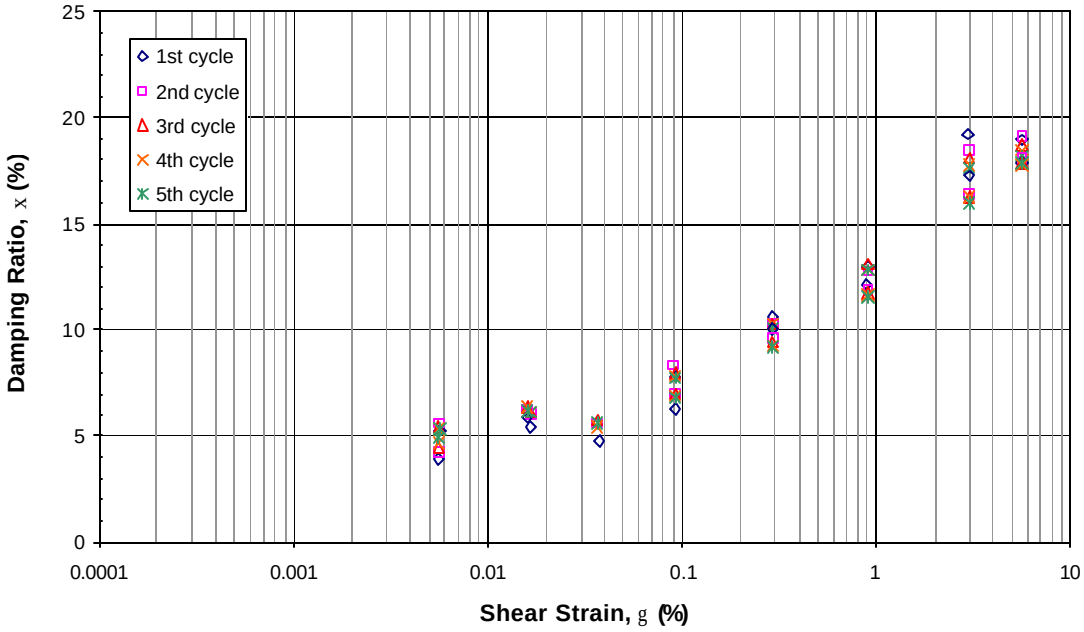

Appendix B: Stress-Strain Data for a Representative Test (Sample 9)

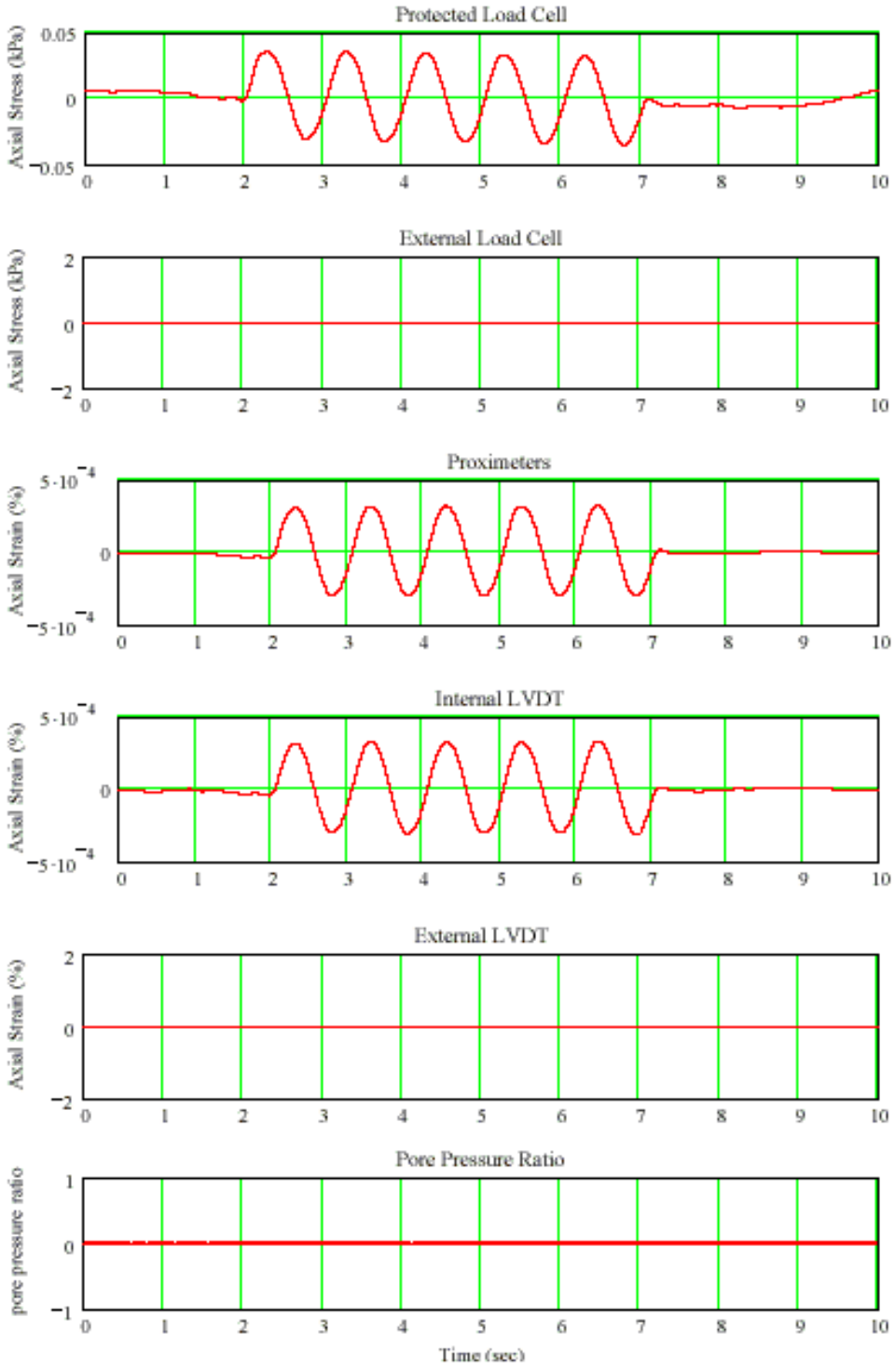
Protected Load Cell
Axial Stress (kPa)
0.05
0
−0.05
0 1 2 3 4 5 6 7 8 9 10
External Load Cell
Axial Stress (kPa)
2
0
−2
0 1 2 3 4 5 6 7 8 9 10
Proximeters
Axial Strain (%)
5·10⁻⁴
0
−5·10⁻⁴
0 1 2 3 4 5 6 7 8 9 10
Internal LVDT
Axial Strain (%)
5·10⁻⁴
0
−5·10⁻⁴
0 1 2 3 4 5 6 7 8 9 10
External LVDT
Axial Strain (%)
2
0
−2
0 1 2 3 4 5 6 7 8 9 10
Pore Pressure Ratio
pore pressure ratio
1
0
−1
0 1 2 3 4 5 6 7 8 9 10
Time (sec)

Internal Load Cell vs. Average Proximeter

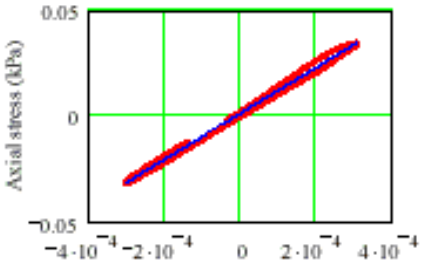

Loop 1:

$E_{0,0} = 10943$ kPa

$G_{0,0} = 3648$ kPa

$\xi_{0,0} = 0.033$

$\gamma_{0,0} = 4.55 \times 10^{-4}$ %

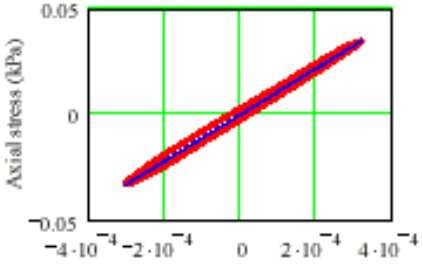

Loop 2:

$E_{1,0} = 11030$ kPa

$G_{1,0} = 3677$ kPa

$\xi_{1,0} = 0.043$

$\gamma_{1,0} = 4.64 \times 10^{-4}$ %

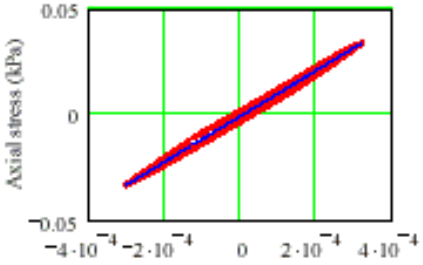

Loop 3:

$E_{2,0} = 10881$ kPa

$G_{2,0} = 3627$ kPa

$\xi_{2,0} = 0.036$

$\gamma_{2,0} = 4.66 \times 10^{-4}$ %

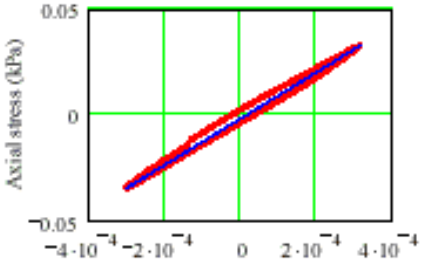

Loop 4:

$E_{3,0} = 11008$ kPa

$G_{3,0} = 3669$ kPa

$\xi_{3,0} = 0.042$

$\gamma_{3,0} = 4.61 \times 10^{-4}$ %

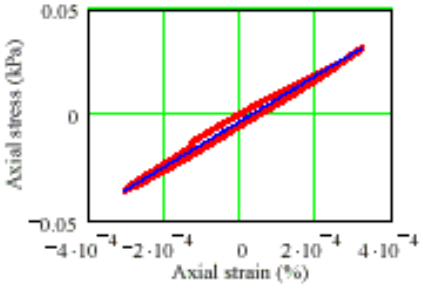

Loop 5:

$E_{4,0} = 10846$ kPa

$G_{4,0} = 3615$ kPa

$\xi_{4,0} = 0.034$

$\gamma_{4,0} = 4.66 \times 10^{-4}$ %

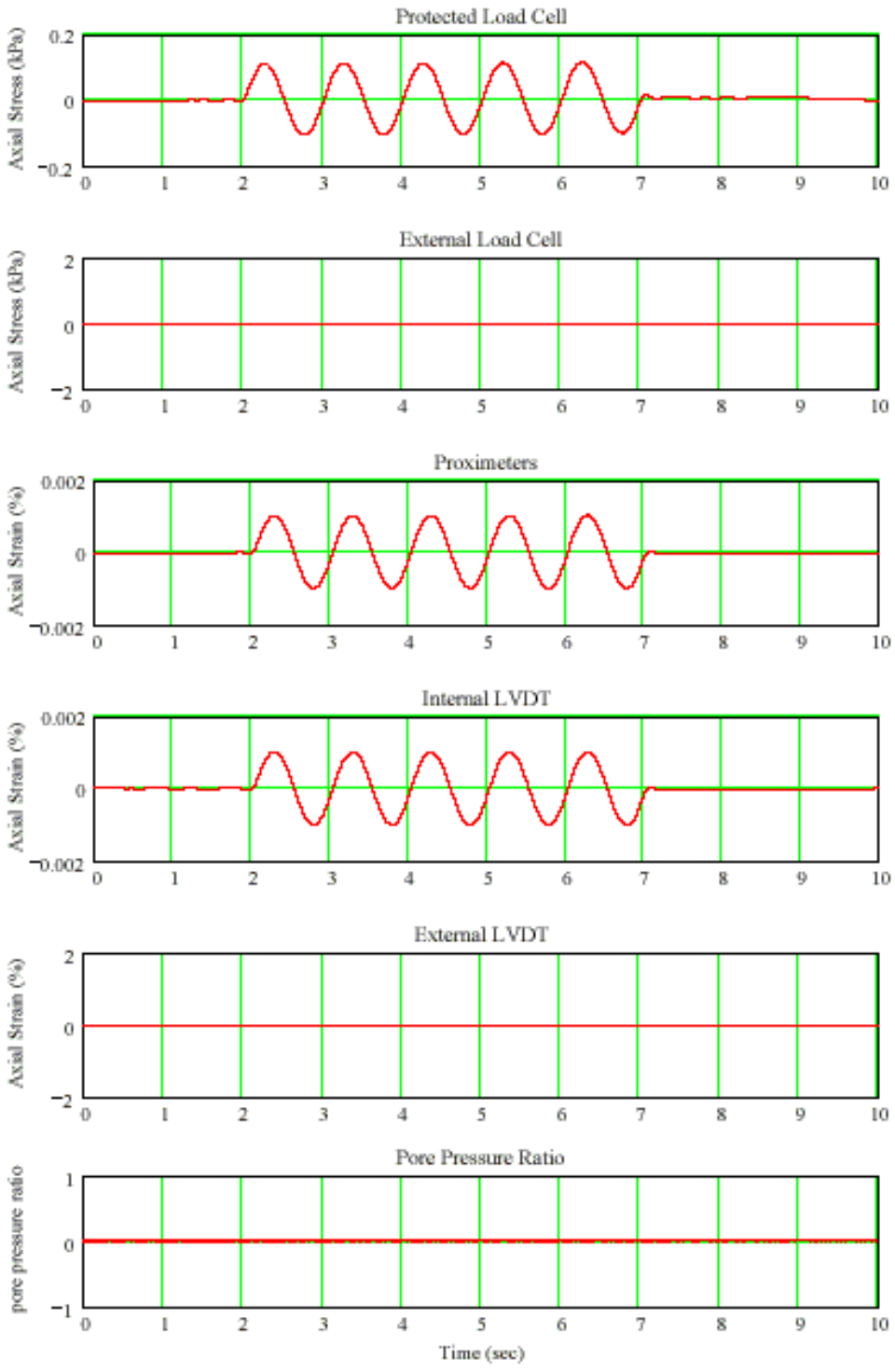
Protected Load Cell
Axial Stress (kPa)
0.2
0
−0.2
External Load Cell
Axial Stress (kPa)
2
0
−2
Proximeters
Axial Strain (%)
0.002
0
−0.002
Internal LVDT
Axial Strain (%)
0.002
0
−0.002
External LVDT
Axial Strain (%)
2
0
−2
Pore Pressure Ratio
pore pressure ratio
1
0
−1
0 1 2 3 4 5 6 7 8 9 10
Time (sec)

Internal Load Cell vs. Average Proximeter

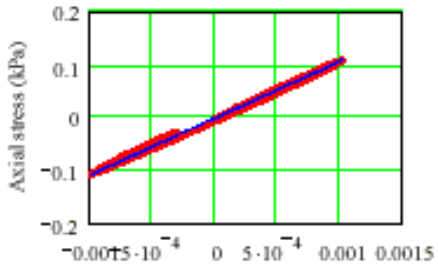

Loop 1:

$E_{0,0} = 10794$ kPa

$G_{0,0} = 3598$ kPa

$\xi_{0,0} = 0.033$

$\gamma_{0,0} = 1.51 \times 10^{-3}$ %

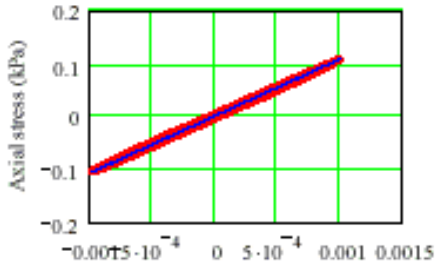

Loop 2:

$E_{1,0} = 10824$ kPa

$G_{1,0} = 3608$ kPa

$\xi_{1,0} = 0.036$

$\gamma_{1,0} = 1.49 \times 10^{-3}$ %

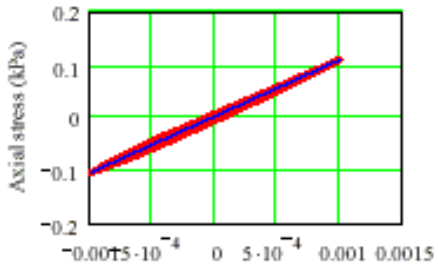

Loop 3:

$E_{2,0} = 10738$ kPa

$G_{2,0} = 3579$ kPa

$\xi_{2,0} = 0.032$

$\gamma_{2,0} = 1.5 \times 10^{-3}$ %

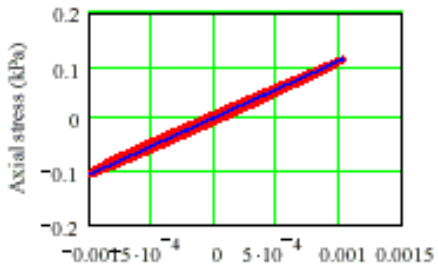

Loop 4:

$E_{3,0} = 10797$ kPa

$G_{3,0} = 3599$ kPa

$\xi_{3,0} = 0.038$

$\gamma_{3,0} = 1.51 \times 10^{-3}$ %

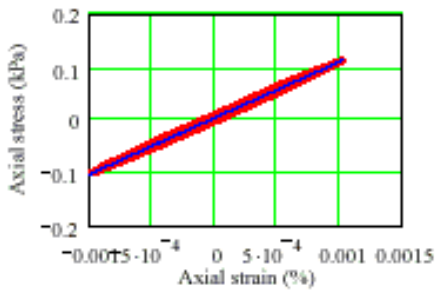

Loop 5:

$E_{4,0} = 10669$ kPa

$G_{4,0} = 3556$ kPa

$\xi_{4,0} = 0.038$

$\gamma_{4,0} = 1.51 \times 10^{-3}$ %

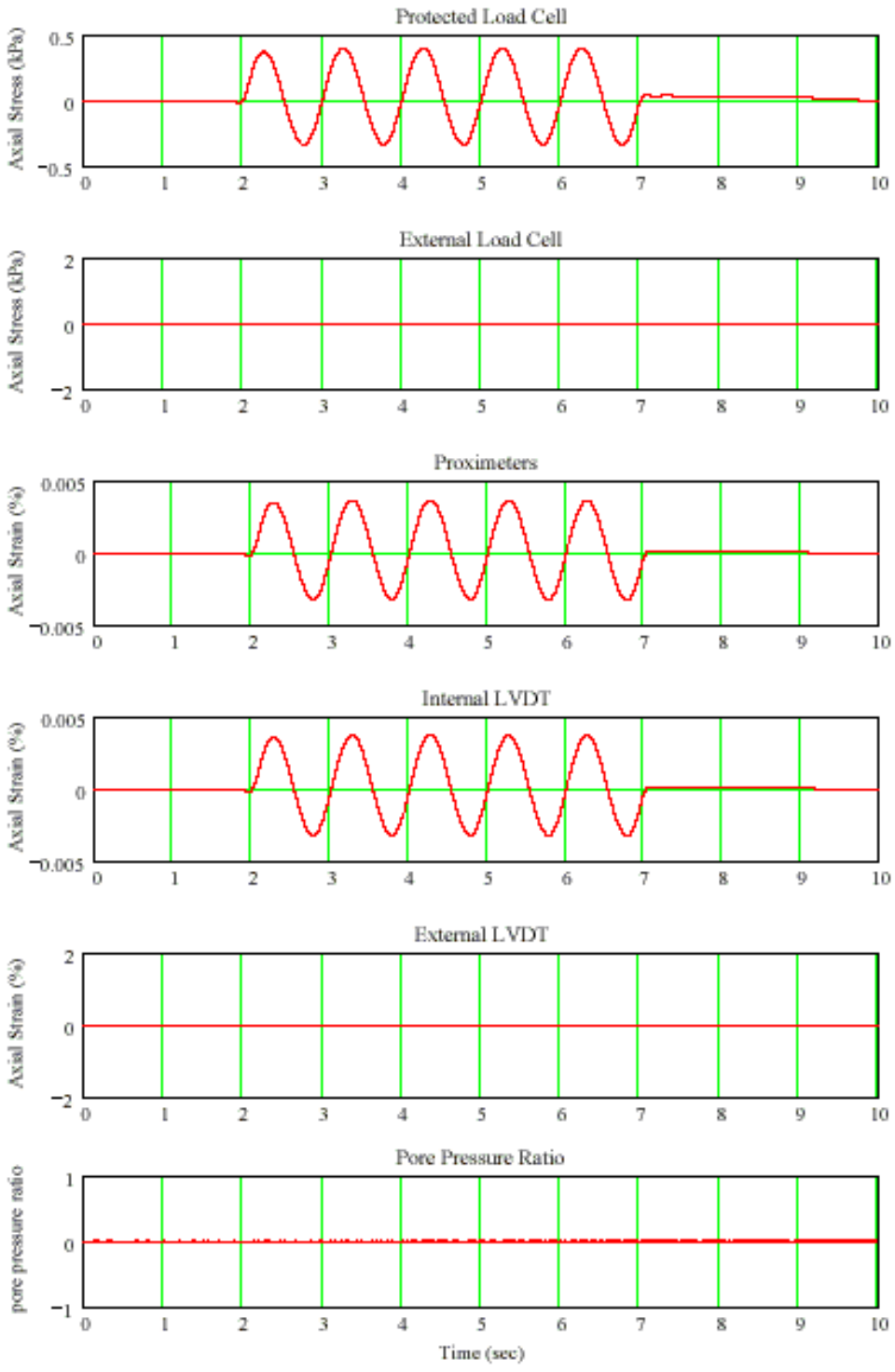
Protected Load Cell
Axial Stress (kPa)
0.5
0
−0.5
0 1 2 3 4 5 6 7 8 9 10
External Load Cell
Axial Stress (kPa)
2
0
−2
0 1 2 3 4 5 6 7 8 9 10
Proximeters
Axial Strain (%)
0.005
0
−0.005
0 1 2 3 4 5 6 7 8 9 10
Internal LVDT
Axial Strain (%)
0.005
0
−0.005
0 1 2 3 4 5 6 7 8 9 10
External LVDT
Axial Strain (%)
2
0
−2
0 1 2 3 4 5 6 7 8 9 10
Pore Pressure Ratio
pore pressure ratio
1
0
−1
0 1 2 3 4 5 6 7 8 9 10
Time (sec)

Internal Load Cell vs. Average Proximeter

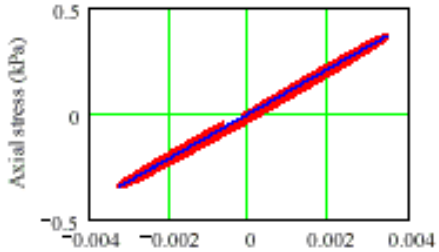

Loop 1:

$E_{0,0} = 10598$ kPa

$G_{0,0} = 3533$ kPa

$\xi_{0,0} = 0.031$

$\gamma_{0,0} = 5.01 \times 10^{-3}$ %

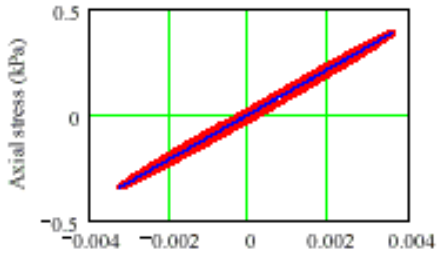

Loop 2:

$E_{1,0} = 10692$ kPa

$G_{1,0} = 3564$ kPa

$\xi_{1,0} = 0.035$

$\gamma_{1,0} = 5.13 \times 10^{-3}$ %

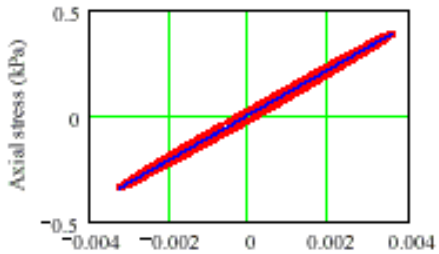

Loop 3:

$E_{2,0} = 10682$ kPa

$G_{2,0} = 3561$ kPa

$\xi_{2,0} = 0.034$

$\gamma_{2,0} = 5.16 \times 10^{-3}$ %

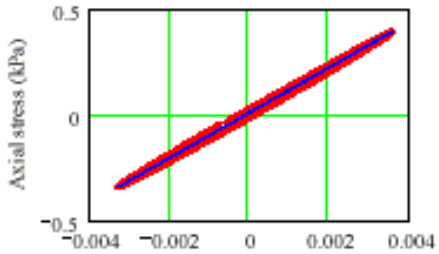

Loop 4:

$E_{3,0} = 10679$ kPa

$G_{3,0} = 3560$ kPa

$\xi_{3,0} = 0.034$

$\gamma_{3,0} = 5.17 \times 10^{-3}$ %

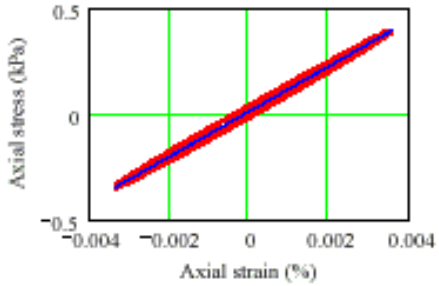

Loop 5:

$E_{4,0} = 10667$ kPa

$G_{4,0} = 3556$ kPa

$\xi_{4,0} = 0.034$

$\gamma_{4,0} = 5.19 \times 10^{-3}$ %

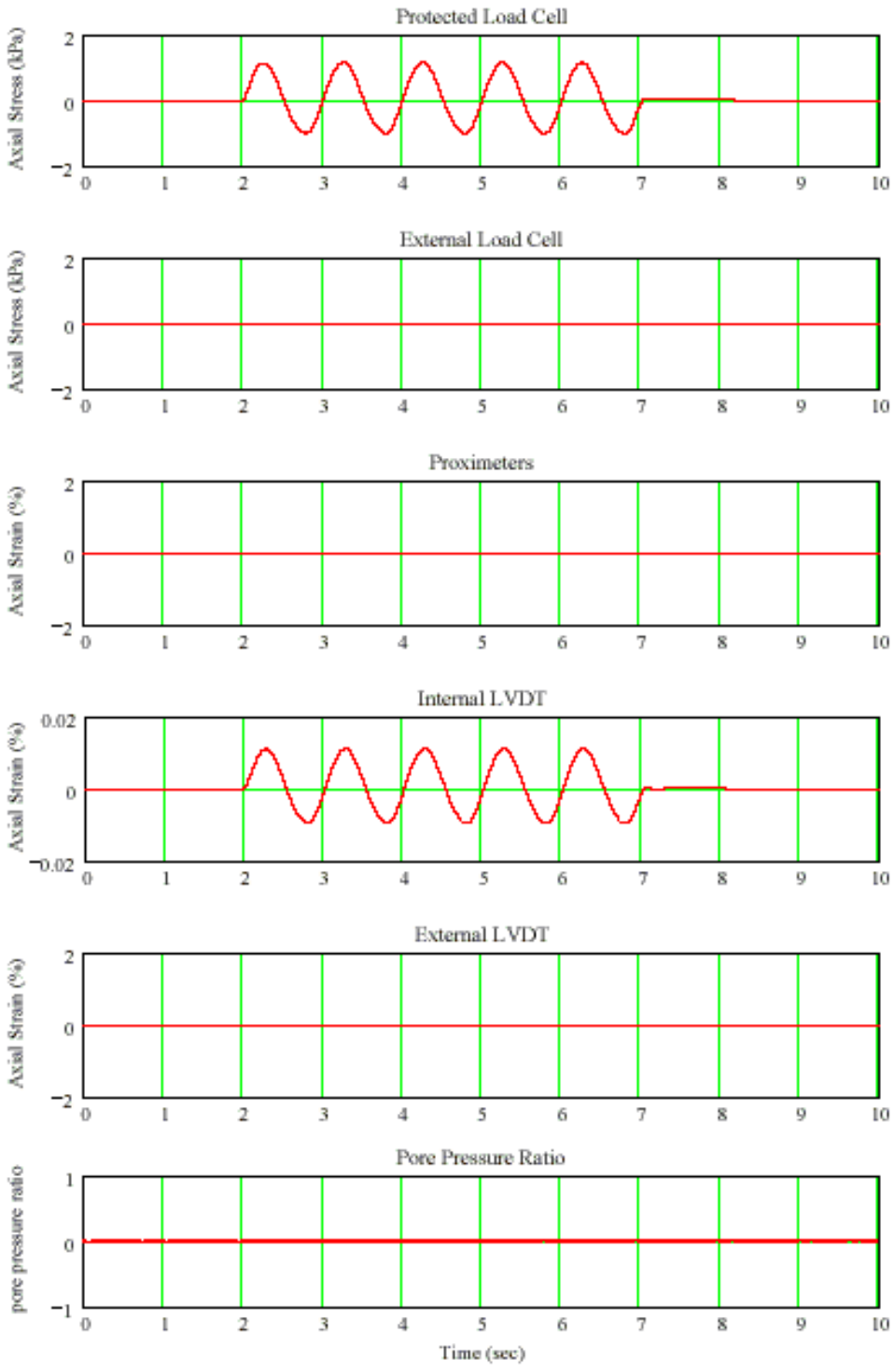
Protected Load Cell
Axial Stress (kPa)
2
0
−2
0 1 2 3 4 5 6 7 8 9 10
External Load Cell
Axial Stress (kPa)
2
0
−2
0 1 2 3 4 5 6 7 8 9 10
Proximeters
Axial Strain (%)
2
0
−2
0 1 2 3 4 5 6 7 8 9 10
Internal LVDT
Axial Strain (%)
0.02
0
−0.02
0 1 2 3 4 5 6 7 8 9 10
External LVDT
Axial Strain (%)
2
0
−2
0 1 2 3 4 5 6 7 8 9 10
Pore Pressure Ratio
pore pressure ratio
1
0
−1
0 1 2 3 4 5 6 7 8 9 10
Time (sec)

Internal Load Cell vs. Internal LVDT

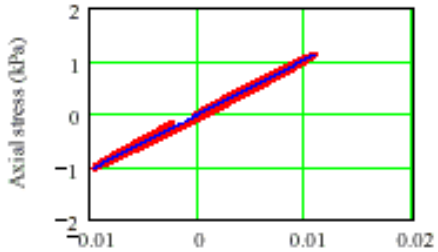

Loop 1

$E_{0,1} = 10468$ kPa

$G_{0,1} = 3489$ kPa

$\xi_{0,1} = 0.034$

$\gamma_{0,1} = 1.53 \times 10^{-2}$ %

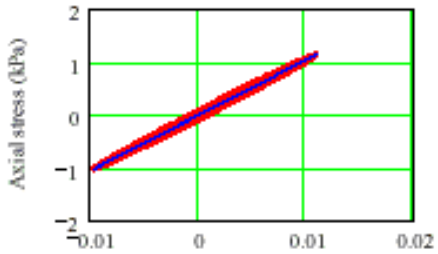

Loop 2

$E_{1,1} = 10504$ kPa

$G_{1,1} = 3501$ kPa

$\xi_{1,1} = 0.039$

$\gamma_{1,1} = 1.54 \times 10^{-2}$ %

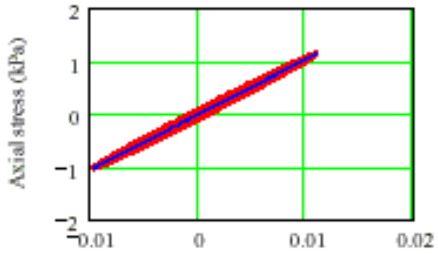

Loop 3

$E_{2,1} = 10486$ kPa

$G_{2,1} = 3495$ kPa

$\xi_{2,1} = 0.038$

$\gamma_{2,1} = 1.54 \times 10^{-2}$ %

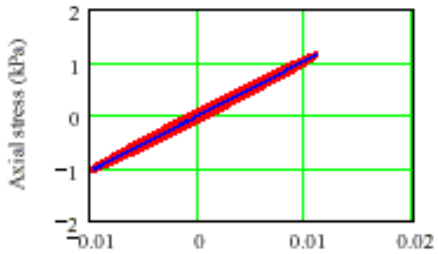

Loop 4

$E_{3,1} = 10477$ kPa

$G_{3,1} = 3492$ kPa

$\xi_{3,1} = 0.038$

$\gamma_{3,1} = 1.55 \times 10^{-2}$ %

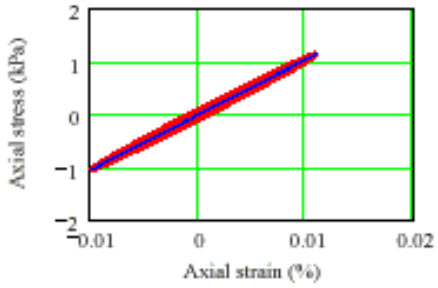

Loop 5

$E_{4,1} = 10491$ kPa

$G_{4,1} = 3497$ kPa

$\xi_{4,1} = 0.038$

$\gamma_{4,1} = 1.55 \times 10^{-2}$ %

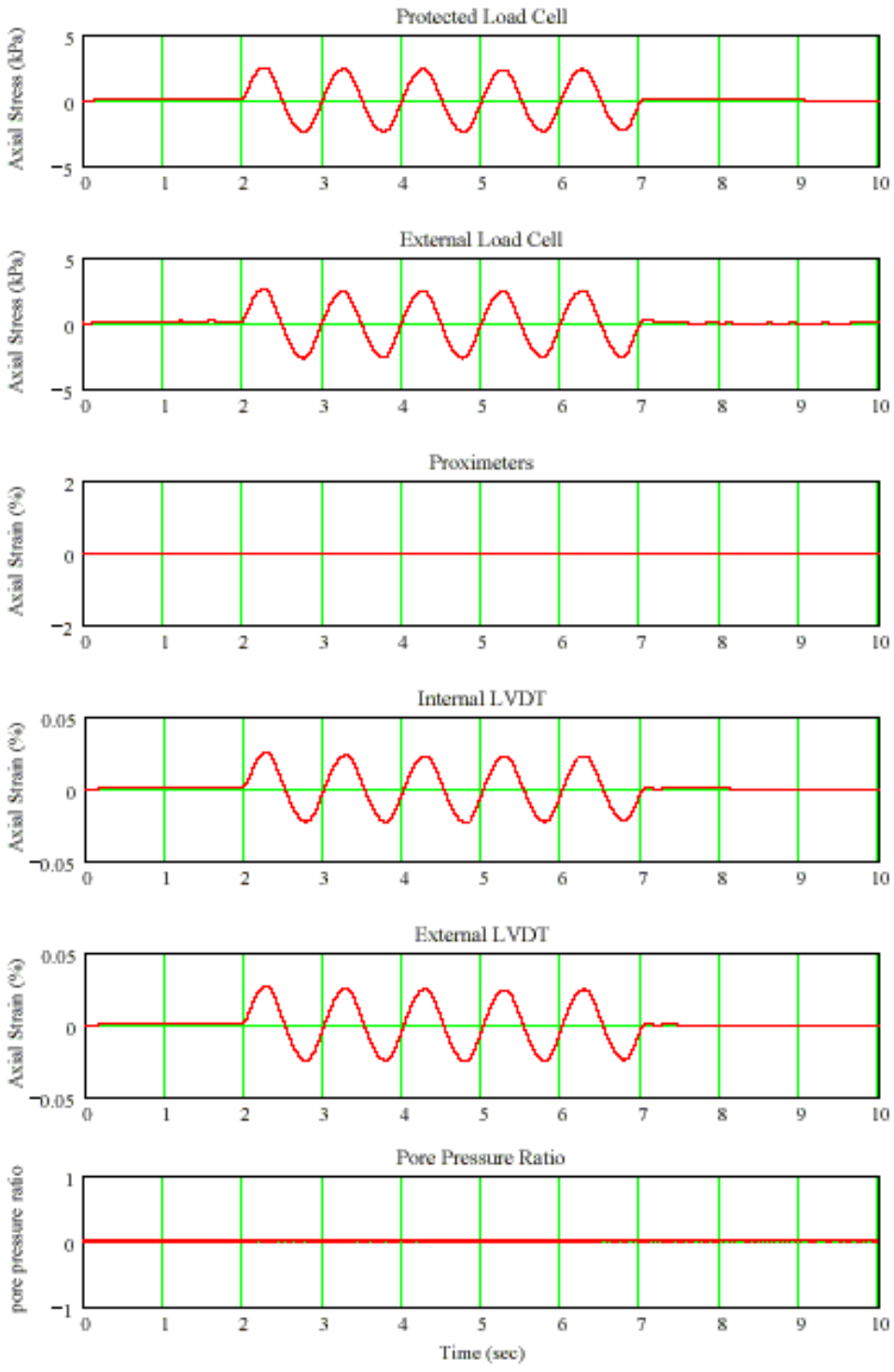
Protected Load Cell
Axial Stress (kPa)
5
0
−5
0 1 2 3 4 5 6 7 8 9 10
External Load Cell
Axial Stress (kPa)
5
0
−5
0 1 2 3 4 5 6 7 8 9 10
Proximeters
Axial Strain (%)
2
0
−2
0 1 2 3 4 5 6 7 8 9 10
Internal LVDT
Axial Strain (%)
0.05
0
−0.05
0 1 2 3 4 5 6 7 8 9 10
External LVDT
Axial Strain (%)
0.05
0
−0.05
0 1 2 3 4 5 6 7 8 9 10
Pore Pressure Ratio
pore pressure ratio
1
0
−1
0 1 2 3 4 5 6 7 8 9 10
Time (sec)

Internal Load Cell vs. Internal LVDT

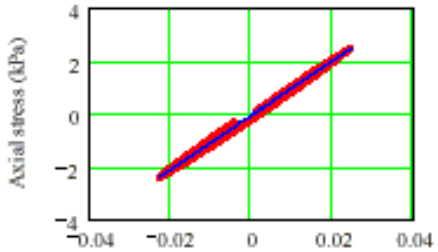

Loop 1

$E_{0,1} = 10308$ kPa

$G_{0,1} = 3436$ kPa

$\xi_{0,1} = 0.035$

$\gamma_{0,1} = 3.56 \times 10^{-2}$ %

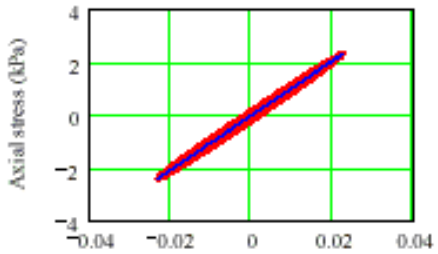

Loop 2

$E_{1,1} = 10335$ kPa

$G_{1,1} = 3445$ kPa

$\xi_{1,1} = 0.04$

$\gamma_{1,1} = 3.45 \times 10^{-2}$ %

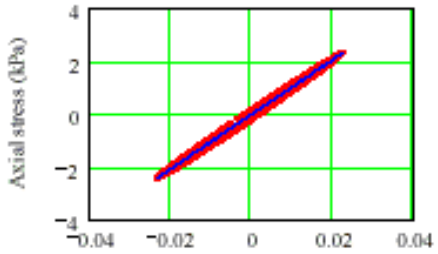

Loop 3

$E_{2,1} = 10335$ kPa

$G_{2,1} = 3445$ kPa

$\xi_{2,1} = 0.04$

$\gamma_{2,1} = 3.45 \times 10^{-2}$ %

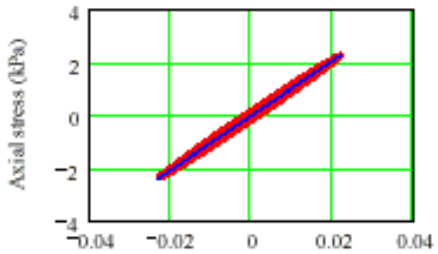

Loop 4

$E_{3,1} = 10345$ kPa

$G_{3,1} = 3448$ kPa

$\xi_{3,1} = 0.04$

$\gamma_{3,1} = 3.38 \times 10^{-2}$ %

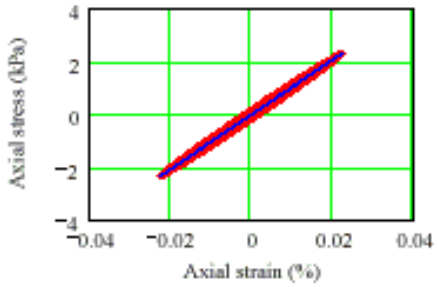

Loop 5

$E_{4,1} = 10352$ kPa

$G_{4,1} = 3451$ kPa

$\xi_{4,1} = 0.04$

$\gamma_{4,1} = 3.37 \times 10^{-2}$ %

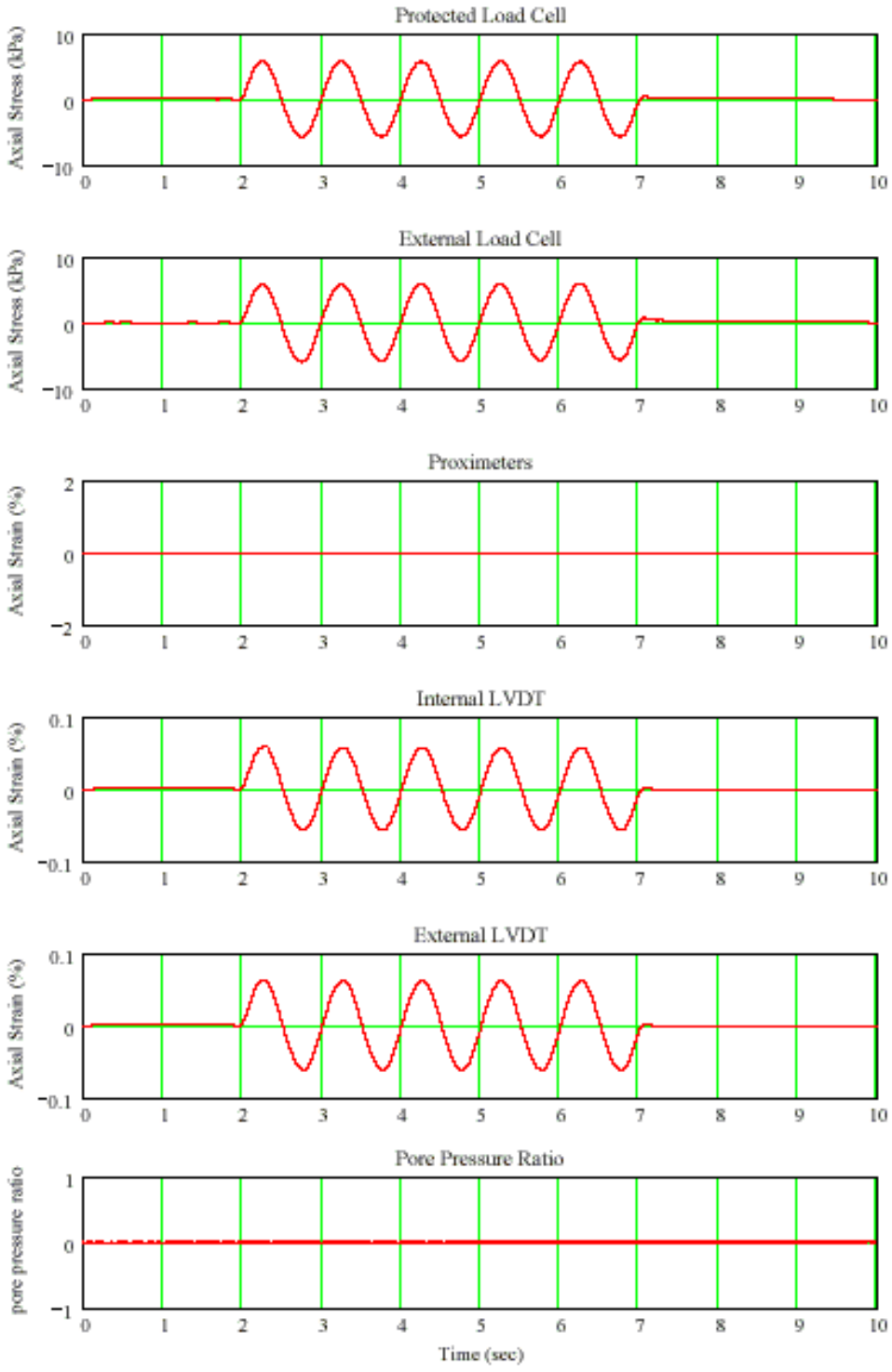
Protected Load Cell
Axial Stress (kPa)
10
0
−10
0 1 2 3 4 5 6 7 8 9 10
External Load Cell
Axial Stress (kPa)
10
0
−10
0 1 2 3 4 5 6 7 8 9 10
Proximeters
Axial Strain (%)
2
0
−2
0 1 2 3 4 5 6 7 8 9 10
Internal LVDT
Axial Strain (%)
0.1
0
−0.1
0 1 2 3 4 5 6 7 8 9 10
External LVDT
Axial Strain (%)
0.1
0
−0.1
0 1 2 3 4 5 6 7 8 9 10
Pore Pressure Ratio
pore pressure ratio
1
0
−1
0 1 2 3 4 5 6 7 8 9 10
Time (sec)

Internal Load Cell vs. Internal LVDT

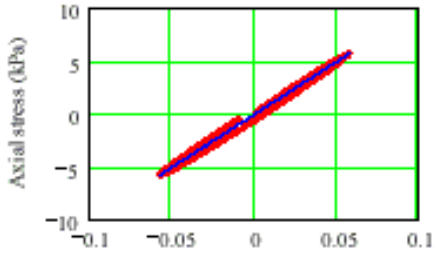

Loop 1

$E_{0,1} = 9992$ kPa

$G_{0,1} = 3331$ kPa

$\xi_{0,1} = 0.042$

$\gamma_{0,1} = 8.65 \times 10^{-2}$ %

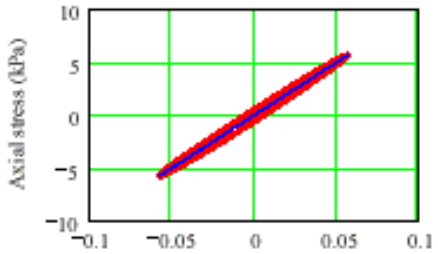

Loop 2

$E_{1,1} = 9997$ kPa

$G_{1,1} = 3332$ kPa

$\xi_{1,1} = 0.047$

$\gamma_{1,1} = 8.58 \times 10^{-2}$ %

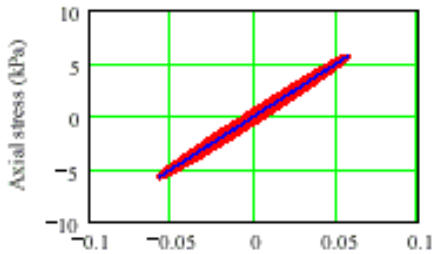

Loop 3

$E_{2,1} = 9976$ kPa

$G_{2,1} = 3325$ kPa

$\xi_{2,1} = 0.047$

$\gamma_{2,1} = 8.57 \times 10^{-2}$ %

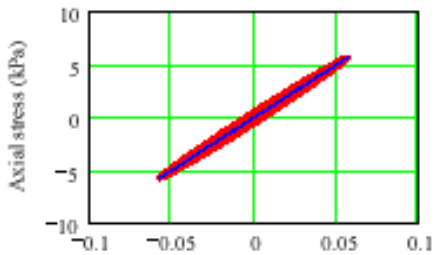

Loop 4

$E_{3,1} = 9983$ kPa

$G_{3,1} = 3328$ kPa

$\xi_{3,1} = 0.047$

$\gamma_{3,1} = 8.56 \times 10^{-2}$ %

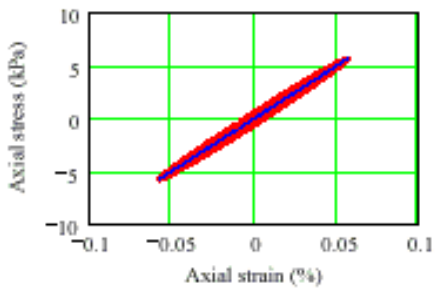

Loop 5

$E_{4,1} = 9970$ kPa

$G_{4,1} = 3323$ kPa

$\xi_{4,1} = 0.047$

$\gamma_{4,1} = 8.57 \times 10^{-2}$ %

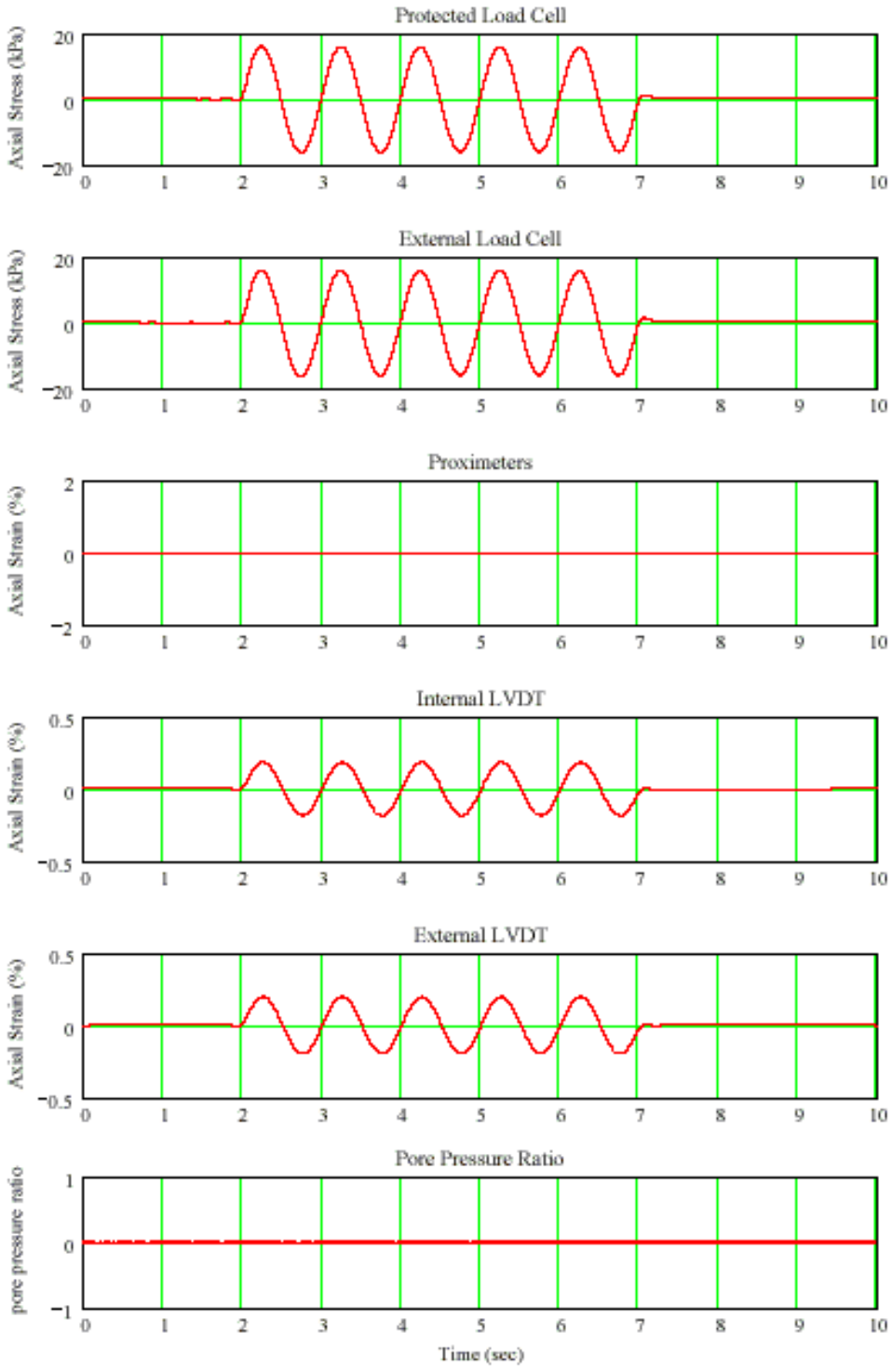
Protected Load Cell
Axial Stress (kPa)
20
0
−20
0 1 2 3 4 5 6 7 8 9 10
External Load Cell
Axial Stress (kPa)
20
0
−20
0 1 2 3 4 5 6 7 8 9 10
Proximeters
Axial Strain (%)
2
0
−2
0 1 2 3 4 5 6 7 8 9 10
Internal LVDT
Axial Strain (%)
0.5
0
−0.5
0 1 2 3 4 5 6 7 8 9 10
External LVDT
Axial Strain (%)
0.5
0
−0.5
0 1 2 3 4 5 6 7 8 9 10
Pore Pressure Ratio
pore pressure ratio
1
0
−1
0 1 2 3 4 5 6 7 8 9 10
Time (sec)

Internal Load Cell vs. Internal LVDT

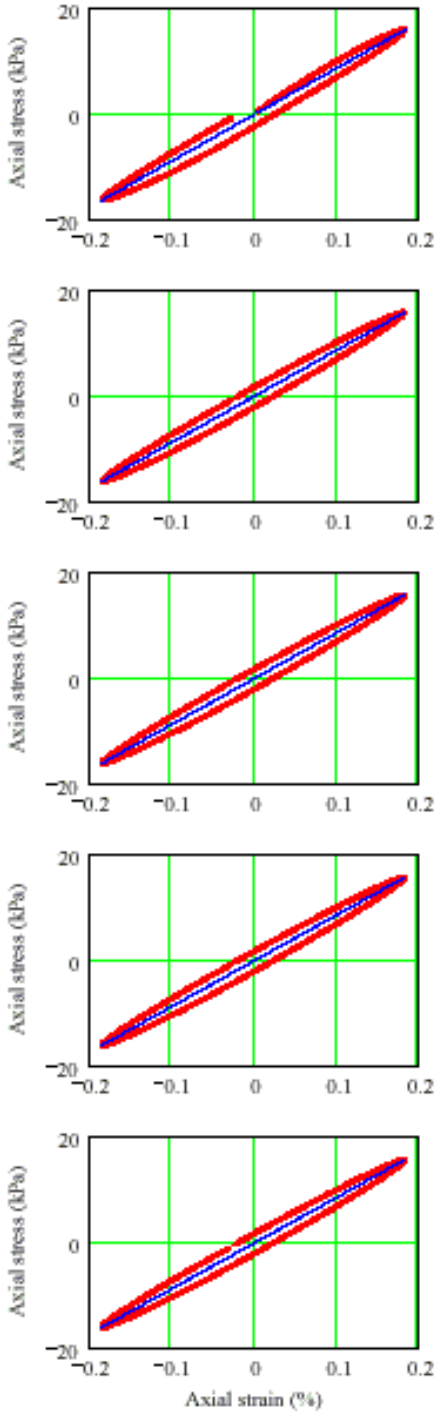

Loop 1

$E_{0,1} = 8768$ kPa

$G_{0,1} = 2923$ kPa

$\xi_{0,1} = 0.058$

$\gamma_{0,1} = 2.76 \times 10^{-1}$ %

Loop 2

$E_{1,1} = 8713$ kPa

$G_{1,1} = 2904$ kPa

$\xi_{1,1} = 0.06$

$\gamma_{1,1} = 2.75 \times 10^{-1}$ %

Loop 3

$E_{2,1} = 8667$ kPa

$G_{2,1} = 2889$ kPa

$\xi_{2,1} = 0.06$

$\gamma_{2,1} = 2.75 \times 10^{-1}$ %

Loop 4

$E_{3,1} = 8644$ kPa

$G_{3,1} = 2881$ kPa

$\xi_{3,1} = 0.06$

$\gamma_{3,1} = 2.75 \times 10^{-1}$ %

Loop 5

$E_{4,1} = 8628$ kPa

$G_{4,1} = 2876$ kPa

$\xi_{4,1} = 0.06$

$\gamma_{4,1} = 2.75 \times 10^{-1}$ %

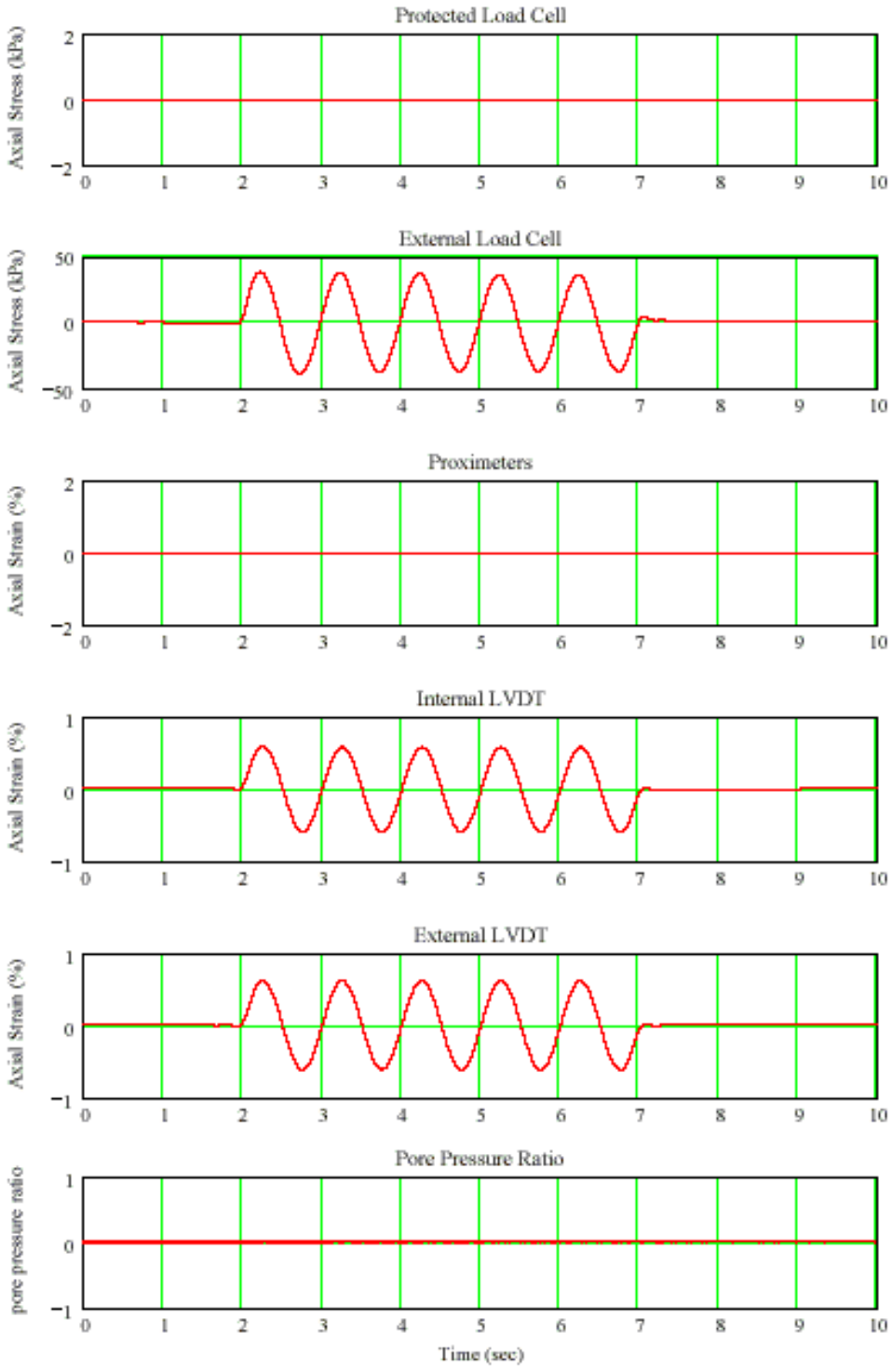
Protected Load Cell
Axial Stress (kPa)
2
0
−2
0 1 2 3 4 5 6 7 8 9 10
External Load Cell
Axial Stress (kPa)
50
0
−50
0 1 2 3 4 5 6 7 8 9 10
Proximeters
Axial Strain (%)
2
0
−2
0 1 2 3 4 5 6 7 8 9 10
Internal LVDT
Axial Strain (%)
1
0
−1
0 1 2 3 4 5 6 7 8 9 10
External LVDT
Axial Strain (%)
1
0
−1
0 1 2 3 4 5 6 7 8 9 10
Pore Pressure Ratio
pore pressure ratio
1
0
−1
0 1 2 3 4 5 6 7 8 9 10
Time (sec)

External Load Cell vs. Internal LVDT

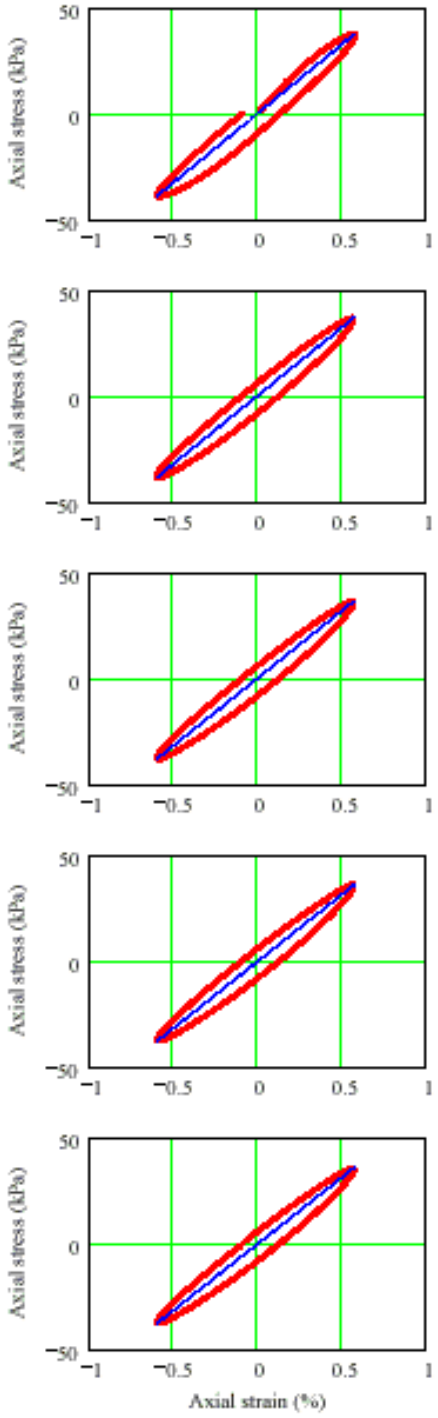

Loop 1

$E_{0,2} = 6521$ kPa

$G_{0,2} = 2174$ kPa

$\xi_{0,2} = 0.095$

$\gamma_{0,2} = 8.79 \times 10^{-1}$ %

Loop 2

$E_{1,2} = 6437$ kPa

$G_{1,2} = 2146$ kPa

$\xi_{1,2} = 0.095$

$\gamma_{1,2} = 8.76 \times 10^{-1}$ %

Loop 3

$E_{2,2} = 6373$ kPa

$G_{2,2} = 2124$ kPa

$\xi_{2,2} = 0.094$

$\gamma_{2,2} = 8.75 \times 10^{-1}$ %

Loop 4

$E_{3,2} = 6305$ kPa

$G_{3,2} = 2102$ kPa

$\xi_{3,2} = 0.094$

$\gamma_{3,2} = 8.76 \times 10^{-1}$ %

Loop 5

$E_{4,2} = 6275$ kPa

$G_{4,2} = 2092$ kPa

$\xi_{4,2} = 0.093$

$\gamma_{4,2} = 8.76 \times 10^{-1}$ %

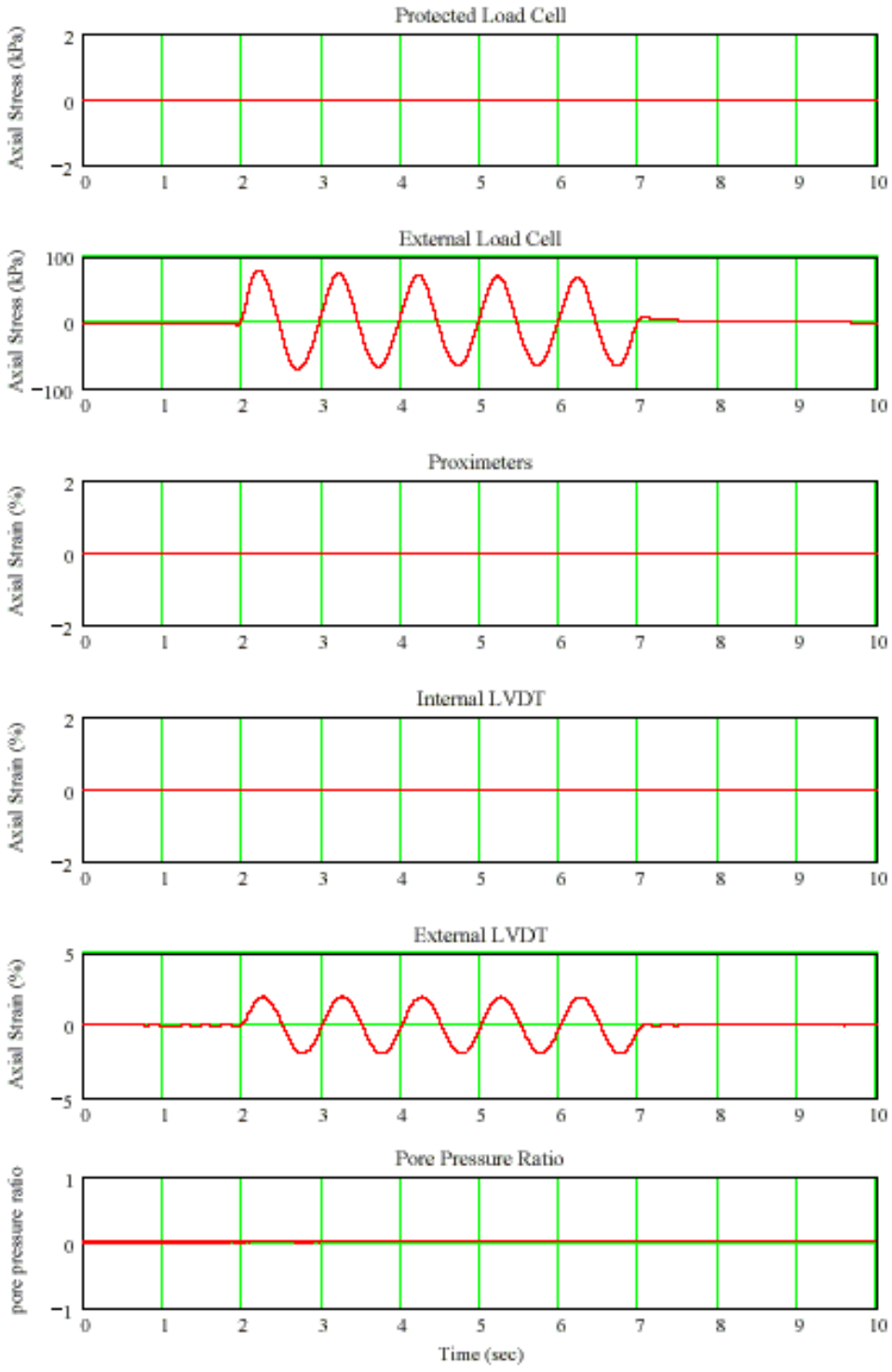
Protected Load Cell
Axial Stress (kPa)
2
0
−2
0 1 2 3 4 5 6 7 8 9 10
External Load Cell
Axial Stress (kPa)
100
0
−100
0 1 2 3 4 5 6 7 8 9 10
Proximeters
Axial Strain (%)
2
0
−2
0 1 2 3 4 5 6 7 8 9 10
Internal LVDT
Axial Strain (%)
2
0
−2
0 1 2 3 4 5 6 7 8 9 10
External LVDT
Axial Strain (%)
5
0
−5
0 1 2 3 4 5 6 7 8 9 10
Pore Pressure Ratio
pore pressure ratio
1
0
−1
0 1 2 3 4 5 6 7 8 9 10
Time (sec)

External Load Cell vs. External LVDT

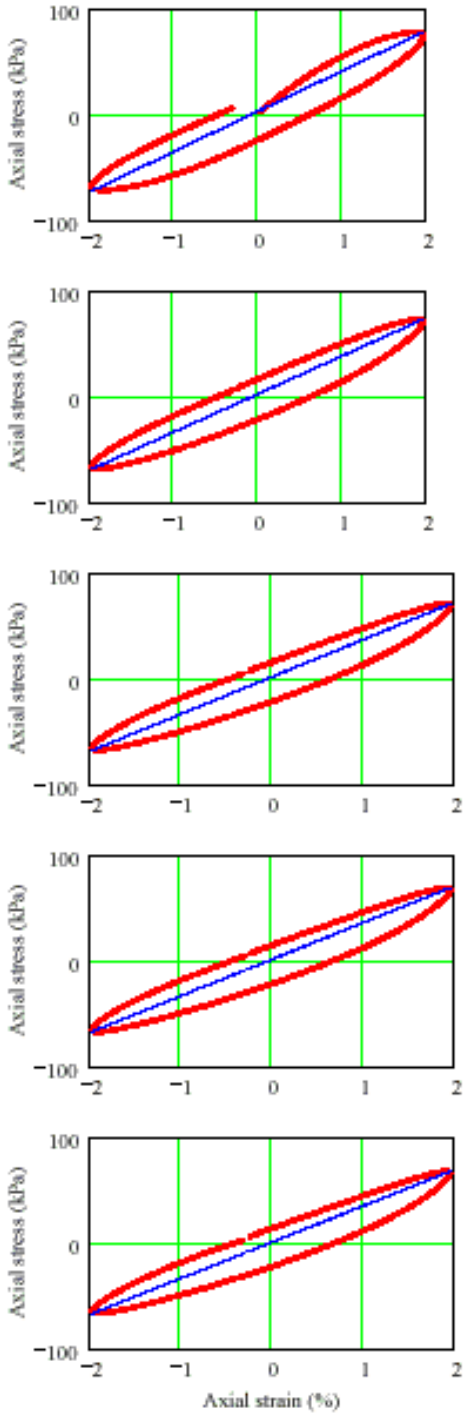

Loop 1

$E_{0,3} = 3812$ kPa

$G_{0,3} = 1271$ kPa

$\xi_{0,3} = 0.144$

$\gamma_{0,3} = 2.9 \times 10^{0}$ %

Loop 2

$E_{1,3} = 3598$ kPa

$G_{1,3} = 1199$ kPa

$\xi_{1,3} = 0.141$

$\gamma_{1,3} = 2.92 \times 10^{0}$ %

Loop 3

$E_{2,3} = 3522$ kPa

$G_{2,3} = 1174$ kPa

$\xi_{2,3} = 0.14$

$\gamma_{2,3} = 2.92 \times 10^{0}$ %

Loop 4

$E_{3,3} = 3463$ kPa

$G_{3,3} = 1154$ kPa

$\xi_{3,3} = 0.138$

$\gamma_{3,3} = 2.93 \times 10^{0}$ %

Loop 5

$E_{4,3} = 3425$ kPa

$G_{4,3} = 1142$ kPa

$\xi_{4,3} = 0.137$

$\gamma_{4,3} = 2.93 \times 10^{0}$ %

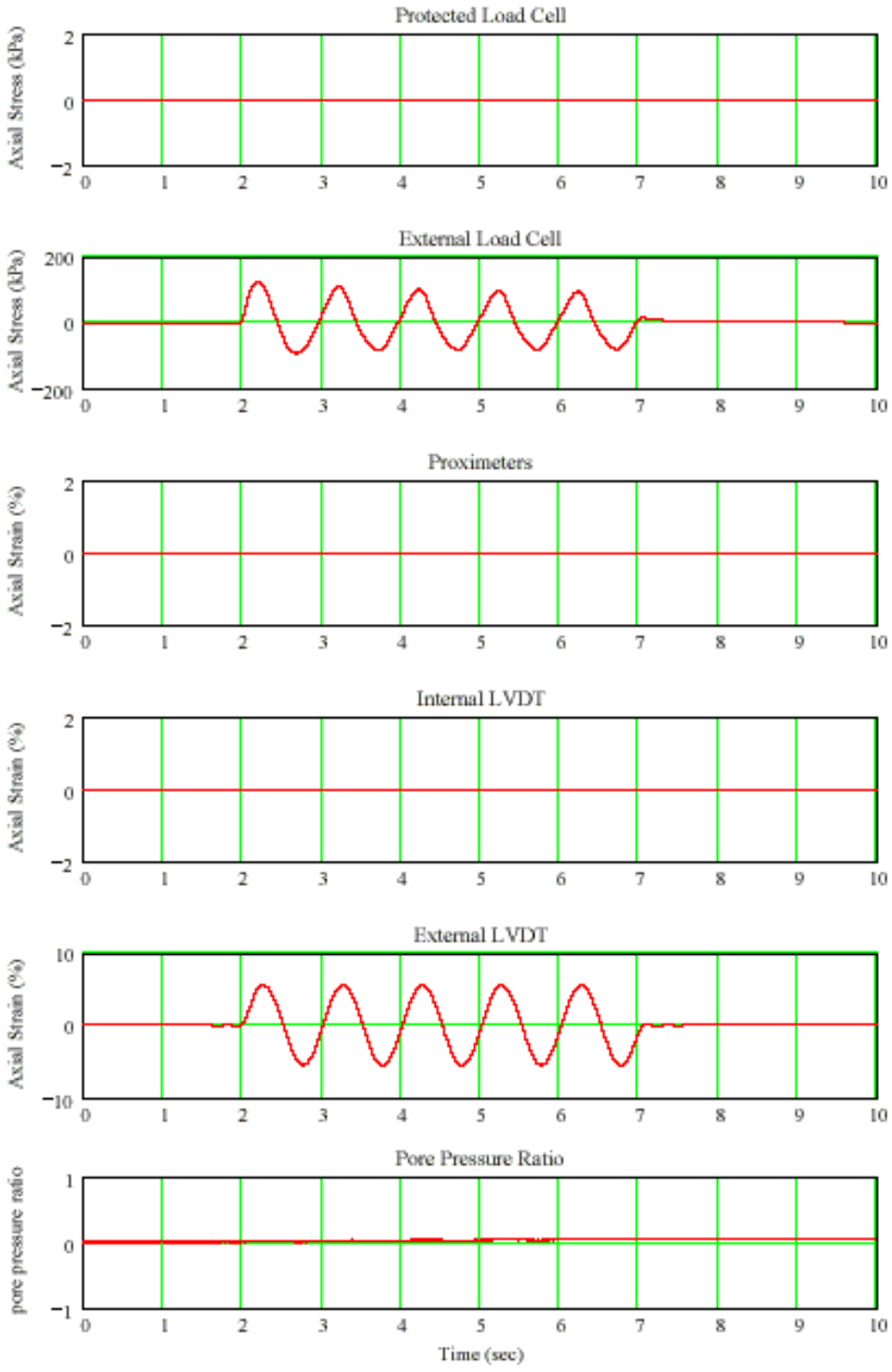
Protected Load Cell
Axial Stress (kPa)
2
0
−2
0 1 2 3 4 5 6 7 8 9 10
External Load Cell
Axial Stress (kPa)
200
0
−200
0 1 2 3 4 5 6 7 8 9 10
Proximeters
Axial Strain (%)
2
0
−2
0 1 2 3 4 5 6 7 8 9 10
Internal LVDT
Axial Strain (%)
2
0
−2
0 1 2 3 4 5 6 7 8 9 10
External LVDT
Axial Strain (%)
10
0
−10
0 1 2 3 4 5 6 7 8 9 10
Pore Pressure Ratio
pore pressure ratio
1
0
−1
0 1 2 3 4 5 6 7 8 9 10
Time (sec)

External Load Cell vs. External LVDT

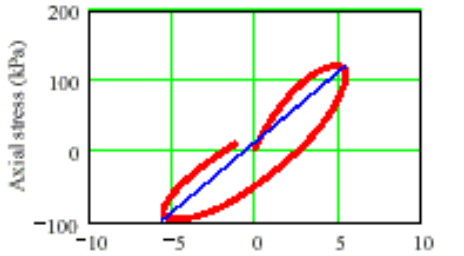

Loop 1

$E_{0,3} = 1978$ kPa

$G_{0,3} = 659$ kPa

$\xi_{0,3} = 0.209$

$\gamma_{0,3} = 8.04 \times 10^{0}$ %

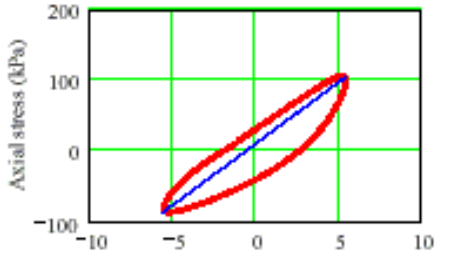

Loop 2

$E_{1,3} = 1738$ kPa

$G_{1,3} = 579$ kPa

$\xi_{1,3} = 0.197$

$\gamma_{1,3} = 8.19 \times 10^{0}$ %

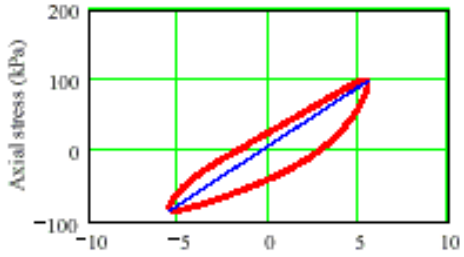

Loop 3

$E_{2,3} = 1667$ kPa

$G_{2,3} = 556$ kPa

$\xi_{2,3} = 0.191$

$\gamma_{2,3} = 8.19 \times 10^{0}$ %

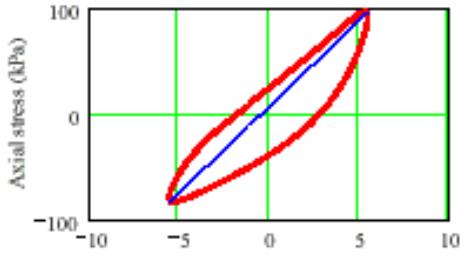

Loop 4

$E_{3,3} = 1625$ kPa

$G_{3,3} = 542$ kPa

$\xi_{3,3} = 0.188$

$\gamma_{3,3} = 8.19 \times 10^{0}$ %

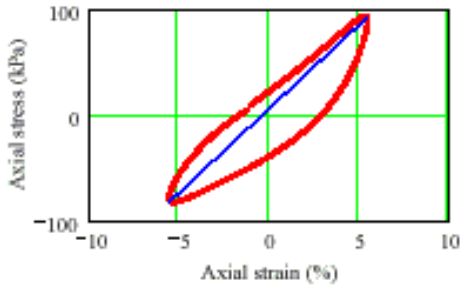

Loop 5

$E_{4,3} = 1586$ kPa

$G_{4,3} = 529$ kPa

$\xi_{4,3} = 0.186$

$\gamma_{4,3} = 8.21 \times 10^{0}$ %